

C O N T E N T S

	<u>PAGE</u>
<u>Chapter 1: Introduction</u>	1
1.1 The nature of surfaces	1
1.2 Techniques used for the analysis of surfaces	2
1.2.1 Thermal input	2
1.2.2 Electron probes	3
1.2.3 Ion probes	8
1.2.4 Photon probes	10
1.2.5 Electric and Magnetic field probes	13
1.2.6 Other techniques and Raman spectroscopy	15
1.3 Vibrational spectroscopy	17
1.3.1 Infrared spectroscopy	18
1.3.2 The Raman effect	19
1.3.3 Comparison of Infrared and Raman spectroscopy at surfaces	25
1.3.4 Survey of Laser Raman spectroscopy at surfaces	27
<u>Chapter 2: Instrumentation</u>	31
2.1 Illumination sources	31
2.2 Sample area	35
2.3 Monochromators	38
2.4 Detectors	42
2.5 Signal processing	44
2.6 The Coderg T800 Raman spectrometer	45
<u>Chapter 3: Optimization of the illumination and collection optics</u>	49
3.1 Analysis of the illumination and collection optics	49
3.2 Experimental determination of the optimum conditions	56

3.2.1 Lens collection optics	56
3.2.2 Cassegrain collection optics	57
3.3 Results	58
3.3.1 Lens collection optics	58
3.3.2 Cassegrain collection optics	60
<u>Chapter 4: Raman spectroscopy at oxide surfaces</u>	63
4.1 Adsorption at oxide surfaces	63
4.1.1 Characterisation of surfaces	64
4.2 Raman cells for the study of surfaces	66
4.3 Vacuum and furnace system	70
4.4 Sample activation and fluorescence	72
4.4.1 Surface properties on activation	72
4.4.2 Fluorescence and its elimination from oxides	74
4.5 Coloured adsorbents	76
<u>Chapter 5: Adsorption and reaction of Uranium hexa-fluoride at oxide surfaces</u>	78
5.1 Handling and reactions of UF_6	78
5.2 Uranium oxyfluorides	80
5.2.1 UO_2F_2	80
5.2.2 UOF_4	81
5.2.3 $U_2O_3F_6$	84
5.2.4 $U_3O_5F_8$	84
5.3 Oxide adsorbents	87
5.4 Adsorption on SiO_2	87
5.4.1 Characterisation of the surface	87
5.4.2 Adsorption of UF_6	90

5.5 Adsorption on other non Laser absorbing oxides	93
5.5.1 γ -Al ₂ O ₃	97
5.5.2 ZnO	103
5.5.3 TiO ₂	105
5.5.4 MgO	105
5.6 Adsorption on Laser absorbing coloured oxides	105
5.6.1 NiO	105
5.6.2 Fe ₂ O ₃	108
<u>Chapter 6: Conclusions</u>	109

UNIVERSITY OF SOUTHAMPTON

ABSTRACT

FACULTY OF SCIENCE

CHEMISTRY

Master of Philosophy

RAMAN SPECTROSCOPY OF ADSORPTION AND REACTION OF URANIUM
HEXAFLUORIDE AT OXIDE SURFACES.

by John Hugh Prior

The collection and illumination optics for Raman spectrometers has been optimized for the study of surfaces, and the maximum Raman signal is collected when the slit image on the surface is fully illuminated. The optimum demagnification of the slits was found to be significantly different from that used in commercial spectrometers. At the optimum conditions the radiant flux density on the surface is greatly reduced, and the decomposition/desorption problem frequently encountered in adsorbed species is reduced.

In the system, oxide + UF_6 , very little physisorbed UF_6 was found on the surface of $\gamma-Al_2O_3$, ZnO and MgO . UF_6 does not chemisorb to surfaces which have Lewis sites present, but SiO_2 activated at $950^{\circ}C$ which has siloxane bridges on the surface chemisorbes UF_6 strongly, and less than 0.05 monolayers of UF_6 could be detected. No fluorination of the surface with UF_6 could be detected at room temperature.

The oxy-fluorides UO_2F_2 , UOF_4 and $U_2O_3F_6$ have been prepared and the Raman spectra recorded for use in identifying oxy-fluorides formed on the oxide surface through hydrolysis of UF_6 with physisorbed water and chemisorbed hydroxyl groups. UO_2F_2 and $U_2O_3F_6$ are both present on hydrolysis of UF_6 over oxide surfaces containing Lewis sites. UOF_4 which precedes $U_2O_3F_6$ in the hydrolysis system of UF_6 is absent from the surface species formed.

ACKNOWLEDGEMENTS

I wish to thank Dr. P.J. Hendra and Dr. G.J. van Schalkwyk for their helpful discussions during the course of this study.

Chapter 1Introduction1.1 The nature of surfaces

The universe consists of three phases, solids, liquids and gases, and it is becoming increasingly accepted that the boundary between these phases is fundamentally different and must be identified as a separate "surface phase". Most chemical reactions occur at surfaces, and the surface chemistry of catalysis, corrosion, adhesion, sintering and semiconductors is of major industrial importance, yet we know little about the nature of these surfaces. This is due to the experimental arrangements used such as X-ray and electron diffraction, molecular and elemental analysis which give valuable information about the bulk material but nothing about the surface. The contribution from the surface is very small indeed, as it is at most two atomic or molecular layers thick. Most successful investigation has undoubtedly been carried out at the solid-gas interface, and this is the one of interest here.

A solid surface is a very abrupt discontinuity, and Haber (1) has expressed the view that an atom at the surface of a solid is only partly saturated on its inner side and therefore possesses "residual valences" on the outer side. Langmuir extended the idea that these "residual valences" were responsible for the adsorption of foreign atoms or molecules on the surface, and formulated an equation for adsorption equilibrium. This begins to answer the many questions which were posed about the forces that cause adsorption, the interaction between the adsorbed atom and the surface, and the kinetics of adsorption.

Most of the elegant techniques which have been developed for the analysis of surfaces investigate only chemically clean and hence, in a sense meaningful surfaces. For years questions have been asked whether a surface is "clean" or not, and what kind of a vacuum and/or thermal environment is necessary to prepare and keep a surface "clean" for studying. In the 1960's reasoned guesses

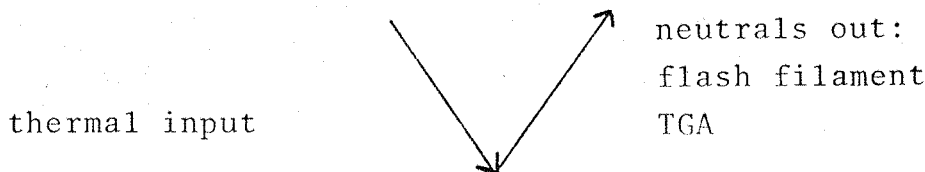
were made that a surface was "clean", based upon the reproducibility obtained in LEED (low energy electron diffraction) patterns, and now known to be wrong on the basis of measurements made using AES (auger electron spectroscopy). Furthermore, surfaces treated simply by outgassing and/or chemical reduction, known intuitively to be "dirty", have been shown to be "clean".

An idea of the speed of surface contamination may be seen if a sheet of mica is cleaved and one surface is sprayed immediately with distilled water from an atomizer and the surface is uniformly wetted, now if the other surface is sprayed several seconds later, the water will bead up in distinctly visible droplets due to contamination by organic vapours in the atmosphere. At a vacuum of 10^{-6} Torr a complete monolayer of contamination can condense in \sim one second, and at 10^{-10} Torr in \sim two hours. This requires that for most sophisticated techniques it is necessary to establish the cleanliness of the surface in advance of every experiment.

1.2 Techniques used for the analysis of surfaces

Over the past few years there has been an explosion of interest in surface studies, and a simultaneous increasing development of new methods of surface analysis. In this section the most important techniques are reviewed and their sensitivity and usefulness for studying adsorbed species are discussed. The techniques are grouped together under headings which relate to the type of particle or field probe which is used.

1.2.1 Thermal input:

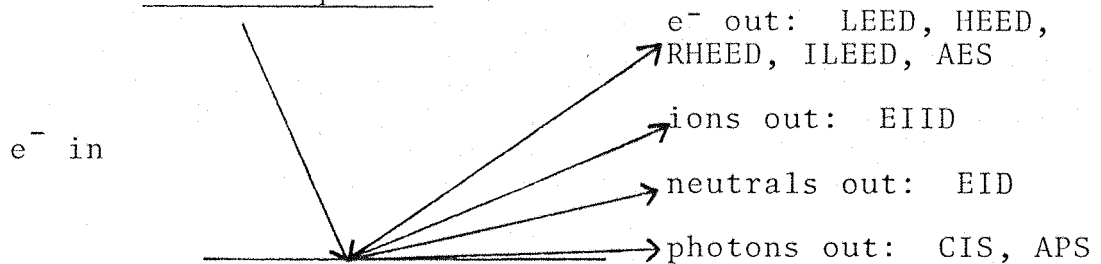


Flash filament is undoubtedly the simplest technique. The sample, usually a refractory metal (principally tungsten) in the form of a ribbon or wire is rigorously

ly cleaned under U.H.V. conditions, the adsorbate is then introduced. The total sample is then heated rapidly by passing a current through the metal and the pressure of the desorbing molecules is monitored by an ion gauge. From the desorption kinetics, the activation energy, rate constants and the order of the reaction can be established. This technique is very sensitive as fractions of a monolayer are easily detected from wires of low surface area. Using this technique molecular nitrogen has been shown to dissociate into atoms on a tungsten surface (2), and carbon monoxide, isoelectronic with nitrogen, has been shown not to dissociate when adsorbed on tungsten (3).

Gravimetric analysis has been used to determine adsorption isotherms (4), from which the surface area of the sample may be calculated. If hysteresis is present in the isotherm, additional information about the pore volume and sizes may be obtained. Thermo-gravimetric analysis (TGA) is widely used and is of great importance in determining the concentration of water and hydroxyl groups on adsorbents. The sample is normally heated in vacuum and suspended from a microbalance. The sensitivity is proportional to the surface area of the sample, and a mass resolution of 1 μ g is obtainable. Dzis'ko (5) has shown from TGA that the water left remaining on silica gel at 115°C is present as a monolayer of hydroxyl groups, and the number of hydroxyl groups is proportional to the surface area of the silica gel.

1.2.2 Electron probes:



Scanning electron microscopy is one of the oldest microanalytical methods developed. The surface can be

studied directly, though if the surface is non-conducting on thin conducting film must be evaporated onto it. The sample under high vacuum is scanned by the electron probe and the output is displayed on a television monitor. Features of the order of 20nm in height and width can be resolved. The surface area and range of pore diameters may be determined. Silica gel has been studied by this method at various temperatures (6). Magnesia (7), γ -Alumina (8,9) and transition metal catalysts (10) have also been examined.

Low energy electron diffraction (LEED) has been known for over 50 years. The technique is very sensitive to the outermost layers of the surface, but requires clean surfaces under UHV conditions. The electrons in the probe beam must have a wavelength comparable with the expected periodicity of the surface, this restricts the electron energies to the range 20-200 eV. The electron beam is focused to a diameter of $\sim 1\text{mm}$ at the selected crystal surface. Only the elastically diffracted electrons (i.e. those which have not lost any energy) play a part in the formation of the diffraction patterns, and grids are used to repel all electrons which have lost a part of their energy. The diffraction pattern is similar to the back reflection Laue method of X-ray diffraction. The diffraction pattern is made visible on a fluorescent screen which is raised to an accelerating potential of 3-5 kV and is on the same side of the crystal surface as the incoming electron beam. The great surface sensitivity of this technique is due to the low energy of the electrons used which cannot penetrate and be elastically diffracted from anything but the outermost layers of the surface. Any adsorbed species will give rise to an extra set of spots in the diffraction pattern, and although it is not difficult to obtain a spot pattern, it is clearly not simple to analyse. This has resulted in LEED often being used in conjunction with another technique capable of identifying the adsorbed species. LEED has been used to study the interaction of oxygen with

single crystal Cu surfaces (11), and the adsorption of CO₂ on a W (100) surface (12), the results indicating that the CO₂ is dissociated on the surface. Ni(111) (13), Cu (110) (14) and Fe (110) (15) surfaces have been investigated in the presence of adsorbed CO.

Although most people interested in electron diffraction use low energy electrons, experiments can be done using high energy electrons, where the experiment is called high energy electron diffraction (HEED). Very thin films are used and the transmission electron diffraction pattern is observed. This technique is not as surface sensitive as LEED but has been used to study the interaction of oxygen with single crystal surfaces of Cu (11).

High energy electrons can be made more surface sensitive by probing the surface at a glancing angle. This technique is known as reflection high energy electron diffraction (RHEED), and the scattered electrons are reflected from the surface layers. RHEED has been used in a kinetic study of the initial oxidation of a Ni (001) surface (16).

Inelastic low energy electron diffraction (ILEED) is the technique where a spatial analysis is carried out on the electrons which have been inelastically scattered from the surface. Carefully controlled energy selection is used to observe only the electrons which have lost a specific amount of their energy, resulting in a smaller output signal. Due to the complexity of the experimental system ILEED has only been used on a limited scale, although additional information about the surfaces of cleaved graphite, W (110) and Cu (100) has been obtained (17).

Auger electron spectroscopy (AES) has emerged as one of the most widely used analytical techniques for obtaining the chemical composition of solid surfaces. AES has a high sensitivity for chemical analysis in the surface layers, a rapid data acquisition speed and the ability to detect all elements above H_e, and in many cases provides

information on the status of chemical bonding. Clean surfaces and UHV conditions are required.

Auger (18) discovered the effect in 1925, but the high sensitivity of the technique was not realised until 1968 when Harris (19) demonstrated the use of differentiation of the energy distribution curves to obtain Auger spectra in the present familiar form. The Auger effect is produced when an electron in the energy range 1000-3000 eV produces core level excitation of an atom on the surface and removes a core electron from the atom. The excited state atom relaxes back to the ground state, and the liberated energy can be emitted as a photon, giving conventional X-ray emission or the excess energy can be transmitted to another of the electrons in the atom which then has sufficient energy to leave the atom and the material surface. The kinetic energy of this Auger electron is uniquely determined by the energy levels of the atom from whence it came and is independant of the primary electron beam.

The grids in a standard LEED system are easily converted to be used as an energy analyser, and makes it possible to do AES and LEED on the same sample. Unfortunately the LEED grid structure used as an energy analyser gives only a small signal-to-noise ratio and is not used much for AES. The cylindrical mirror analyser (20) is now used almost exclusively in modern AES apparatus, and with its improved signal-to-noise ratio it enables scanning to be carried out 100-1000 times faster. The high surface sensitivity of AES is due to the limited mean free path of electrons in the kinetic energy range 20-2500 eV. Auger electrons which lose energy i.e. come from deeper down in the sample, contribute to the nearly uniform background on which the Auger peaks are superimposed. In practice Auger electrons can be detected from a maximum depth of 1-3 nm. Scanning Auger microscopy was first attempted by MacDonald (21). The electron beam is scanned across the surface and a two dimensional surface Auger image is displayed on a television monitor.

AES has been used in many adsorption and desorption studies to monitor surface coverage. The coverage is usually calibrated from a supplementary technique such as LEED (22) and it is possible to detect adsorbed species down to 0.01 monolayer. Palmberg (23) used the peak-to-peak amplitude in the differentiated spectrum as a measure of surface coverage in a study of Xe adsorption on a Pd (100) surface. Hooker (24) used AES to study the adsorption of oxygen on a clean Ni surface. Hopkins (12) used AES in conjunction with LEED to study CO₂ adsorption on a W (100) surface. Adsorption-desorption studies are sometimes complicated by dissociation or desorption caused by the electron beam. In most cases the electron beam effects are easily recognised and the problem overcome by lowering the beam current, defocussing the beam or using pulsed current techniques (25).

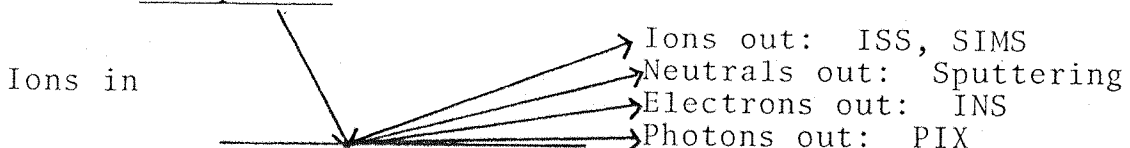
Electron induced ion desorption (EIID), sometimes called electron probe surface mass spectrometry (EPSMS) is a sensitive technique for analysing adsorbed species. Bombarding adsorbed atoms or molecules with 100eV electrons will cause some to undergo dissociative ionization and some will have sufficient excess kinetic energy to leave the surface. The desorbed ions are analysed by a mass spectrometer. Since the desorbing probability is $\sim 10^{-5}$ ions per electron, a sensitive mass spectrometer using an electron multiplier detector must be used. Only the outermost adsorbed monolayer on the surface contributes to the desorbed ions as the electrons used are of such low energy they are not able to penetrate the surface. Lichtman (26) has shown that the electron induced O⁺ signal of CO adsorbed on Mo comes from a weakly bound state of CO.

Electron induced neutral desorption (EID) has the promise of providing considerable information about the surface monolayer. The basic problem is that in EIID the desorbing ions can be directed to the detector with appropriate electric fields, but desorbing neutrals leave the surface in all directions and the collection effi-

ciency is only 10^{-4} to 10^{-2} times that of EIID, presenting a formidable task.

Characteristic isochromat spectroscopy (CIS) (27) and appearance potential spectroscopy (APS) (28) depend on detecting photons emitted from a surface when bombarded with an electron beam. The systems are not simple and provide information from a region considerably thicker than the surface monolayer. The generation of the electron probe beam is simple but the detection and analysis of the emitted photons is difficult. The emitted photons leave the surface in all directions and only a very small fraction can be collected and detected. If the photons are generated in the visible or U.V., a very carefully designed system is needed to reduce scattered light from the filaments. This problem is reduced by using high energy electrons which penetrate the surface, decreasing the surface sensitivity and generating photons in the X-ray region.

1.2.3 Ion probes



A major difference in using ion probes compared with electron probes is that considerable kinetic energy exchange can occur because the ion particles have masses comparable with those of the substrate. This may cause considerable sputtering and therefore change the surface. Extra care is therefore needed when using ion probes so that the surface being studied is not destroyed before information has been obtained about it.

Ion scattering spectrometry (ISS) (29) is a very surface sensitive technique. It is assumed that the bombarding ion undergoes a simple collision with a substrate atom and loses energy according to simple kinetic energy exchange. If the primary beam were to penetrate the substrate, the possibility of undergoing a simple binary collision inside the bulk material and then scattering back

out without losing any additional energy is very small indeed. The scattered ions are energy analysed to produce a spectrum. The peak positions are very close to the values predicted on the basis of the simple binary collision. The resolution of the system is rather limited at present and does not allow the form of the atom which does the scattering to be ascertained i.e. scattering oxygen atoms cannot be specified if they are due to adsorbed oxygen, or adsorbed CO, or part of the surface oxide. Although there are a number of limitations, the technique does provide chemical identification of the surface components with a rather simple experimental arrangement.

If instead of energy analysing the reflected primary ions, the sputtered ions are mass analysed, then the technique is referred to as secondary ion mass spectrometry (SIMS) (30). The number and type of both positive and negative ions emitted from the surface can be determined. The spectra are generally complex with many lines, but the resolution of the analyser is significantly greater than in ISS. SIMS has a detection sensitivity of $< 10^{-4}$ monolayer for the majority of elements, is able to do isotopic analysis and analysis of low atomic number elements. UHV conditions are needed otherwise the arrival rate of gaseous species from the vacuum environment can exceed the arrival rate of incoming ions in a low current beam. The median escape depth of secondary ions is usually $< 1\text{nm}$ but a fraction of the ions do originate from layers deeper below the surface. Secondary ion images that provide a two-dimensional elemental characterisation of the surface are available. Lateral resolutions of $1\text{ }\mu\text{m}$ have been achieved with direct imaging instruments (31). SIMS has been used to study the surface species present on a silver catalyst used for the oxidation of ethylene (32), the adsorption of oxygen on copper (33), and the oxidation of aluminium (34).

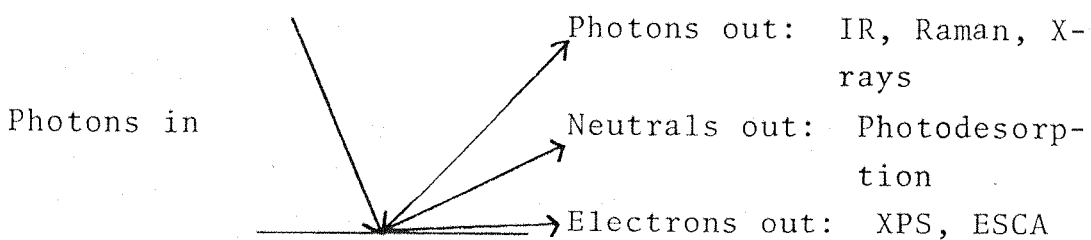
Ion bombardment of surfaces also leads to consider-

rable desorption of neutral atoms and molecular fragments. The problem of analysing these sputtered neutrals is the same as in EID, i.e. only a small fraction of the sputtered neutrals would reach the detector. Controlled sputtering of surfaces is used in conjunction with many techniques to give depth concentration profiles e.g. in AES and SIMS.

Ion probes also cause electron emission from surfaces and Hagstrum (35) has done work on ion neutralisation spectroscopy (INS). The technique provides information about the electronic nature of the surface, but has not been much pursued as it is easier to produce secondary electrons with a primary electron probe.

The technique of bombarding a surface with ions and analysing the emitted photons has been concentrated in the X-ray region. The depth of material contributing to the signal is thus very much larger than in SIMS. Some recent efforts have been directed towards using proton induced X-ray analysis (PIX) (36) which has an advantage that protons produce the least amount of damage to the surface compared to other ion particles.

1.2.4 Photon probes:



Photon probes have two characteristics which make them well suited for surface analysis. Firstly, they have negligible momentum and produce a minimum of disturbance on the surface. Secondly, being neutral they eliminate the problems of maintaining optimum electric and/or magnetic fields in the vicinity of the surface.

The vibrational behavior of molecules is easily studied using infrared spectroscopy (IR). When a molecule adsorbs on a surface it is perturbed from its free state and from the changes in the vibrational spectrum deduc-

tions can be made about the nature of the surface eg. the types of sites occupied by the molecule and the strength of adsorption. IR has vast applications in chemistry and has an advantage that clean surfaces are not necessary. IR is mainly applied to surfaces in two ways, by transmission or by reflection.

Most IR instruments are normally used in the transmission mode. The substrates must have sufficient transmission in the wavelength region of interest, and this requires the use of thin films and thin pressed discs. Vibrational bands of the substrate are also present in the spectrum, but it is possible to cancel them out by using a substrate sample in the reference beam of a double beam spectrometer. The surface of silica-aluminas has been characterised by the adsorption of ammonia and pyridine (37), NH_3 being adsorbed at Lewis sites and NH_4^+ at Brönsted sites. The adsorption of pyridine on alumina (38) has shown that strong Lewis sites are predominant.

Infrared reflection-absorbtion spectroscopy (RA) makes it possible to study surfaces which are opaque to infrared radiation eg. metals. The sensitivity is greater than in transmission IR and the substrate does not interfere. Usually between one and thirty reflections are used, but the optimum number must be determined for each surface. Yates (39) has been able to detect 0.04 monolayer of CO adsorbed on W using RA.

Raman spectroscopy also investigates the vibrational behaviour of molecules. This will be discussed in section 1.2.6.

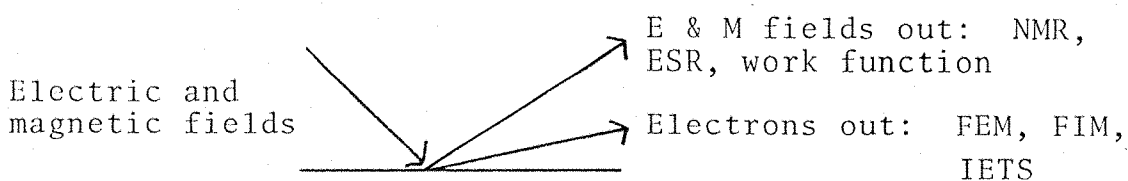
X-rays penetrate the bulk material, and the X-ray diffraction data reveal only properties of the bulk material, but are used to distinguish different crystalline structures. Low angle X-ray scattering is surface sensitive and is used for the determination of surface area (40). Tamagusuku (41, 42) has determined the surface areas of many silica-aluminas and the results are in good agreement with the surface areas determined by adsorption.

The interaction of UV photons with adsorbed molecules produces photodesorption. Wavelengths below 300nm and preferably below 200nm are required for the process to occur. Photodesorption has been found to occur basically on semiconductor surfaces, and has an almost zero cross-section on metals. With the limited number of substrates and the restricted amount of information to be gained about the surface, this technique has only seen a limited use.

The photoelectric effect is well known, normally the number and energy of emitted electrons is a function of the incident wavelength (usually visible and UV). With the advent of high resolution electron energy analysers and using photons in the X-ray region, X-ray photoelectron spectroscopy (XPS) is used to determine the electronic structure of solid surfaces as well as to identify the chemical components. When used for chemical analysis it is known as electron spectroscopy for chemical analysis (ESCA). A monoenergetic beam of X-ray photons are directed at the sample, atoms in the surface absorb the photons and promptly emit an electron with kinetic energy equal to the difference of the incident photon energy and the binding energy of the electron in the atom. The electrons generally come from the internal K and L shells although electrons from all orbitals with a binding energy less than the photon energy are possible. The observation depth of ESCA is limited by the mean free path of the electrons which is typically 0.5 - 2.5 nm for metals and metal oxides and up to 10nm for organic and polymeric materials. UHV conditions are not necessary since many of the surfaces to be studied are not atomically clean. Each element has characteristic peaks in the spectrum and a chemical shift is resolvable which enables the valency of the atoms to be determined. Aluminium covered with a thin oxide layer has two peaks 3eV apart due to the metal and Al^{3+} . Most elements can be detected at 0.1 at.% abundance. The adsorption of CO on Mo and W films has been studied using ESCA (43) and it is possible to dis-

tinguish the different forms of the adsorbed CO.

1.2.5 Electric and magnetic field probes:



Nuclear magnetic resonance (NMR) and electron spin resonance (ESR) have primarily been used for bulk analysis, one factor being the considerable number of atoms required to obtain a reasonable signal-to-noise ratio. A d.c. magnetic field is applied to the sample and a transmitted r.f. signal is analysed for absorption by the sample. The absorbed signal frequency corresponds to the frequency of magnetic resonance induced by the applied magnetic field on the nucleons or electrons. Gay and Fritz (44) studied the adsorption of butenes on silica and sodium exchanged silica by measuring the ^{13}C NMR chemical shifts. They deduced that neither the hydroxyl groups or the sodium ions were responsible for the observed chemical shifts of the adsorbed butenes. Freude, Muller and Schmiedel (45) have studied the NMR lineshapes of hydroxyl groups on Y-zeolites to obtain detailed information about the geometrical arrangements of the hydroxyl groups on the surface. Rooney and Pink (46) studied the adsorption of anthracene on a silica-alumina catalyst by ESR, the paramagnetic species being a positive radical ion formed by electron transfer at a Lewis acid site on the surface. The sensitivity for hydrocarbons is $\sim 10^{-9}$ mole, and they suggest the use of ESR to directly determine the number of active sites on a surface by measuring the radical concentration. Miller and Haneman (47) used ESR to study the adsorption of oxygen on low surface area GaAs and AlSb. They found O_2^- ions to be adsorbed on the surface.

Work function measurements can be made in a variety of ways, the best known method is that in which a vibrating condenser is employed (Kelvin probe). To study ad-

sorption on a surface (working electrode), the reference electrode must be made passive as regards adsorption. The variations of work function observed during adsorption indicate the changes in the distribution of electrons in the neighbourhood of the surface which arise from the adsorption.

Field emission microscopy (FEM) and field ion microscopy (FIM) are perhaps the most precise surface analysis techniques available. The sample is usually a relatively refractory metal with a very small radius tip and is placed on the central axis of a hemispherical fluorescent screen. In FEM a very high electric field ($> 10^6 \text{ Vmm}^{-1}$) is applied to the tip and the emitted electrons produce a very enlarged image on the screen, with a resolving power of $\sim 2\text{nm}$. As the work function of the electrons vary as a function of the crystallographic orientation of the metal, the image obtained on the screen is directly linked to the symmetry of the crystal surface. The adsorption of a gas on the surface is accompanied by a change in work function and is shown up directly on the fluorescent screen. The adsorption of hydrogen on tungsten has been thoroughly investigated and the heats of adsorption on the main planes measured.

FIM uses the same arrangement as FEM but the potential is reversed and $\sim 10^{-4}\text{Torr}$ of helium introduced into the vacuum chamber. Under the effect of the intense field the helium ionises, and the helium ions form an image on the screen as in FEM. A resolution of 0.2nm can be obtained making it possible to identify individual atoms on the surface. Desorbed ions selected from a small area of the image are mass analysed in a time-of-flight atom probe (TOF). FIM has been used to study the interaction of hydrogen with metals, and TOF has been used to identify the hydride ions BeH^+ , NiH^+ and FeH^+ (48) which were formed. Nitrogen which is supposed to be only molecularly adsorbed on a noble metal such as Rh is found to form N_2^+ , N^+ and some RhN^+ ions by FIM.

A relatively new technique is inelastic electron

tunneling spectroscopy (IETS) which allows the molecular structure of an adsorbate to be determined in a similar manner to that used in IR and Raman spectroscopy. The substrate preparation is not easy as it needs to be in the form of a metal-oxide-metal tunneling junction sandwich with an oxide thickness of $\sim 2.5\text{nm}$. After introducing the adsorbate and with one metal in the superconducting state (otherwise thermal contributions cause line width broadening up to 300 cm^{-1}), a bias potential is applied across the two metal electrodes and electrons tunnel through the junction and can undergo inelastic collisions with the adsorbate and raise it to allowed vibrational states. A plot of current versus the applied potential shows steps where the inelastic collisions occur, and cover a spectral range of 300 to 4000 cm^{-1} . Lewis, Moseman and Weinberg (49) have used IETS to study acetic acid adsorbed on alumina and they could detect acetic acid down to 0.03 monolayer, indicating the high sensitivity of the technique.

1.2.6 Other techniques and Raman spectroscopy:

The adsorption-desorption isotherm of a gas or vapour on a solid adsorbent can reveal much of the physical nature of the solid. Adsorption can occur in two forms: physisorption or chemisorption. Physisorption is due to a weak interaction between the adsorbate and the surface. The bonds involved are analogous to those existing in liquids where van der Waal's forces are involved. The energies associated with these bonds are low, generally $< 20\text{ kJ mole}^{-1}$, and multimolecular layers are possible. Chemisorption is attributable to the adsorbate being co-ordinated to the surface by a transfer of electrons, and can only form a monolayer though it may be covered with physisorbed layers. There are a variety of isotherm models, the best known are those of Brunauer, Emmett and Teller (BET) (50) which covers multimolecular physical adsorption, and Langmuir which covers physical and chemical adsorption. The surface area of the adsorbent may

be calculated from the monolayer capacity (derived from the isotherm) and a knowledge of the cross-sectional area of the adsorbate. Non-specific physisorption is required to determine the total surface area, and nitrogen is the most commonly used although other gases such as helium, argon and krypton are also used. The heat of adsorption may be determined from a set of isotherms at different temperatures.

Gas chromatography (GC) is mainly used for product analysis but has been applied to determine isotherms and heats of adsorption. Surface area determinations carried out using GC have not been in agreement with those obtained by the BET method (51), and the experiment must be carried out at a high temperature to prevent sorption of the carrier gas.

Calorimetry provides the heat of adsorption directly and is a very useful complementary technique. Differential scanning calorimetry (DSC) provides additional information eg. the energy distribution of acid sites on the surface (52). Glass and Ross (7, 8) have extensively investigated the adsorption of sulphur dioxide on aluminas, magnesias and transition metal catalysts by calorimetry.

Raman spectroscopy was first applied to surfaces in 1962 by Karagcunis and Issa (53) who reported the spectra of aromatic and olefinic hydrocarbons adsorbed on silica and porous glass. The molecular vibrations of the adsorbate can be used to reveal a part of the nature of the surface. The single biggest problem is sensitivity, but this has been partially offset by the high density monochromatic source available from a laser. Recently (54) it has been shown possible to detect pyridine adsorbed on γ -alumina down to 0.03 monolayer. Raman has advantages over many of the other surface techniques in that atomically clean surfaces and UHV conditions are not required. Raman spectroscopy has the appearance of continually growing in importance as regards its application to surface analysis, particularly with the great improvements in

performance available with the advent of multiplex spectrometers.

1.3 Vibrational spectroscopy

If a molecule were observed in free space it would appear to be carrying out random motions, actually a combination of vibrations, rotations and translations. Since every atom has three degrees of freedom a molecule of n atoms has $3n$ degrees of freedom of which 3 are translational and 3 are rotational (2 for a linear molecule). The total number of modes of vibration for the molecule are $3n - 6$ for a non-linear molecule and $3n - 5$ for a linear molecule.

All molecules at all temperatures including even absolute zero are continually executing vibrational motions ie. motions in which the distances between atoms and the internal angles of the molecule change periodically without producing any net translation of the centre of mass or imparting any net angular momentum to the molecule. Observing from the centre of gravity of the molecule, only the internal vibrations will be observed and a close inspection and proper analysis of these vibrations reveals a basic regularity and simplicity. These seemingly aperiodic internal motions of the molecule are the result of the superposition of the relatively simple $3n - 6$ (or $3n - 5$ for a linear molecule) normal modes of vibration. These vibrational motions can not take up just any amount of energy as the vibrational energy is quantized and has very specific energy levels. The positions of these energy levels may be obtained from the vibrational spectrum which is most conveniently studied using infrared and Raman spectroscopy. The rule of mutual exclusion applies to molecules with a centre of symmetry ie. any infrared active vibration is not Raman active and vice versa. Molecules of low symmetry can have many common infrared and Raman vibrations.

1.3.1 Infrared spectroscopy:

A necessary condition for absorbtion or emission of infrared radiation to occur is that the dipole moment (μ) of the molecule should change periodically with the vibration, i.e. $\frac{d\mu}{dq} \neq 0$, where q is the vibrational coordinate. The absorbtion of infrared radiation is a resonance effect and an infrared active vibration will only be excited by a photon with the same energy as the energy spacing between the relevant vibrational levels ie. no other but the correct wavelength radiation will excite the vibration. When recording an IR spectrum the percentage transmission is monitored. The relationship between the incident intensity (I_0) and the transmitted intensity (I) is given by the Beer-Lambert law:

$$\frac{I}{I_0} = e^{-\varepsilon cl}$$

Where ε = extinction coefficient
 c = concentration of absorbing species
 l = pathlength of absorbing species

Infrared grating spectrometers cover the range 4000 - 250 cm^{-1} , the region below 250 cm^{-1} is known as the far infrared (FIR) and requires a separate special spectrometer.

The concept of group frequencies has greatly simplified analytical IR spectroscopy. Every functional group has a characteristic frequency ie. when the functional group is changed to a different environment or placed in another molecule, the frequency of the vibration does not change very much eg. the $\text{C} = \text{O}$ group frequency is nearly always found in the region 1700 - 2200 cm^{-1} , and is easily characterised. Fingerprinting is often useful in identifying unknown compounds, since each compound has its own unique spectrum. The unknown spectra is compared with reference spectra of known compounds until a match is obtained.

Some examples of the many systems of adsorbed species studied by IR are given in Table 1.1

Table 1.1

Adsorbate	Adsorbent	Reference
Ammonia	Silica, Silica-alumina	55, 37
Pyridine	Alumina, Silica, Silica-alumina	38, 56, 37
Acetone	Magnesium oxide	57
Trimethylamine	Silica	56
Diisopropylketone	Alumina	58
Hydrogen chloride	Silica, alumina	59
Hydrogen sulphide	Alumina	60
Sulphur dioxide	Alumina	60
Carbon monoxide	Zinc oxide, Alumina	61, 62
Acetylene	Alumina	63
Water	Silica	55

1.3.2 The Raman effect

The Raman effect was predicted theoretically by Smekal (65) in 1923 and discovered by Raman (64) in 1927 after whom the phenomenon is named.

Classical theory describes most of the Raman effects adequately. When a sample is exposed to monochromatic radiation of frequency ν_0 (usually in the visible between 400 and 700 nm and $\nu_0 \gg \nu_{\text{vib}}$) with an associated electric field E , an oscillating dipole is induced in the sample with a dipole moment M , and

α is the polarizability which may be thought of as proportional to the volume of the electron orbitals relative to the nuclei as they move under the influence of

the applied electric field. α may be expanded in terms of the vibrational coordinate q .

where α_0 is the equilibrium polarizability. The vibrational coordinate q is a function of the vibrational frequency ν_{vib} and time, t .

The electric field of the monochromatic radiation oscillates with a frequency ν_0

Combining equations (1), (2), (3) and (4) we obtain an expression for the induced dipole moment.

$$M = \alpha_0 E_0 \cos(2\pi v_0 t) + q_0 E_0 \left(\frac{d\alpha}{dq}\right) \cos(2\pi v_0 t) \cdot \cos(2\pi v_{\text{vib}} t)$$

expanding the second term we obtain:

ie. we expect to see scattered radiation at v_o , $v_o + v_{vib}$ and $v_o - v_{vib}$. The elastically scattered component (Rayleigh scatter) at v_o is normally $\sim 10^{-4}$ of the incident intensity I_o , although if the scatterer is turbid or reflecting the total scatter can be 10% of I_o . The scatter at $v_o + v_{vib}$ is the anti-Stokes Raman, and that at $v_o - v_{vib}$ is the Stokes Raman. Since $\alpha_o \gg q_o \left(\frac{d\alpha}{dq} \right)$, the Rayleigh scatter is much stronger than the Raman scatter. Generally the Raman scatter is $\sim 10^{-8}$ of I_o .

From equation (5) we see that the Raman scattered components are only active if $(\frac{d\alpha}{dq}) \neq 0$. CO_2 a linear triatomic molecule can be used to demonstrate Raman activity. The fundamental vibrational modes of CO_2 are represented in Fig. 1.1. A plot of polarizability (α) as a function of the vibrational coordinate (q) will show whether a vibration is Raman active or not. This is done for CO_2 in Fig. 1.2

The slope of the curves at the equilibrium position are all zero except for ν_1 , ie. $(\frac{d\alpha}{dq}) \neq 0$ for ν_1 , and hence only ν_1 is Raman active (as is found experimentally). ν_3 and ν_4 are identical except for the direction of the deformation and are therefore indistinguishable and are called degenerate modes. ν_2 , ν_3 and ν_4 all involve a change in dipole moment during vibration and are IR active. The vibrational modes of small and simple molecules can be inspected visually to see if there is a change in polarizability during vibration. For larger molecules, group theory is applied to the symmetry elements of the molecule to determine its Raman activity.

From equation (5) we expect the Stokes and anti-Stokes lines to be of equal intensity, but in practice the Stokes lines are stronger. This may be explained by considering the quantum properties of the Raman effect. The relative populations of the vibrational ground state and excited state determine the intensities.

$$\frac{I_{\text{STOKES}}}{I_{\text{ANTI-STOKES}}} = \frac{(v_0 - v_{\text{vib}})^4}{(v_0 + v_{\text{vib}})^4} \cdot \frac{\hbar v_{\text{vib}}}{R \cdot T} \dots \dots \dots \quad (6)$$

Fig 1.3 shows the possible Raman transitions of CO_2 , the molecular system is excited by incident radiation of frequency v_0 and produces a polarized state from which the molecule relaxes to either the same state (Rayleigh scattering) or to another state (Raman scattering). From equation (6) it is clear that as v_{vib} increases the ratio of Stokes to anti-Stokes increases, and so normally

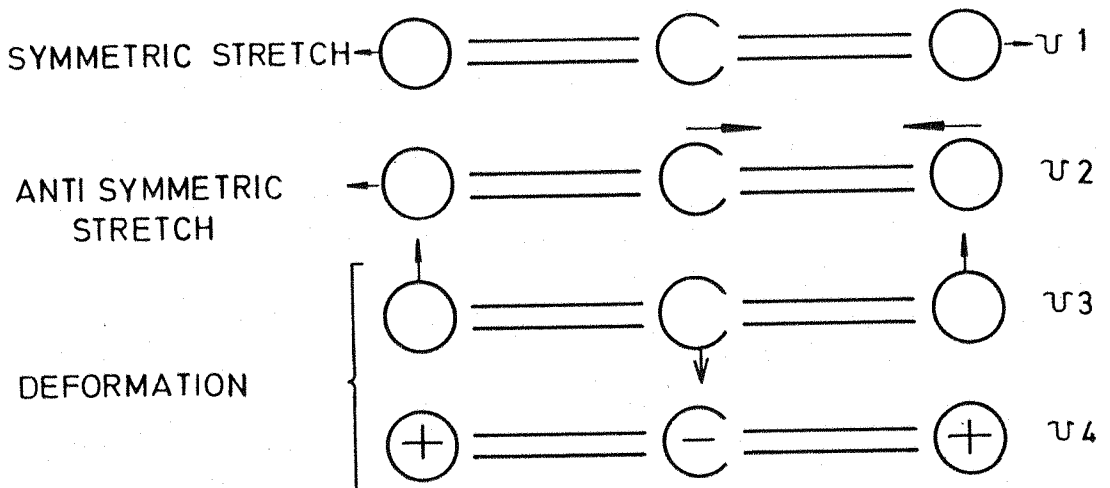
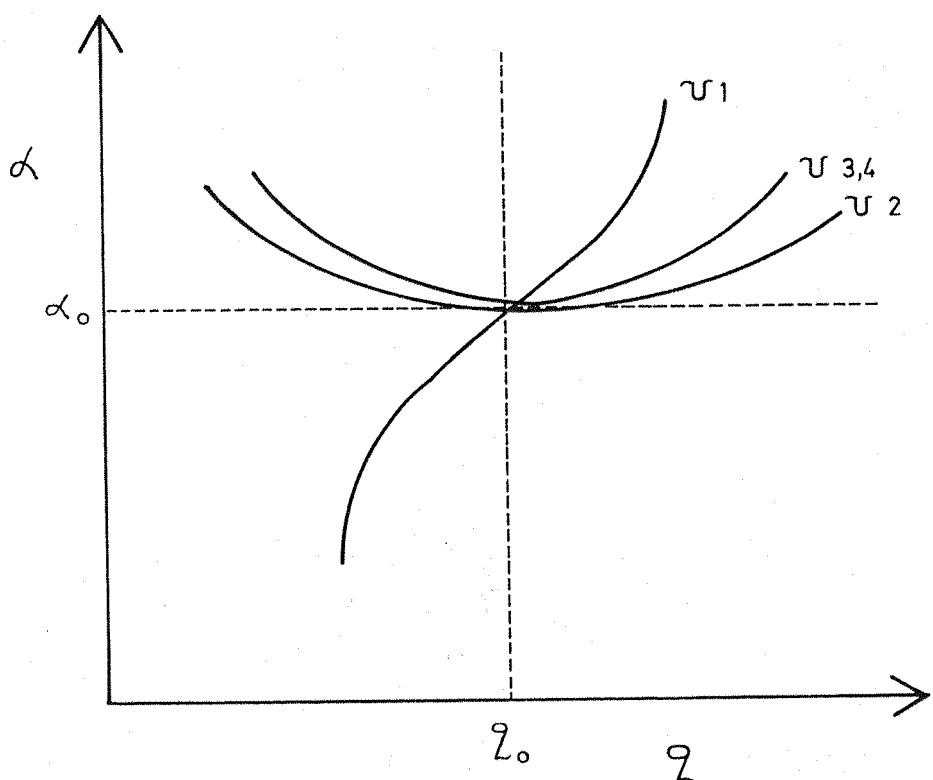


Fig. 1.1

FUNDAMENTAL VIBRATIONAL MODES OF CO_2 Fig. 1.2 POLARIZABILITY OF THE NORMAL MODES OF CO_2

the Stokes side of ν_0 is scanned for a Raman spectrum. The Raman spectrum is displayed as a frequency shift ($\Delta\nu$) from the exciting line ν_0 .

$$\Delta\nu = (\nu_0 - \nu)$$

Where ν is the absolute frequency of the emitted photon. The Raman intensity varies linearly with concentration in transparent or non-absorbing media.

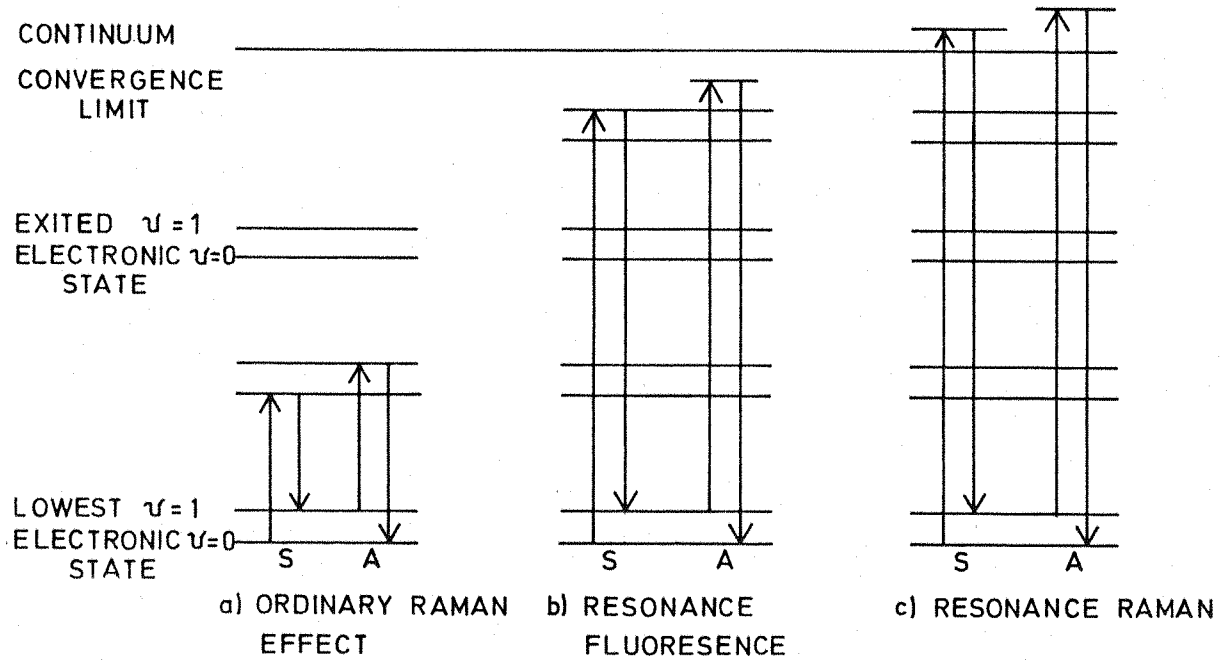
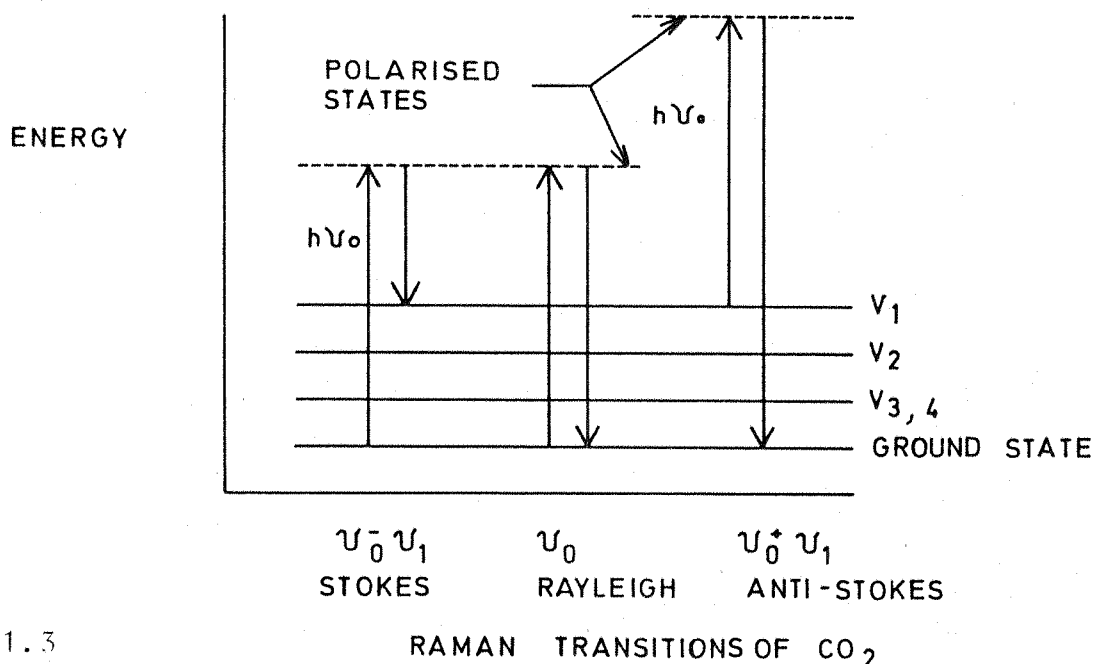
If plane polarized light is used as the source, the Rayleigh scatter at right angles to the source has a polarization close to that of the source. A fully symmetric Raman mode will behave similarly and for any lower symmetry the scattered light is scrambled. If a polarization filter is used to analyse the scattered light, the ratio of the intensities with the polarizer set crossed to the source to the polarizer set parallel to the source is defined as the depolarization ratio, p_s , and is given by

$$p_s = \frac{I_{\perp}}{I_{\parallel}}$$

A laser source with Brewster windows has an output that is almost 100% plane polarized and a totally symmetric mode has $p_s \approx 0$, for lower symmetry modes $p_s < 0.75$ and $p_s = 0.75$ for asymmetric modes.

Due to the natural weakness of Raman scattering, resonance enhancement effects are important. Enhancements of up to 10^5 are possible, making spectra easier to obtain and/or more dilute species detectable. The enhancement occurs when the exciting photon energy ($h\nu_0$) approaches or enters the region of electronic absorption of the molecule.

Fig. 1.4(a) shows the ordinary Raman effect, Fig. 1.4(b) shows the resonance fluorescence condition where excitation is to the convergence limit and Fig. 1.4(c) shows the resonance Raman effect where excitation is into the continuum, here the enhancement of the spectrum is



S = STOKES, A = ANTI-STOKES

Fig. 1.4 ENERGY LEVEL DIAGRAMS FOR RAMAN EFFECTS

strongly dependant on the electronic absorbtion coefficient at the incident source frequency. The effect is used to its greatest advantage by using a tuneable dye laser and tuning it to a frequency which has the maximum electronic absorbtion in the continuum. One of the problems associated with using resonance enhancement is that for each sample the correct excitation frequency must be found before any spectra can be recorded.

1.3.3 Comparison of Infrared and Raman spectroscopy at surfaces.

Since IR spectroscopy was first applied to surfaces it had gained a strong foothold before Raman spectroscopy gained sufficient sensitivity to detect the small quantities of adsorbate present. The development of the laser has greatly increased the sensitivity of Raman spectroscopy. Raman and IR generally complement one another, but it is possible to use the vibrational information from either technique to monitor the processes occurring at the surface. Raman and IR have many relative advantages and disadvantages when applied to surfaces, the most important of which are discussed below.

Raman scatter is very weak, $\sim 10^{-8}$ of the intensity of the incident source, compared to IR where the absorbtion or transmission of the molecules is measured directly. This basic lack of intensity is the main drawback of Raman spectroscopy and optimum experimental conditions must be used. The spectrometer should have a high efficiency collection optics system and a high discrimination against stray light as reflected light from a solid surface at ν_0 is added to the Rayleigh scatter. A high dispersion is also preferable to allow relatively large slit widths to be used to obtain a high throughput.

Vibrational bands extend out to 4000 cm^{-1} and Raman spectroscopy can easily scan the range from $< 50 \text{ cm}^{-1}$ to 4000 cm^{-1} provided a photomultiplier is used which

covers the range of frequencies. IR spectrometers cover the range from 4000 to 250 cm^{-1} and from 250 to $< 50\text{ cm}^{-1}$ a separate FIR spectrometer is needed.

The adsorbents used are mainly oxides (preferably with a high surface area). Generally they are not transparent to infrared below 1200 cm^{-1} , thus severely limiting the application of IR. Raman does not suffer greatly from interference from the adsorbent.

For IR the adsorbents need to be pressed into thin discs under high pressure to allow sufficient IR transmission. These discs are usually fragile and it is difficult to carry out other experiments (eg. isotherms) on the same sample. It has been found that there is a general decrease in surface area on pressing and water molecules in the interior of the disc become somewhat inaccessible. For Raman spectroscopy adsorbents may be used unpressed in powder or granular form. Water must be excluded as far as possible from an IR cell as it absorbs strongly, whereas water has a weak Raman spectrum and does not interfere. IR cells require windows of a suitable material such as KBr, NaCl or AgBr etc. and must be chemically stable to the adsorbates used. Raman cells may be made of glass or quartz as both have only a weak Raman spectrum and usually do not interfere. Samples may be activated *in situ* at temperatures up to 1200°C in quartz and isotherms carried out in the same sample cell.

Coloured samples present a problem in Raman spectroscopy as a large part of the incident beam can be absorbed causing localised heating. Since the scattered light originates from a finite depth element of the sample, some of the scattered light is also absorbed decreasing the intensity. Spinning cells have been used to decrease the heating effect and by using a different laser line which is less strongly absorbed by the sample. Red laser lines are popular for coloured samples as the energy carried by a red photon is intrinsically less than that of a green or blue photon. Excitation in the

red usually leads to a loss of intensity of the Raman signal as can be seen from equation (6) in section 1.3.2.

Photomultiplier tubes are generally less sensitive in the red than in the blue or green, although GaAs photomultiplier tubes are sensitive to 900 nm.

Fluorescence is a major problem in Raman spectroscopy as most oxides exhibit a fluorescence background. Even feeble fluorescence can swamp out Raman bands. The origin of this type of fluorescence is thought to involve transition metal impurities. The fluorescence normally takes on the form of a broad background and the intensity is very dependant on the temperature of activation of the sample. Several methods are available to reduce the fluorescence to a tolerable level, usually involving activation at high temperatures and/or the burning out of impurities with oxygen.

1.3.4 Survey of laser Raman spectroscopy at surfaces

Karagounis and Issa (53) were the first to apply Raman spectroscopy to the study of surfaces. They used mercury discharge lamps as the exciting source and the resulting spectra were of poor quality. With the development of the laser, Hendra and Loader (66, 67) were the first to apply this technique to surfaces using laser excitation. They investigated the adsorption of carbon tetrachloride, carbon disulphide, bromine, trans dichloroethylene and acetaldehyde on silica gel, and showed that there is little interference from the adsorbent. The acetaldehyde was shown to polymerise on the surface to form physisorbed paraldehyde. Their results aroused interest about other possible surface systems which may be studied using laser Raman spectroscopy.

Table 1.2 is a summary of some of the surface systems which have been investigated using laser Raman methods.

Table 1.2

Adsorbate	Adsorbent	Reference
Pyridine	Silica gel, Cab-O-Sil Porous Vycor glass, Aerosil, Silica-alumina, Titanium dioxide, magnesium oxide	68, 69, 70
Pyridine	NH_4^+ mordenite	70
Pyridine	η and γ alumina	69, 70, 72
Pyridine	Na Y zeolite	69
2-Chloropyridine	Silica gel	68
Piperidine	γ -alumina	72
Benzene	Porous Vycor glass	69, 71, 73
Benzene	Aerosil	74
Chlorobenzene	Porous Vycor glass	69
Carbon tetrachloride	Silica gel, Aerosil	75, 74
Bromine	Silica gel	75
Carbon disulphide	Silica gel	75
trans dichloroethylene	Silica gel, Aerosil	75, 74
Acetaldehyde	Silica gel	67
Acetonitrile	Silica gel, Aerosil	75
Acetonitrile	X, Y zeolites	76
Benzonitrile	Silica gel	75
trans stilbene	Cab-O-Sil	75
Styrene	Silica gel, Cab-O-Sil and Aerogel	77
Propylene	Porous Vycor glass	73
Propylene	A, X and Y zeolites	76
Ethylene	Porous Vycor glass	73
Carbon dioxide	X and Y zeolites	76

Adsorbate	Adsorbent	Reference
Acrolein	Y zeolite	76
Aniline	Porous glass	69
Benzylamine	Porous glass	69
tert-butyl cyanide	Aerosil	74
Oxygen	Nickel, tungsten	78

In order to characterise a surface it is necessary to have a suitable "tell-tale" molecule, ie. one which exhibits measurable changes in its spectrum on changing its environment. Pyridine is just such a molecule and has been widely used (68, 69, 70, 72). The pyridine ring breathing vibrations are sensitive to the environment, and the molecule can chemisorb on the surface by donating the lone pair of electrons on the nitrogen atom to a Lewis site on the surface to form a coordinate bond with the surface. A pyridinium ion can be formed by the abstraction of a proton from a Brönsted site, or a hydrogen bond to a surface hydroxyl group can form. Each type of adsorbed pyridine has a characteristic set of bands which enables the sites on the surface to be determined. Alumina, silica-alumina and titanium dioxide all show Lewis coordinated pyridine. Kagel (68) found that whereas pyridine is hydrogen bonded to a silica gel surface, 2-chloropyridine only physisorbs due to steric hinderance of the chloride ion preventing the hydrogen bond formation.

Egerton et. al. (69) found that while the Raman bands of benzene adsorbed on porous glass are close in position to those in the liquid, the 994 cm^{-1} ring breathing vibration decreases in intensity, this being consistent with a lowered polarizability of the ring electrons resulting from their interaction with surface hydroxyls. Loader (77) studied styrene adsorbed on different silicas, and found it to chemisorb on silica gel with the

appearance of two new lines in the carbon-carbon double bond stretching region, whereas Cab-O-Sil and Aerosil only showed physisorption. Angell (76) investigated the adsorption of acetonitrile, propylene and acrolein on a number of zeolites and found that only physisorption occurred. Linnett et. al. (78) have observed a series of sharp bands in the 40 to 60 cm^{-1} region on tungsten and nickel surfaces in air and in vacuum. The sharp bands disappeared on oxidising the surfaces, and the origin of the bands is thought to be from the lateral vibrations of adsorbed oxygen.

Chapter 2Instrumentation

A system for Raman spectroscopy consists basically of five parts:

- a) A high intensity source of monochromatic radiation (usually a laser)
- b) The sample area where the laser beam is focussed down onto the sample and the scattered light is collected and focussed onto the entrance slit of the spectrometer.
- c) The monochromators where the scattered light is dispersed into its component frequencies.
- d) A photon detector (photomultiplier tube) to detect the quantity of light being transmitted through the exit slit of the spectrometer.
- e) Electronic processing of the detected signal with analogue or digital output for recording or computer processing of the Raman signal.

A diagram of a Raman system is shown in Fig. 2.1

2.1 Illumination sources:

The ideal source is an intense, highly monochromatic beam of radiation in the visible region. It is necessary to maintain $\nu_0 >> \nu_{\text{vib}}$, and by choosing ν_0 in the visible spectrum enables glass optics to be used in the spectrometer.

The mercury discharge lamp was the most important source used for many years. This has many disadvantages compared with the laser as the output is not a collimated beam and large amounts of electric power are consumed to illuminate a large volume of sample. The sensitivity obtainable when using these lamps is low because they suffer from polychromaticity and a continuous "white" noise background away from the emission lines. The maximum resolution attainable is limited as each emission line consists of a multiplet of lines and each line is pressure broadened, as high pressure lamps are necessary to achieve a high output.

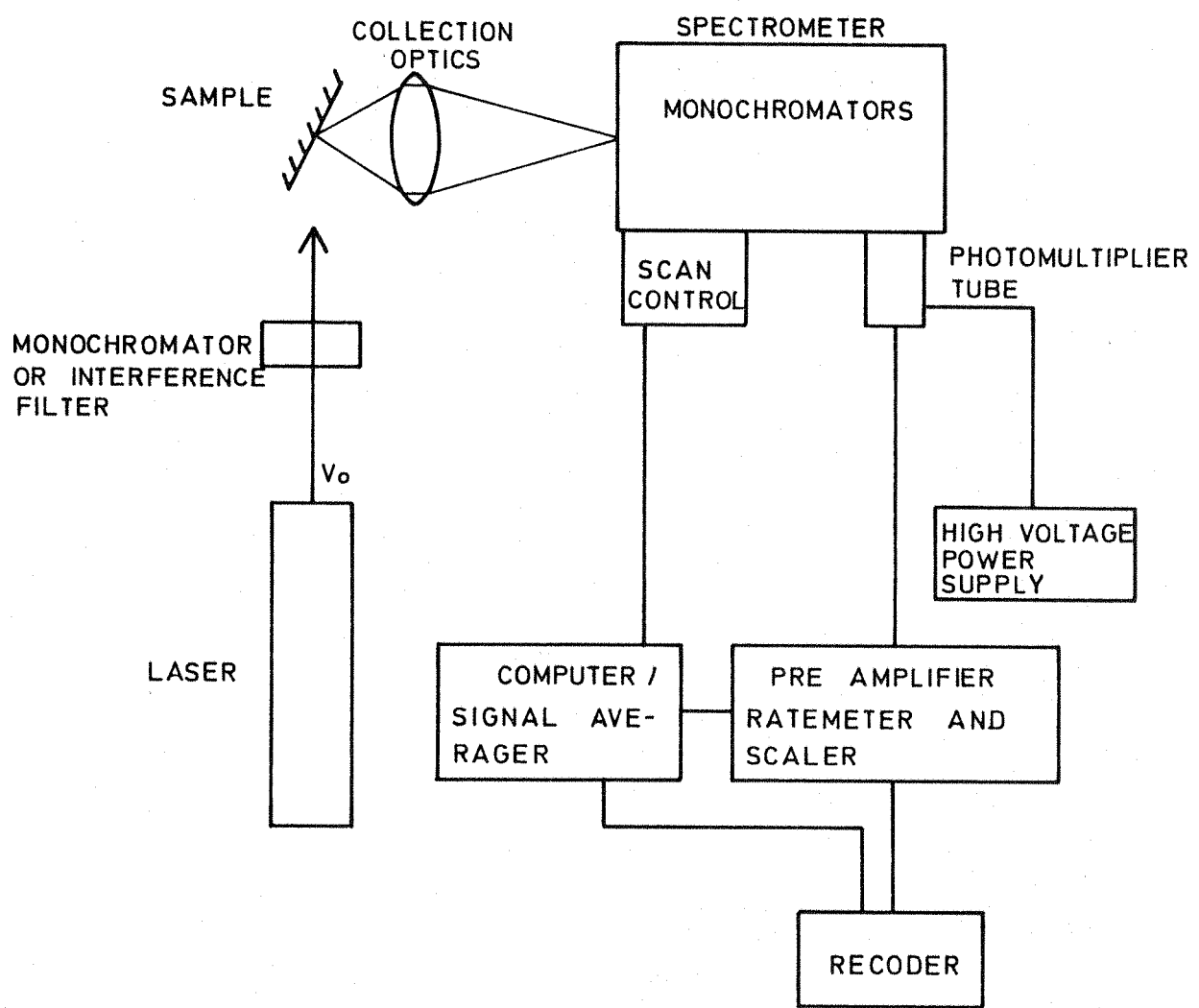


Fig. 2.1

RAMAN SPECTROSCOPY SYSTEM

With the development of the laser, Raman spectroscopy has become easier. The highly monochromatic, collimated output from a laser coupled with the high power densities that are available has revitalised Raman spectroscopy. Porto and Wood (79) showed that only 50 - 100 pulses from a ruby laser were necessary to obtain a spectrum, although of poor quality. Other solid state lasers such as Nd/glass or Nd/YAG can be run pulsed or CW but suffer from a broad emission output and need to be frequency doubled for Raman spectroscopy.

Gas lasers are far superior and offer many further advantages. Kogelnik and Porto (80) first used a He/Ne laser to demonstrate its feasibility for Raman spectroscopy. The gas lasers are CW output and apart from the normal illumination of a sample, transparent samples may be used intra-cavity, greatly increasing the intensity of excitation. The principal lasers used for Raman spectroscopy are the Ar^+ , Kr^+ , Ar^+/Kr^+ , He/Ne and He/Cd. The Ar^+ laser is the most popular choice as it has the highest available output power although the output bandwidth is typically 0.25 cm^{-1} compared with 0.05 cm^{-1} for the He/Ne laser. The Ar^+ output bandwidth may be reduced by using a suitable etalon intra-cavity resulting in a loss of output power. The characteristics of some commercially available lasers are compared in Table 2.1.

Table 2.1

Type	Output Wavelength nm.	Colour	Maximum output Power mW
Ar^+	632.8	red	70
	514.5	green	7500
	488.0	blue	6500
	476.5	blue	2700
	496.5	blue	2500
	501.7	green/blue	1500
Kr^+	647.1	red	500
	568.2	yellow	200
Ar^+/Kr^+	647.1	red	200
	514.5	green	200
	488.0	blue	200

Only the strongest outputs are shown in Table 2.1, many other lines of lower output powers are also available. The Ar^+ laser is the most common source for Raman spectroscopy as the blue and green lines which are the most powerful fall in the region of peak photomultiplier sensitivity. The intensity of a Raman band is dependant amongst other things on the exciting frequency used, known as the fourth power Raman intensity law:

$$I_{\text{Raman}} \propto (v_o - v_{\text{VIB}})^4$$

Where $(v_o - v_{\text{VIB}})$ is the frequency of the Stokes line. This effect results in Raman signals being 2.8 times larger per unit power when using the 488.0 nm line compared to the 632.8 nm line.

When a laser beam is incident upon a sample, some absorbtion occurs causing local heating. In many instances this heating effect can be serious, leading to decomposition of the sample. Therefore it is preferable to use a laser line which coincides with a minimum of absorbtion of the sample. Most samples can be catered for by using an Ar^+/Kr^+ laser which has lines from red through to blue, or separate Ar^+ and Kr^+ lasers which are capable of higher outputs. Alternatively a dye laser may be used and can be tuned over a range of frequencies, depending on what dye is used. Dye lasers are usually pumped from an Ar^+ laser and the output is on the low frequency side of the Ar^+ line used. Dye lasers have a high background away from the exciting line, but this may be overcome by using a suitable premonochromator.

Filters are available for the main laser lines. These are etalons with a combined blocking filter to the longer wavelength side, and have a maximum transmission of 50% and an output bandwidth of 1nm. Filters cannot be used for anti-stokes Raman spectroscopy as they allow through background and "plasma lines" on the shorter wavelength side of the exciting frequency. A prism premonochromator has the advantage of having a throughput of up to 85% and

an output bandwidth of 0.4 nm.

2.2 Sample area:

The imaginary image of the entrance slit at the sample is usually demagnified six to seven times by the collection optics. This requires that the laser beam be focussed down to a suitably small cross section to effectively illuminate the sample area or volume that is being seen by the spectrometer. The intensity of the beam at the focus is dependant on the power of the laser beam, the diameter of the beam and the focal length of the lens used to focus the beam down to match the imaginary image of the slit. Barrett and Adams (81) have shown that according to confocal theory the volume most effectively illuminated in a Raman sample is a cylinder of length b and radius W_0 when the sample is transparent.

$$\text{where } b = \frac{8\lambda f^2}{\pi d^2}$$

$$\text{and } W_0 = \frac{2\lambda f}{\pi d}$$

λ is the exciting wavelength, f the focal length of the lens and d the beam diameter. Fig. 2.2 depicts the geometry of the focal region.

Using typical values: A 10 cm focal length lens, a 2 mm diameter beam of 100 mW at 514.5 nm. The beam radius at the focus is 16.4 μm and the beam cross section is 0.0008 mm^2 . At the focus the power density is 12 kW cm^{-2} . Using a 6:1 demagnification of the slits, a slit width of 0.2 mm is needed to match the size of the focussed beam.

Three methods of sample illumination have been used, namely 0° , 90° and 180° illumination. The geometrical arrangements are shown in Fig. 2.3.

The most commonly used method is 90° illumination as it is the simplest and the most versatile as it is applicable to gas, liquid and solid samples. This method allows the depolarization ratio of the Raman bands to be

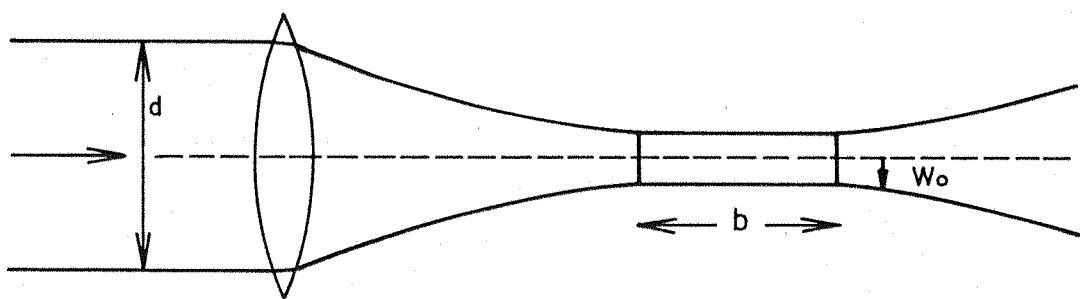
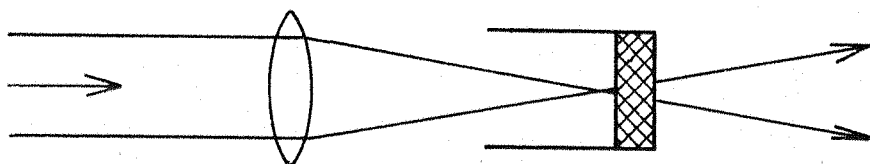
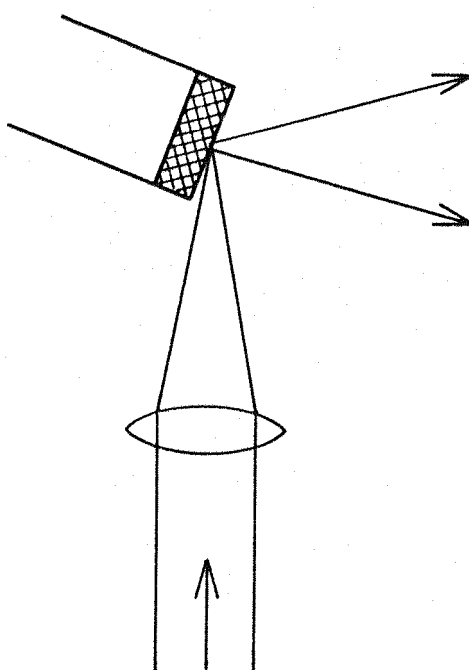


Fig. 2.2

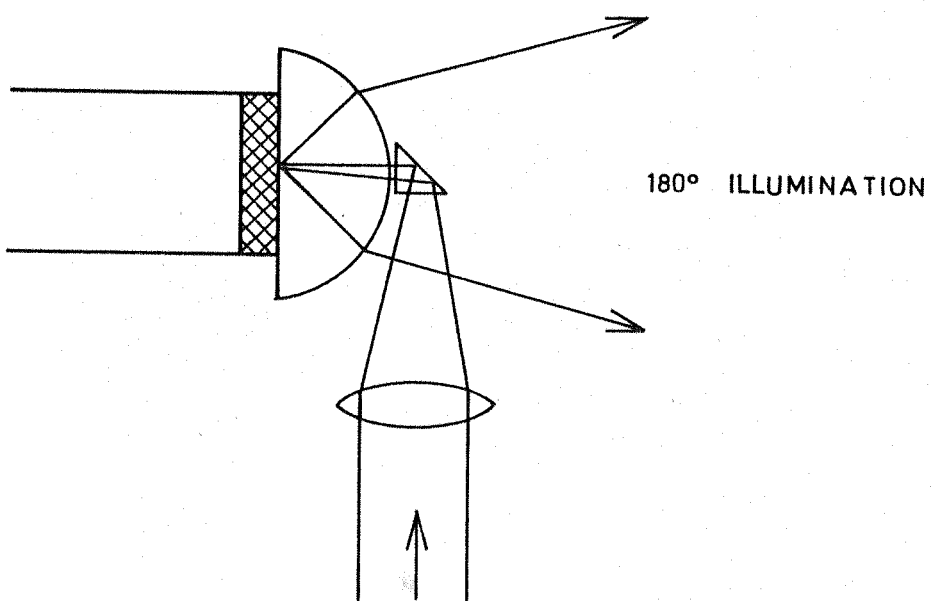
THE LASER FOCUS



0° ILLUMINATION



90° ILLUMINATION



180° ILLUMINATION

Fig. 2.3

SAMPLE ILLUMINATION

determined. The 0° method can only be applied to transparent samples and is not used much. The 180° method has many more optical surfaces and the prism blocks off a part of the scattered light.

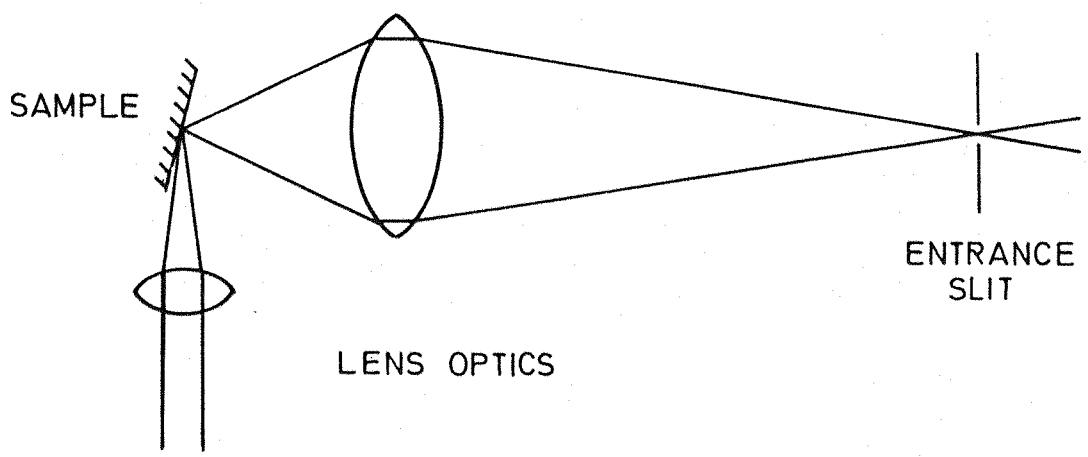
The collection optics of a Raman system focus the scattered light onto the entrance slit of the spectrometer, and since the Raman effect is so weak it is essential to collect as much scattered light as possible as efficiently as possible. Normally a lens is used to couple the collected cone of light to the spectrometer. Cassegrain mirror optics are now commercially available for Raman spectrometers. Since the diameter of the mirror is very much larger than the lens of the lens collection optics, the Cassegrain can collect a larger solid angle cone of scattered light. The geometries of the available collection optics is shown in Fig. 2.4

2.3 Monochromators:

The monochromator separates the weak Raman bands from each other and from the very much more intense Rayleigh scatter and reflected light. The light throughput of a triple monochromator when illuminated with a monochromatic source is typically 10%.

Some terms associated with monochromators are discussed below:

- Resolution: This is defined as the full width of the band at half the maximum intensity (FWHM). The limiting resolution of the spectrometer is the FWHM of an infinitely narrow source, when closing the slits further does not affect the sharpness of the band. In the study of surfaces the adsorbed species usually have very weak signals. Decreasing the resolution (opening the slits) greatly increases the throughput and the signal strength, and since bands due to adsorbed species are usually broad, acceptable results are obtained with 4 cm^{-1} slit widths.
- Discrimination: This is the ability of the monochromator to reject stray light. Real monochromators are less than ideal due to reflections from the gratings



LASER BEAM

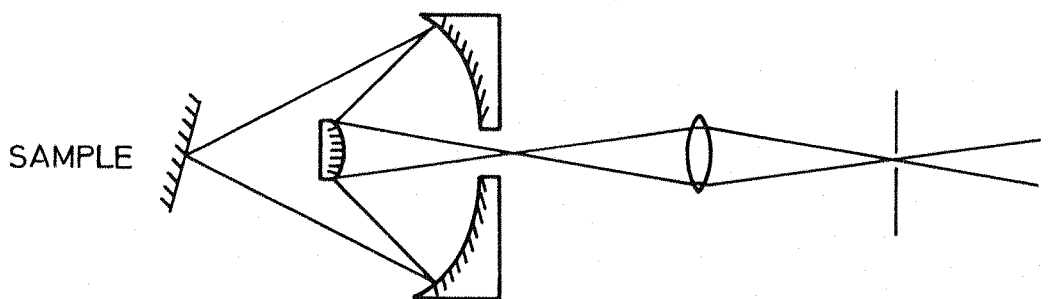


Fig. 2.4

CASSEGRAIN MIRROR OPTICS

COLLECTION OPTICS SYSTEMS

which arise from imperfections in the ruling of the gratings, and stray reflections. Fig. 2.5 shows the ratio of grating scatter to Rayleigh scatter for single, double and triple monochromators.

From Fig. 2.5 it can be seen that a triple monochromator is preferable as it has a higher discrimination, but usually has a lower light throughput than a single or double monochromator.

c) Dispersion: This is the extent that the spectrum has been dispersed at the exit slit of the spectrometer and is expressed as cm^{-1} (wavenumbers) per mm of exit slit width. The dispersion increases with decreasing the frequency, but the increase is usually small (of the order of 1 cm^{-1} per mm slit width in a scan of 2000 cm^{-1}).

d) Spectral bandpass: This is a function of the dispersion and the slit widths, and is the width of spectrum that is transmitted to the detector at any one time. For Raman work a wide spectral band pass is needed to allow more light to the detector to increase the signal-to-noise ratio. This in turn allows a larger volume or area of sample to be illuminated at a lower power density which is especially useful for surface studies.

Of the various types of monochromator mountings available, the Czerny-Turner variant is the one most commonly used as it is the most flexible and has the entrance and exit slits in line at opposite sides of the grating. The aperture of the monochromators are typically f/7 using 500 - 1000 mm focal length. The gratings used are blazed for maximum reflection in the visible spectrum (usually at 500 nm.)

The output from the gratings is curved at the plane of the exit slit. This limits the length of straight slits that may be used without impairing the resolution too ($0.02 \times$ focal length). It is advantageous to use the longest slits possible to get the best light throughput. The Cary 82 spectrometer uses curved slits and the Coderg T800 with an 800 mm focal length uses 20 mm straight

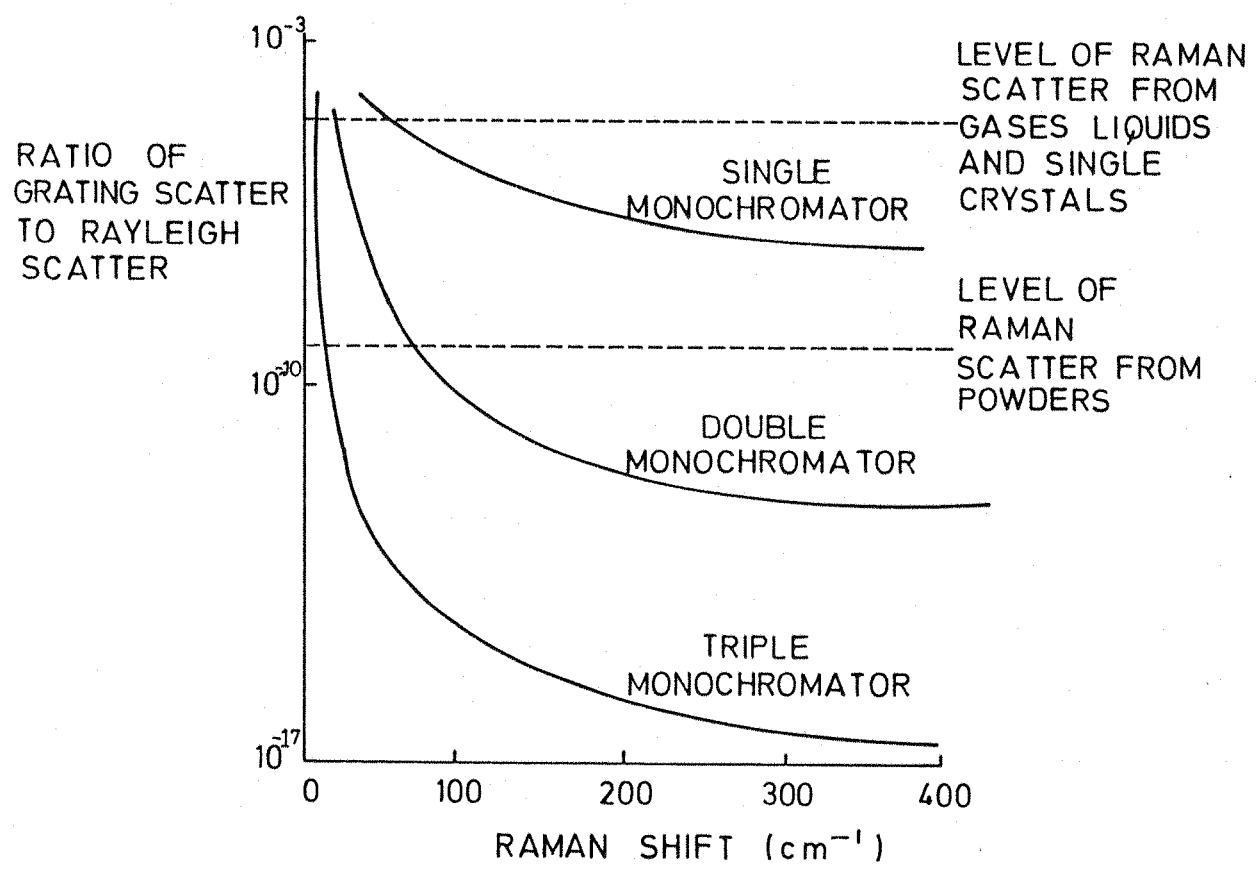


Fig. 2.5

MONOCHROMATOR DISCRIMINATION

slits, curved slits being unnecessary with the long focal length.

Planar holographic gratings have been used to reduce stray light but have a slightly lower throughput compared to ruled gratings.

2.4 Detectors:

The spectrometer disperses light from a source and focusses a small spectral range onto a detector. Since the intensity of the light in this spectral interval is usually very small, the general requirements for a detector are:

- a) A high sensitivity, and preferably constant throughout the visible spectrum to enable the use of different lasers.
- b) A high quantum efficiency conversion of photons into electron pulses.
- c) A low noise level, especially a low dark current, i.e. the noise in the absence of any light falling on the detector.
- d) The response should be linearly proportional to the light input so that accurate photometric measurements can be made.

Photomultiplier tubes satisfy most of these conditions where the photon energy is large enough to free an electron completely from the sensitive cathode and is then avalanched across a series of dynodes until a detectable pulse is produced. Some of the most popular photomultiplier tubes for Raman spectroscopy are the EMI 6256S and 9558 and the RCA CA313034. The absolute sensitivity versus wavelength for these three types are shown in Fig. 2.6.

Of the three types shown, the GaAs photocathode is preferable as it has a response which is nearly constant from 350 to 850 nm and is extremely useful when using the He/Ne and Kr⁺ red lasers.

Photomultiplier tubes are usually cooled to reduce the dark current to an acceptable level, although cooling be-

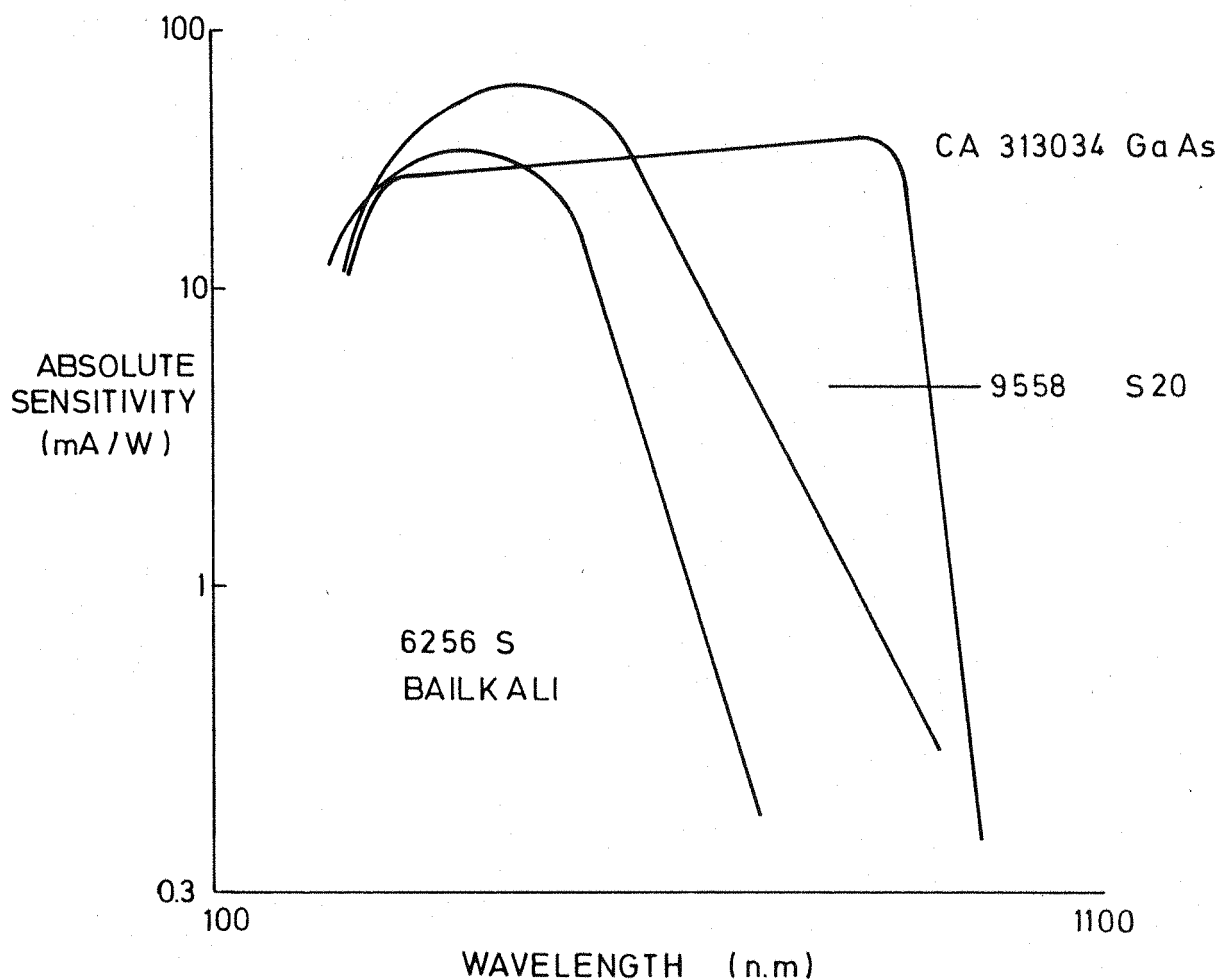


Fig. 2.6.

PHOTOMULTIPLIER RESPONSE

low -20°C has little effect on the dark current but reduces the signal and hence the signal-to-noise ratio. The noise and dark current need to be low as this limits the sensitivity. The 6256S tube has a small bialkali photocathode and an inherently low noise level and needs no cooling to achieve a dark current of < 100 counts per second. The dark current may be reduced by using magnetic defocussing. By placing a circular permanent magnet over the photocathode the effective area of sensitive surface to thermal electrons is greatly reduced and they are deflected away.

2.5 Signal processing:

The signal from the photomultiplier tube is amplified to a level suitable for recording on a recorder and/or inputting to a computer. Three methods of processing are available:

- a) D.C. amplification
- b) Phase sensitive detection
- c) Pulse counting

D.C. amplification is the most convenient and easy to use method, has a high sensitivity except at low light levels where the noise component of the signal is large. This is due to the noise and signal being equally amplified, generally giving a low signal-to-noise ratio. In a system using phase sensitive detection the light beam is chopped, the signal a.c. amplified and phase sensitive detected. The sensitivity is only half that of D.C. amplification but the signal-to-noise ratio is much improved. Additional mechanical components are required to chop the light beam.

Pulse counting or photon rate detection (often inaccurately called photon counting) has been shown to be more sensitive than phase sensitive detection especially at low light levels (82). Each photoelectron pulse arriving at the anode of the photomultiplier is passed through a wide band pre-amplifier then discriminated from low energy noise pulses and high energy pulses due to

cosmic radiation. The signal is then passed through a ratemeter or the pulses counted for preset measurement cycle times. Often the discriminator threshold level is used at too high a setting to reduce the noise level. James (83) has shown that this is incorrect since the information rate is greater at a lower threshold level, and the signal-to-noise ratio is also greater.

The Coderg T800 spectrometer is equipped with repetitive scanning camshafts to allow signal averaging to be carried out. This is useful where weak Raman bands are to be detected in the presence of noise. The true signal increases linearly with the number of scans, while the noise only increases as the square root of the number of scans, thus repetitive scanning results in a better signal-to-noise ratio than slow step scanning. In most cases the spectrum was scanned at least 64 times, giving at least an eight fold improvement in signal-to-noise ratio and lifting weak bands out of the noise.

2.6 The Coderg T800 Raman spectrometer:

The Coderg T800 Raman spectrometer has been used for this investigation. The spectrometer has a triple monochromator using additive dispersion. The symmetrical mount is used for the monochromators with the four slits lying on a common axis and the three gratings mounted on a common shaft. Fig. 2.7 shows the optical layout of the spectrometer.

Since all three gratings rotate on a common shaft this mounting arrangement has good tracking accuracy compared to other mountings. This mounting has less aberrations and a minimum of optical components compared to other mountings.

The gratings used are 90 x 90 mm, ruled at 1800 lines mm^{-1} and blazed at 500 nm for high efficiency. The monochromators are 800 mm focal length with a f/7 aperture. The scan range of the spectrometer is from 10 000 to 24 500 cm^{-1} (1000 to 408 nm) and is suitable for laser sources between 408 and 800 nm. The scan speed is

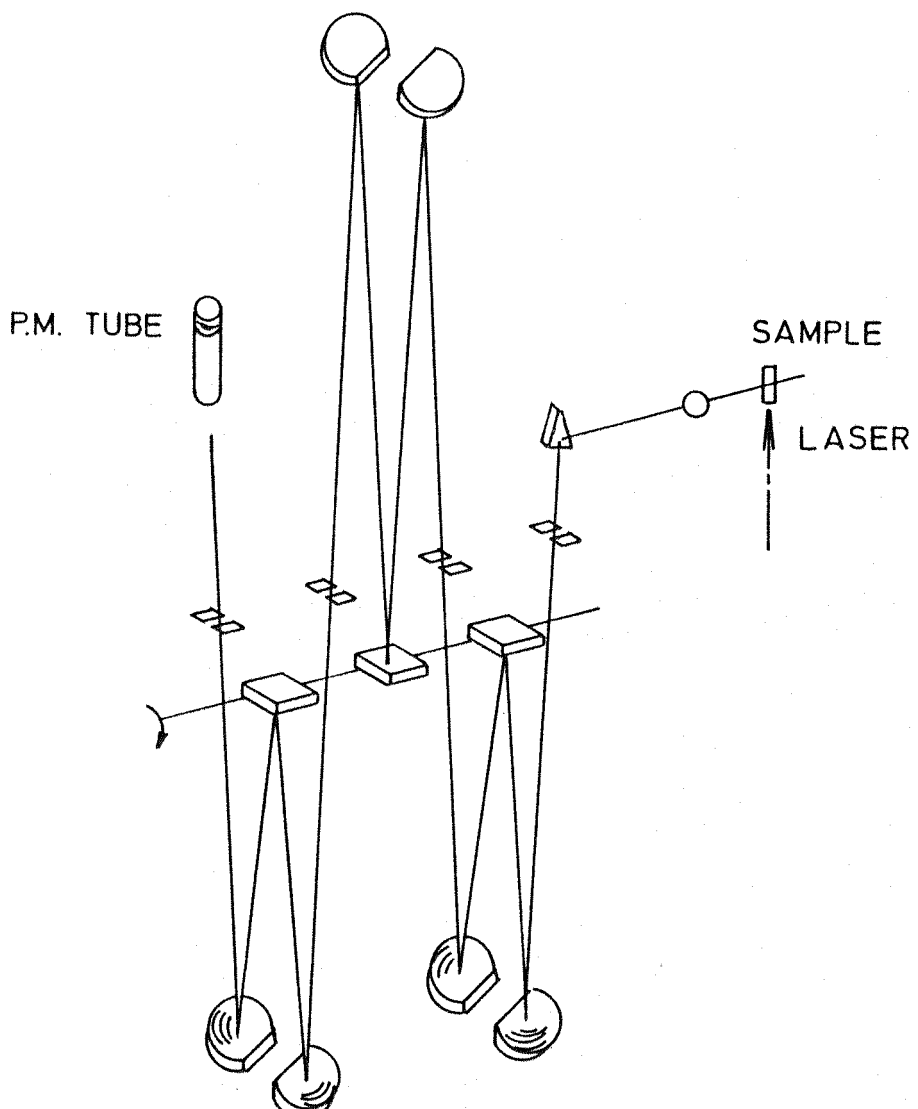


Fig. 2.7 CODERG T 800
 OPTICAL LAYOUT

variable from 1 to 2000 $\text{cm}^{-1} \text{min.}^{-1}$ in 15 steps. The maximum resolution of the spectrometer is 0.3 cm^{-1} at 514.5 nm with a completely filled aperture.

The slit height is 20 mm with straight jaws continuously variable from 0 to 2000 μm . 125 μm slits at 514.5 nm give a 1 cm^{-1} spectral bandpass. At high wave-number shifts the dispersion is increased but the effect is small, and usually ignored. 4 cm^{-1} slit widths were generally used for studying surfaces since the Raman bands of adsorbed species are generally broad.

Initially a f/2 reversed camera lens was used for the collection optics, but was later changed to a f/1.50 mm focal length lens. The demagnification of the slits was about 7 fold and the height of the slit image was 3 mm at the sample.

A Spectra-Physics model 170 Ar^+ laser was used. Technical Optics line filters with 30% transmission and a 1 nm bandwidth were used for the 514.5 and 488.0 nm lines, to remove unwanted laser and plasma lines. Normally between 20 and 150 mW of laser power was used at the sample, focussed down with a cylindrical lens to reduce the radiant flux density on the surface.

Two photomultiplier tubes were used during this investigation. An EMI 6256 S low noise bialkali tube with a peak response in the blue-green part of the spectrum. Beyond 1200 cm^{-1} using the 514.5 nm line the signal intensity drops off, but the useful range can be extended to 2500 cm^{-1} by using the 488.0 nm line. The other tube, an EMI 9558 is more sensitive in the red part of the spectrum and can be used beyond 4000 cm^{-1} with the 514.5 nm line, and can be used with the red lines from the He/Ne and Kr^+ lasers. The EMI 9558 photomultiplier tube requires thermoelectric cooling to -25°C and magnetic defocussing to reduce the dark current to < 100 counts per second.

The signal from the photomultiplier tube was detected with an Ortec-Brookdeal 5CI pulse counting system which incorporates a pre-amplifier, discriminator, rate-

meter and scaler. Measurement cycle times (MCT) of either 0.1 or 1s were normally used, with the availability of MCT from 10^{-6} to 10^5 s.

To obtain an accurate, non-distorted spectrum the spectral bandpass, scan speed and MCT should comply with the following equation:

$$T \leq \frac{15R}{S}$$

where T = MCT in seconds

R = spectral bandpass in cm^{-1}

S = scan speed in $\text{cm}^{-1}/\text{min.}$

Usually a suitable scan speed is selected to match a pre-set spectral bandpass and MCT.

The 5CI converts any 3 consecutive digits of its 8 digit readout into an analogue signal which was recorded on an Oxford Instruments strip chart recorder.

A Hi-Tek PA1 512 channel scaler was used to signal average the output from the 5CI with the spectrometer in the repetitive scanning mode. Repetitive scanning can cover a range of 50, 150 or 450 cm^{-1} from any starting frequency.

Chapter 3: Optimization of the illumination and collection optics.

3.1 Analysis of the illumination and collection optics:

Since Raman scattering is a weak effect and is often applied in spectroscopically unsatisfactory conditions, it is essential to optimize all experimental conditions to provide as large a signal as possible and maintain an optimum S/N ratio.

Benedek and Fritsch (84) have analysed the efficiency of the best illumination and collection geometries for a transparent medium, using a narrow monochromator entrance slit. Barrett and Adams (81) have analysed the illumination geometry for fluids using wide slits.

Schwiesow (85) investigated the problem more generally, covering both the wide and narrow slit cases for the illumination and study of fluids. Pilz (86) has more recently theoretically optimized the efficiency of illumination for a transparent medium, and arrived at results which lie inside the limits found by Schwiesow (85).

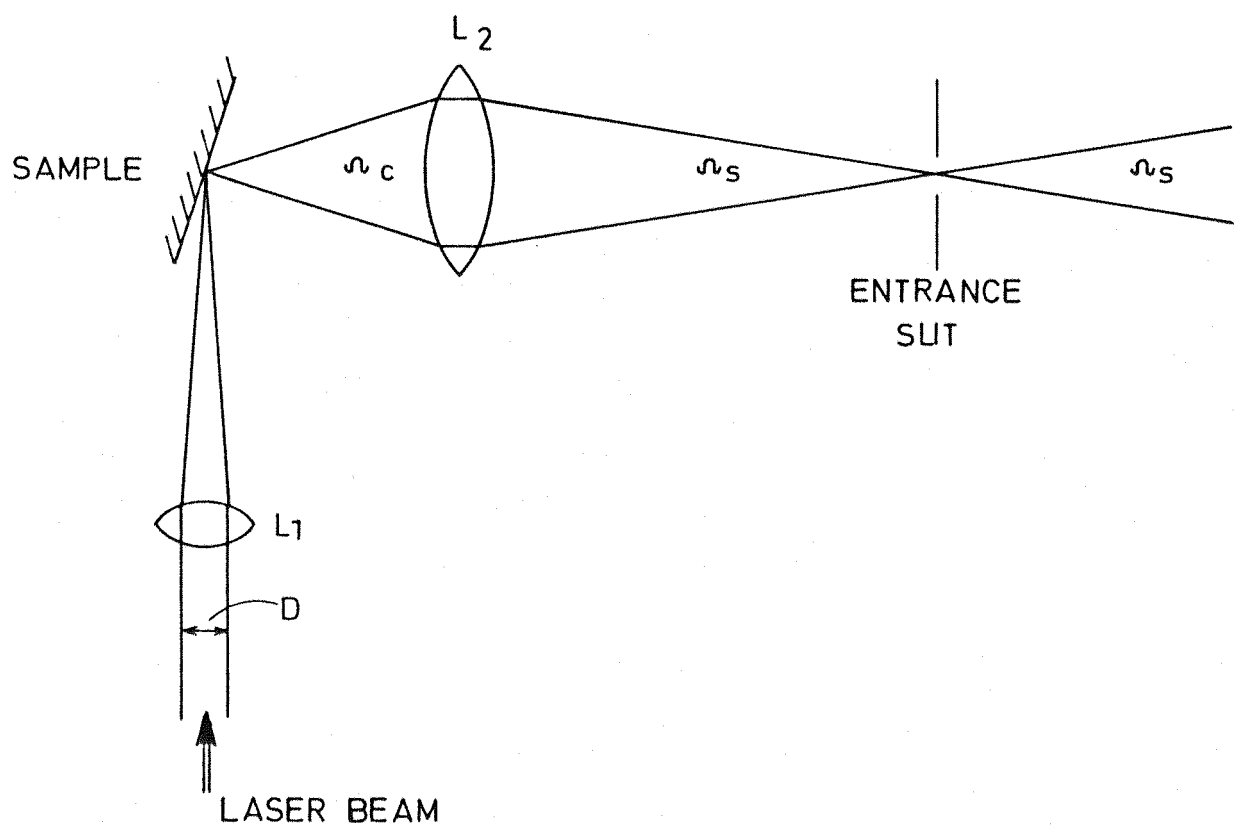
For the investigation of surfaces, the incident laser power density has to be limited to avoid decomposition of the sample, and this introduces a new dimension into the experimental problems.

The photon flux q , collected by the system may be described by:

$$q = \left(\frac{d\sigma}{d\Omega_c} \right) p_m n A \Omega_c$$

where $\left(\frac{d\sigma}{d\Omega_c} \right)$ is the differential scattering probability, p_m is the maximum illumination power density the sample can withstand without decomposing, n is the number density of the scatterers. A is the area on the surface viewed by the spectrometer and illuminated by the laser beam, whilst Ω_c is the solid angle cone of scattered radiation collected by lens L_2 in Fig. 3.1.

The analysis presented here is for a system where the brightness of illumination of the sample p_m is limited by the sample itself and not by the available laser



ILLUMINATION AND COLLECTION OPTICS

Fig. 3.1

power. The demagnification M of the slits at the sample is given by:

$$M = \sqrt{\frac{\Omega_C}{\Omega_S}} = \frac{w}{w_0} = \frac{h}{h_0}$$

where Ω_S is the solid angle of acceptance of the spectrometer (typically $f/7$ aperture). w , h and w_0 , h_0 are the deminsions of the slits and the slit image respectively.

Three cases are considered, where the laser is brought to a focussed spot, and the scattered light illuminating the entrance slit of the spectrometer (Fig. 3.2). These three cases are designated 1, 2 and 3 and correspond to areas I, II and III of Schwiesows (85) Fig. 1.

The photon flux collected for each case may be calculated and compared.

$$\text{Case 1: } q_1 = \left(\frac{d\sigma}{d\Omega_C}\right) p_m n \left[\frac{\pi d_1^2}{4}\right] M^2 \Omega_S$$

where $\left[\frac{\pi d_1^2}{4}\right]$ is the area of the slit image illuminated by the laser, and d_1 , the diameter of the spot illuminated by the laser is determined by D , F , and λ .

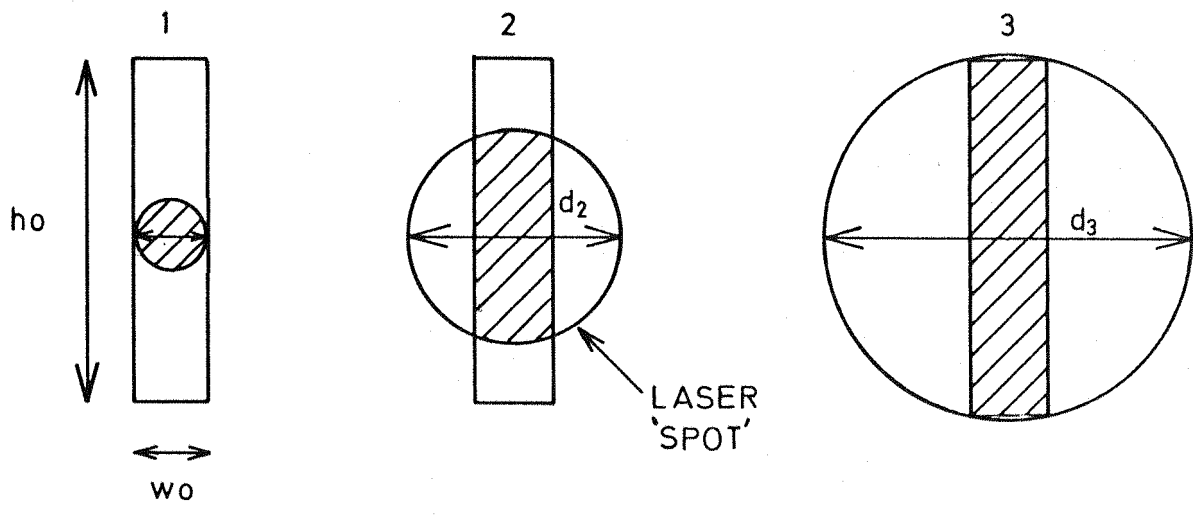
$$\begin{aligned} \text{Case 2: } q_2 &= \left(\frac{d\sigma}{d\Omega_C}\right) p_m n d_2 w_0 \Omega_C \\ &= \left(\frac{d\sigma}{d\Omega_C}\right) p_m n d_2 w M \Omega_S \end{aligned}$$

and

$$\begin{aligned} \text{Case 3: } q_3 &= \left(\frac{d\sigma}{d\Omega_C}\right) p_m n w_0 h_0 \Omega_C \\ &= \left(\frac{d\sigma}{d\Omega_C}\right) p_m n w h \Omega_S \end{aligned}$$

The optimum condition is found by comparing q_1 , q_2 and q_3 .

$$q_1/q_3 = \frac{\pi d_1^2 M^2}{4 w h} \quad \text{and since } d_1 < w_0$$



 AREA OF SAMPLE ILLUMINATED
AND VIEWED BY THE SPECTROMETER

Fig. 3.2

LASER FOCUS AT THE SLIT IMAGE
ON THE SURFACE

$$\text{and } w_0 = \frac{w}{M} \quad \therefore \quad \frac{q_1}{q_3} < \frac{\pi w}{4h}$$

for normal spectrometers $w/h < 1$

($w/h = 0.1$ maximum for the Coderg T800 Raman spectrometer).

$$\therefore \frac{q_1}{q_3} < 1 \text{ i.e. } q_3 > q_1$$

$$\text{and } \frac{q_2}{q_3} = \frac{d_2 M}{h} = \frac{d_2}{h_0} < 1 \quad \therefore q_3 > q_2$$

Thus the maximum q is obtained when the entrance slit of the monochromator is fully illuminated as in Fig. 3.2 [3]. Normal spot focussing of the laser is very wasteful if the above condition is to be met. The laser may be used more efficiently by using a cylindrical lens to focus it down, as it focusses the laser to a strip over the slit image and does not concentrate the heating effect on one spot on the sample but spreads it out over a strip. Barrett and Adams (81) and Schwiesow (85) have shown that for fluids, the optimum conditions are to collect a cone of scattered radiation of as large an angle as possible and then arrange appropriate demagnification between the scatterer and entrance slit. In contrast, from this analysis q_3 is independant of the geometry of the collection system as long as the slits are fully illuminated, implying that the optimum conditions are invariant in M . However there are at least four effects present in the system which may perturb this situation:

- 1) Reflection losses can be high at large off axis angles, hence large aperture collection will be relatively inefficient.
- 2) The Raman scattered radiation is collected from a volume element rather than just an area on the surface of the sample. Depending on the transparency of the sample, the depth of focus of the collection lens (which decreases for lower M) can be a factor which influences the optimum conditions. Both types of sample used (PTFE

Table 3.1

focal length cm	lens diameter cm	subject/lens distance cm	M	LSA cm
5	5	5.7	7.14	-1.8
10	5	14.6	2.18	-1.0

From Table 3.1, the 10cm focal length lens will have a sharper image as far as spherical abberation is concerned, but the lens is normally used at its position where the spherical abberation from all zones of the lens is a minimum, i.e. at the circle of least confusion.

b) Coma occurs for rays that come from object points that are off the lens axis. The amount of coma from a lens can be determined by the lateral length of the comatic flare. For the same two lenses in Table 3.1, the comatic flare of the 5 cm focal length lens is 0.18 cm, and only 0.06 cm for the 10 cm lens. Thus generally a shorter focal length lens will result in a lower definition image and less throughput through the total spectrometer.

c, d) Astigmatism and curvature of field affect points that are removed from the lens axis. They depend approximately on $\tan^2 \beta$ where β is the angle of obliquity of the chief ray and f the lens focal length. The effects are minimal in the collection optics as β is small, but the longer focal length lens (ie lower M) will have less astigmatism and curvature of field.

e) Distortion does not affect the definition of the image but affects the location of an image point in the image plane. The distortion is proportional to $\tan^3 \beta$, and there is effectively no distortion for a thin lens.

The amount of abberation for all five types is less for a longer focal length lens under the conditions that the apertures of the collection optics and the spectrometer are matched. If these apertures are not matched

inefficiencies will arise in the spectrometer.

From the above effects it may be concluded that there will be an optimum demagnification of the slits which is expected to be lower than that used in commercial spectrometers. The above effects are also valid for the Cassegrain mirror optics (Fig. 2.4).

3.2 Experimental determination of the optimum conditions.

3.2.1 Lens collection optics:

The laser beam of diameter $D = 2$ mm (distance between e^{-2} intensity points across the beam) was deliberately not focussed in order to provide a fairly uniform light source over the virtual image of the slit at the sample. The sample was illuminated with 400 mW at $\lambda = 514.5$ nm with the laser in the stabilised "light-mode". Corrections were made where necessary for the approximately Gaussian intensity distribution across the laser beam. A series of 5 cm diameter glass lenses were used to provide focal lengths from 2.5 to 10 cm, projecting the illuminated zone onto the slits at a magnification between 1:10 and 1:1.6 and also to provide optical coupling with the monochromator, maintaining $\Omega_C = M^2 \Omega_S$

Two types of sample were used to determine the optimum conditions.

- The intensity of the symmetric (CF_2) vibration of PTFE at $\Delta\bar{v} = 729$ cm^{-1} (89) was measured as a function of M . The sample in the form of a disc was maintained at 85° incidence to the laser beam, illuminating a strip approximately 2×20 mm at a radiant flux density of 1 $W\ cm^{-2}$. Slit widths $w = 0.35$ mm were used (spectral bandpass ~ 3 cm^{-1}), thus the viewed area on the sample varied in width w_0 from 0.035 to 0.22 mm, and in height h_0 from 2 to 12.5 mm. The correction for the variation in source intensity across the viewed area of the sample was small and is shown in Table 3.2.
- 4g of Spence "H'γ- Al_2O_3 (surface area $125\ m^2\ g^{-1}$) was activated at 10^{-5} Torr for 6 hours at room temperature then 93.6mg pyridine/g Al_2O_3 was adsorbed. This is a

coverage of 1.6 monolayers of pyridine, representing a typical surface scatterer. The intensity of the skeletal vibration of physisorbed pyridine at $\Delta\nu = 992 \text{ cm}^{-1}$ (90) was measured with changing M . The sample cell with a Pyrex optical flat window was maintained at 85° incidence to the laser beam. At this high incident angle approximately 70% of the incident parallel polarised light is reflected from the optical flat, but this does not interfere as it was maintained constant throughout. Slit widths, $w = 0.47 \text{ mm}$ (spectral bandpass $\sim 4 \text{ cm}^{-1}$) were used, thus the viewed area at the sample varied in width w_0 from 0.047 to 0.29 mm.

The correction for the variation in source intensity is shown in Table 3.2

Table 3.2

M	Percentage correction to Raman intensity	
	PTFE	Pyridine/Al ₂ O ₃
1.6	+1.0	+1.7
1.9	+0.6	+1.1
2.4	+0.4	+0.8

3.2.2 Cassegrain collection optics:

By moving the position of the small retro-mirror the focus of the Cassegrain optics can be changed to give a demagnification of the slits from 20 to 3.3, and maintain the correct optical coupling with the spectrometer. No corrections for the Gaussian cross section of the beam were necessary as the minimum demagnification of 3.3 is high enough to view only a very small area on the surface. A PTFE sample was used as in 3.2.1 with slit widths of 0.5 mm (4cm⁻¹ spectral bandpass) and the viewed area at the sample varied in width w_0 from 0.025 to 0.15 mm.

3.3 Results3.3.1 Lens collection optics

The maximum photon flux is collected by the spectrometer at an M value of 3.2 for both PTFE and pyridine adsorbed on $\gamma\text{-Al}_2\text{O}_3$. This M value corresponds to a 7.5 cm focal length collection lens. The normalised Raman intensity versus M is shown in Fig. 3.3

In all modern commercial spectrometers the value of M is selected between 6 and 8. Although this compromise may well be best for gases and liquids, it is not the optimum for surfaces as has been shown.

This analysis only applies where the brightness of illumination is limited by sample absorption and/or instability. This situation is frequently encountered outside surface studies, e.g. in the study of coloured solids, polymers and matrices etc. In some of these cases, complex cell systems are encountered e.g. low temperature or high pressure systems, and the collection aperture is frequently limited.

If the radiant flux density is limited by the sample, Table 3.3 shows that restricted collection aperture (ie low M) need not be a disadvantage.

Table 3.3

	L_1	F_1 cm	M	Incident angle de- grees	Radiant flux density at sample Wcm^{-2}
a	Biconvex	30	7	55	1320
b	cylindrical	30	7	55	36
c	cylindrical	60	3.2	72	16

a, b and c are all calculated for 100mW laser power, $\lambda = 514.5$ nm, $D = 2$ mm and 0.625 mm slits (5 cm^{-1} spectral bandpass, typical for surface studies). The values of F_1 are chosen to provide an illuminated zone of the same width as the slit image.

$$F_1 = \frac{w\pi D}{4\lambda M}$$

w = slit width

D = diameter of beam (2mm)

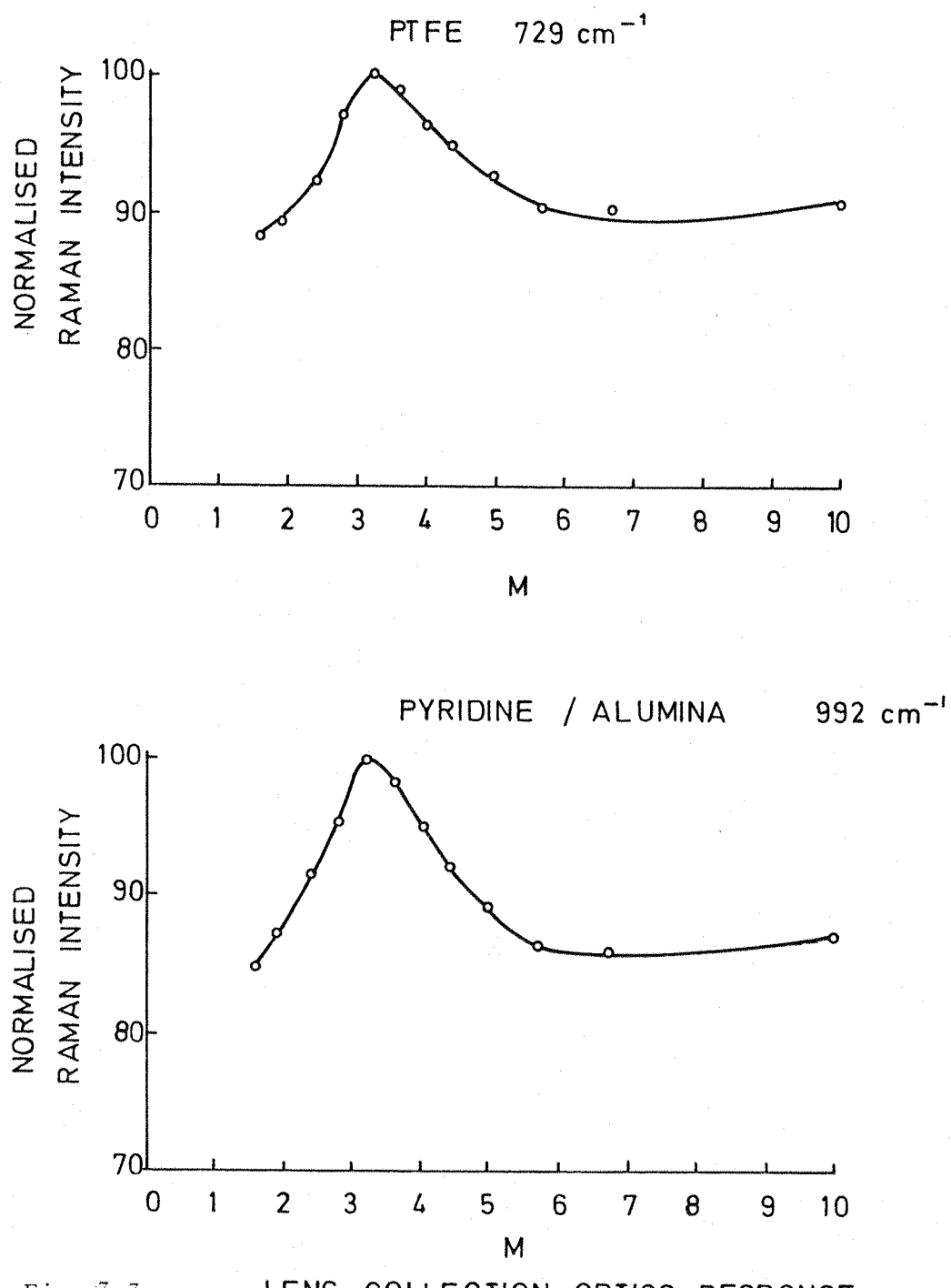


Fig. 3.3

LENS COLLECTION OPTICS RESPONSE

$\lambda = 514.5 \text{ nm.}$

$M = \text{Demagnification of slits.}$

- a) A typical spectrometer with $M = 7$ and a biconvex lens used to focus the laser down to match the slit image. Normally shorter focal length lenses are used, resulting in an even higher radiant flux density at the surface.
- b) The same typical spectrometer except that a cylindrical lens is used to strip focus the laser over the slit image. This decreases the radiant flux density roughly thirty-five fold.
- c) A spectrometer using an optimum value of $M = 3.2$ and matching the slit image with a cylindrical lens, bringing a further two fold reduction in the radiant flux density.

In b) and c) the incident angle is chosen to fill the slit image height with the 2 mm diameter beam through a cylindrical lens. The high angle of incidence required in c) to fill the slit image does not have a detrimental effect on the Raman signal. Greenler and Slager (91) have shown that the maximum Raman intensity for thin films on metal surfaces occurs at incident angles between 60° and 80° , whilst Turner (92) has shown that the maximum Raman intensity from pyridine adsorbed on Al_2O_3 in a quartz optical cell also occurs between 60° and 80° .

3.3.2 Cassegrain collection optics

The maximum photon flux is collected by the spectrometer at a M value of 8. The normalised Raman intensity versus M is shown in Fig. 3.4

The higher fall off of the Raman intensity at high M compared to the lens collection optics is due to the additional loss of Raman scatter caused by the shadow cast by the small retro-mirror on the collection mirror. The optimum value of M is significantly different from that obtained for the lens collection optics. This is to be expected as the geometry of collection is different and the collection mirror is larger than the collection

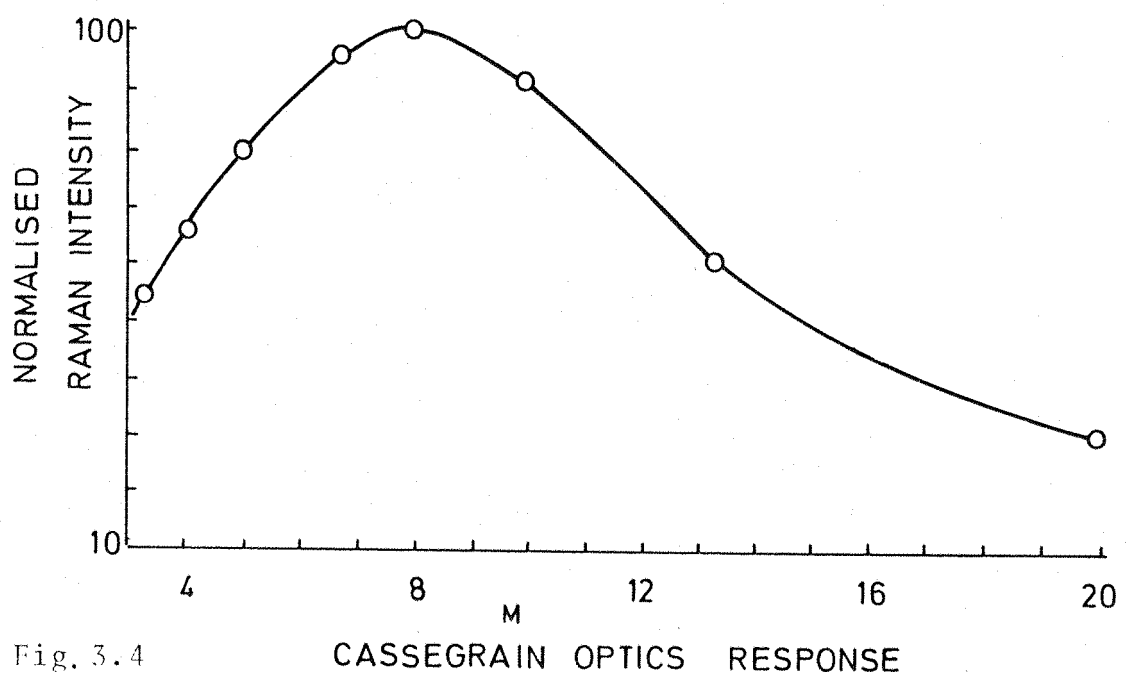


Fig. 3.4

lens. The advantages of using the Cassegrain system at low M values are similar to those for a lens system described in Table 3.3

Thus to conclude, most Raman spectroscopists use commercial spectrometers or variants thereof and tend to illuminate their samples with spot focussed lasers. They normally collect with a high aperture lens or mirror system and focus a magnified image of the illuminated sample area (magnification typically 6 - 8 for lens systems and 13-20 for Cassegrain systems) into the entrance slit of the spectrometer. Where the maximum permitted brightness of illumination of a solid non-transparent sample is limited, the normal collection geometry is not the optimum.

Chapter 4: Raman spectroscopy at oxide surfaces

4.1 Adsorption at oxide surfaces

Raman spectroscopy of an adsorbate at a solid-gas interface can reveal much information about the nature of the surface itself. The surfaces of interest here are those of oxides, in particular those of silicon, aluminium, zinc, magnesium, nickel and iron. All oxide surfaces under atmospheric conditions are covered with a hydroxyl layer and layers of adsorbed water in addition to hydrocarbon impurities.

Adsorption is normally divided into two types, chemisorption and physisorption:

Chemisorption involves the formation of a chemical bond between the adsorbate and the surface. The hydroxyl groups on an oxide surface are present as chemisorbed water with the hydroxyl bonded to a metal ion (see Fig. 4.5). The Raman spectrum of a chemisorbed molecule will be different to that of a free molecule, depending on the nature of the bond that is formed. It is possible for chemisorption to perturb a molecule sufficiently to change its molecular symmetry and so in principle to change its spectrum and make normally inactive vibrations now Raman active. In practice, a molecule is seldom sufficiently perturbed for this to occur. Chemisorbed molecules have a very low vapour pressure and usually require evacuation and strong heating to remove them from the surface as the adsorbate-surface bond has to be broken.

Physisorption involves only weak Van der Waals forces and no chemical bond is formed between the adsorbate and the surface. The molecules are not perturbed from their free state and the Raman spectrum is identical to that of the adsorbent in its gas or liquid state. Physisorbed molecules can form multimolecular layers on the surface in contrast to only a monolayer for chemisorption. Physisorbed molecules do have a finite vapour pressure and may be removed by evacuation.

4.1.1 Characterisation of surfaces.

To be able to characterise a surface ie. to know specifically what surface species are present it is necessary to have a suitable "tell-tale" molecule whose properties are in some way sensitive to the environmental conditions on the surface. Pyridine has been found to be most suitable as it has a relatively strong Raman spectrum and enables low coverages or low surface area samples to be investigated. Further, pyridine can chemisorb via the nitrogen atom to the surface and the ring breathing vibration is very sensitive to the nature of the bond between the nitrogen atom and the surface. Pyridine can also adsorb onto an acidic oxide surface in different ways (see Fig. 4.1).

Chemisorbed pyridine is formed by the donation of the lone pair of electrons on the nitrogen atom to a Lewis acid site and the formation of a coordinate bond. Pyridine can hydrogen bond to the surface and since it is a base, on complete proton abstraction from the hydroxyl group forms a pyridinium cation on the surface which is referred to as Brönsted coordinated pyridine.

The Raman spectra of adsorbed pyridine on Silica gel, Cab-O-Sil, magnesium oxide and alumina were first published by Hendra, Horder and Loader (93) in 1970.

The frequencies of the two ring breathing modes of pyridine in various environments is shown in Table 4.1.

Table 4.1

System	Bonding	Ring breathing vibration (cm ⁻¹) (intensities in brackets)	
liquid pyridine	-	992(10)	1032(8)
pyridine-water	H-bond	1003(10)	1036(5)
C ₅ H ₅ NH ⁺ BF ₄ ⁻	Brönsted	1011(10)	1032(2)
C ₅ H ₅ NZnCl ₂	Lewis	1025(10)	1050(0.4)

The frequencies of the ring breathing vibrations of adsorbed pyridine also depend on the strength of the

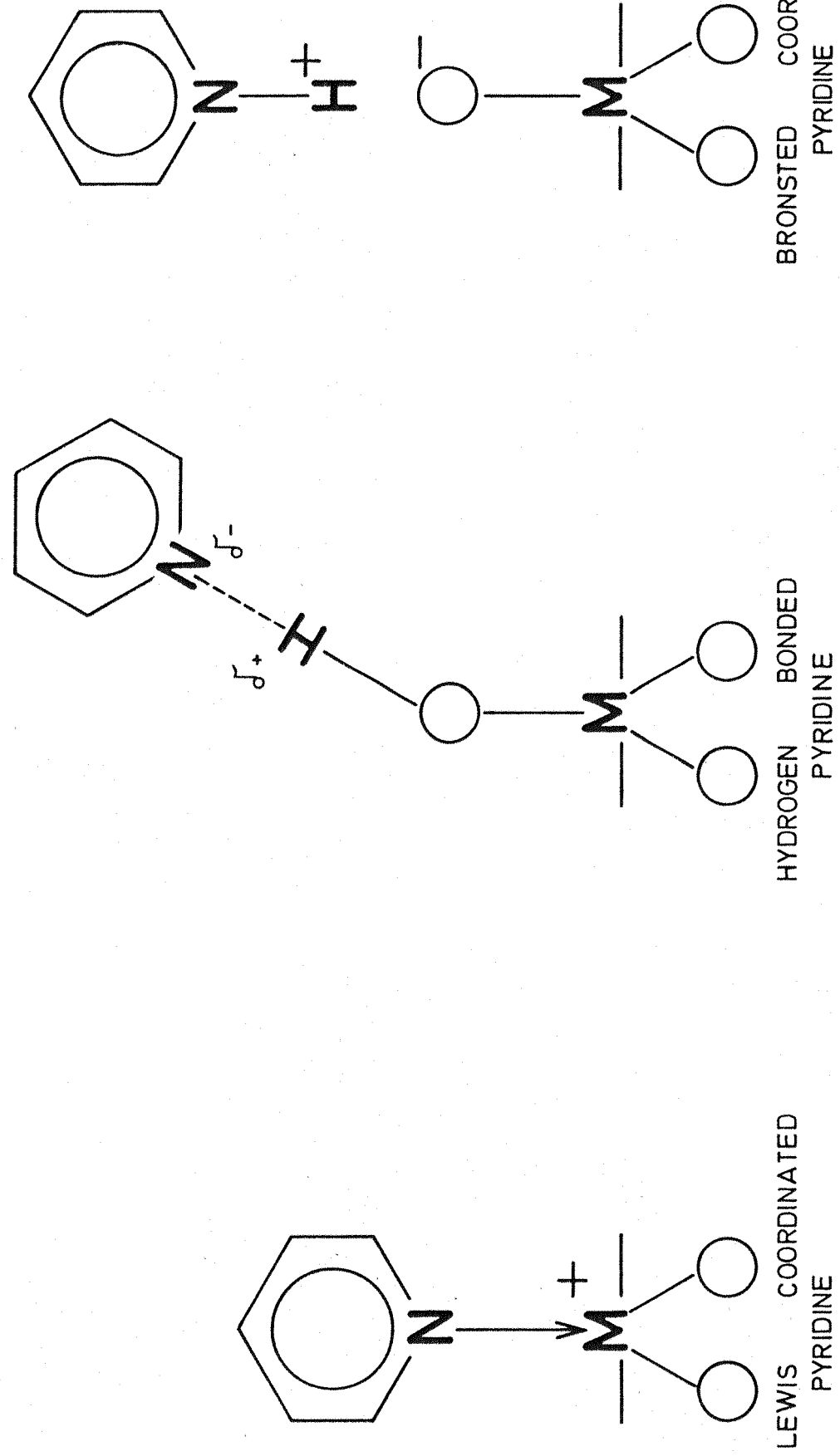


Fig. 4.1 PYRIDINE SURFACE SPECIES

Fig. 4.1

surface site onto which it is adsorbed. The frequencies of hydrogen bonded, Lewis coordinated and Brönsted coordinated pyridine generally fall into groups as shown in Table 4.2.

Table 4.2

Pyridine species	Frequency cm^{-1}	Intensity ratio
Physisorbed pyridine	992, 1032	10 : 8
Hydrogen bonded and Brönsted coordinated	1000-1010, 1028-1036	10 : 7 - 2
Lewis coordinated	1017-1028, above 1040	10 : 8 - 0

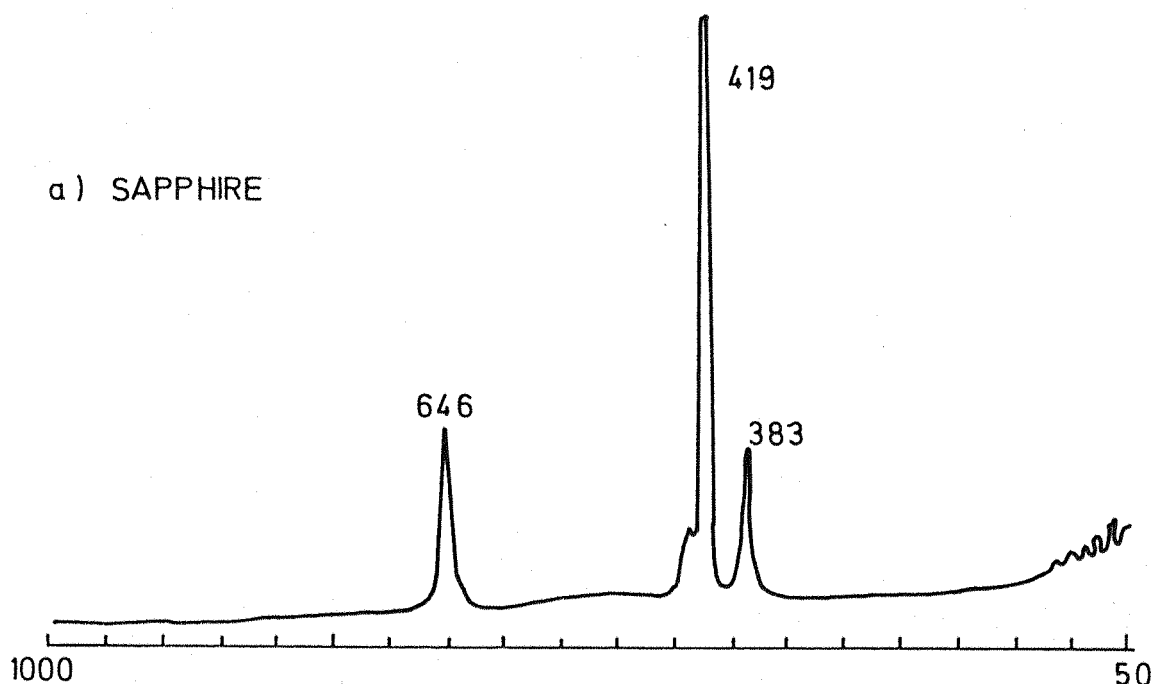
By examining the spectrum of adsorbed pyridine in the 990 to 1100 cm^{-1} region, it is possible to know what surface species are present. The information gained from the adsorption of pyridine may now be applied to the reaction and adsorption of other adsorbates at oxide surfaces.

4.2 Raman cells for the study of surfaces

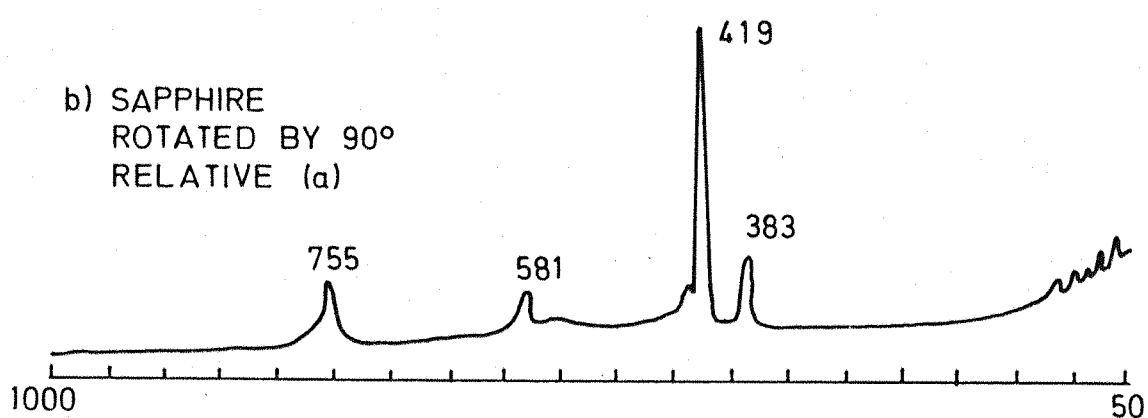
Raman spectra may be conveniently recorded of samples in glass, as glass has a weak Raman spectrum with three broad bands in the region 50 - 1000 cm^{-1} . Since sample activation temperatures of up to 950°C are needed, glass is not a completely satisfactory cell material. Quartz (SiO_2) is more suitable as it can be used at > 950°C. The Raman spectrum of quartz is essentially the same as that of glass (see Fig. 4.2)

Quartz cells were made from a 15 cm length of quartz tube, terminated on one end by a 19 mm diameter quartz optical flat, and on the other by a greased ground glass valve via a graded seal to the quartz tube. Quartz cells have one disadvantage when used in UF_6 systems. UF_6 itself does not attack glass or quartz as long as it is free of HF, but HF vigorously attacks quartz to form H_2O

a) SAPPHIRE



b) SAPPHIRE
ROTATED BY 90°
RELATIVE (a)



QUARTZ

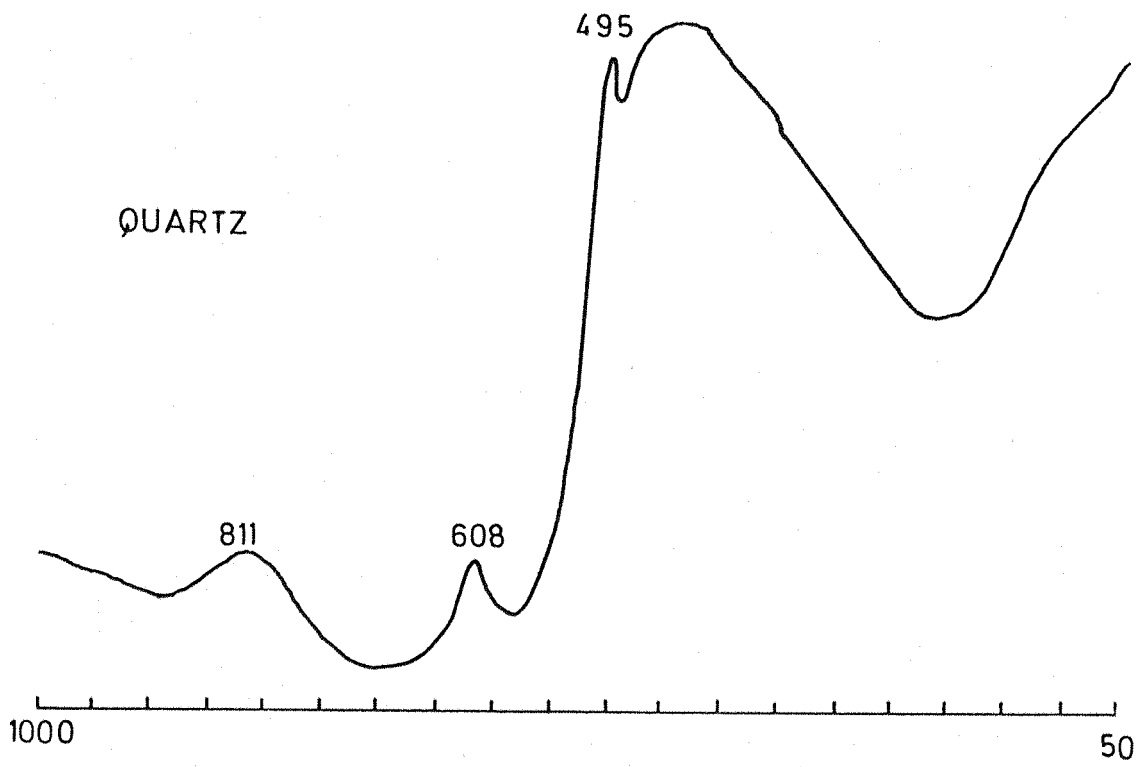


Fig. 4.2 RAMAN SPECTRA OF SAPPHIRE AND QUARTZ

and SiF_4 and in the presence of UF_6 a cyclic reaction occurs where the quartz is continually etched.

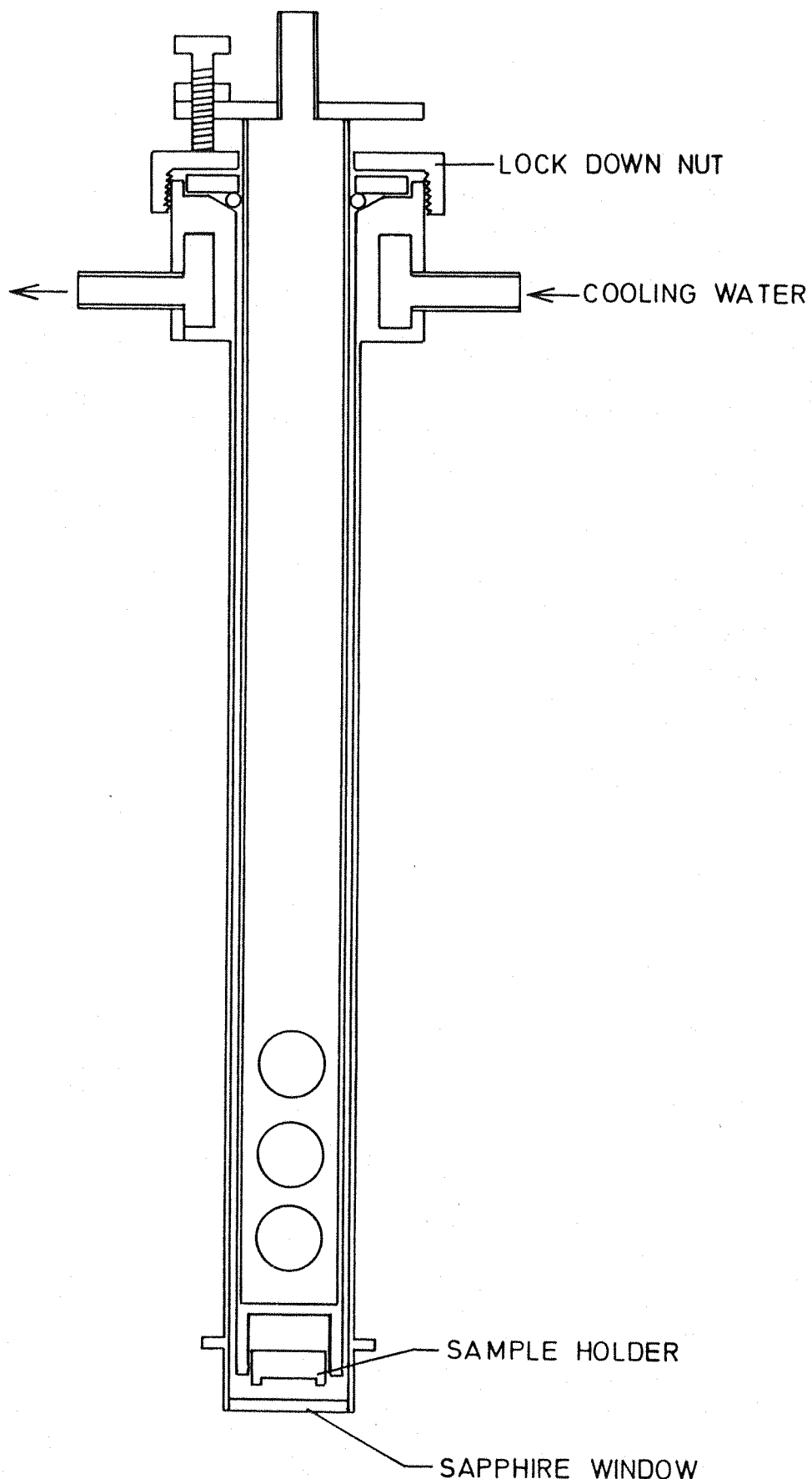


Even a small trace of HF is sufficient to keep the reaction going, and traces of HF are produced from the initial hydrolysis reaction of UF_6 with physisorbed water or surface hydroxyl groups.

Due to unwanted side reactions with quartz it was decided to construct a cell which is UF_6 and HF resistant and would also enable activation at up to 950°C . The most suitable material for the optical window as far as resistance to attack is concerned, is clear sapphire, which is essentially $\alpha\text{-Al}_2\text{O}_3$. The 19 mm diameter sapphire windows, 2 mm thick are supplied hard soldered into a nickel-iron flange (supplied by Anaspec Ltd.) The maximum working temperature of the mounted sapphire is 550°C . This limitation led to a cell design as shown in Fig. 4.3

The cell is made of stainless steel and the inner tube holds the sample holder. To activate a sample, the lock-down nut is loosened and the inner tube withdrawn until the sample is in the centre of the cell and the lock-down nut tightened. The cell is inserted into a tube furnace so that the sapphire window protrudes beyond the hot zone of the furnace. The temperature at the window could be maintained below 300°C . After cooling the cell, the procedure is reversed and the sample pushed up close to the sapphire window. A Viton O-ring is used to seal off the cell and is used ungreased to prevent hydrocarbon contamination of the sample as it has been shown (54) that grease-free activation results in a sample having an acceptably low background.

Since all the oxides used here are powders, the sample holder was made from stainless steel with a shallow recess cut in its lower surface as shown in Fig. 4.3.



SAPPHIRE WINDOW CELL

Fig. 4.3

The oxide sample is merely hand pressed into the holder on a flat surface. In a quartz cell the sample is held under gravity against the window, but in the sapphire cell the sample was purposely held 2 - 3 mm away from the sapphire to reduce the amount of background in the spectrum due to the sapphire. The samples had to be evacuated slowly to avoid them being sucked out of the holder and the valves could only be fully opened once a pressure of $< 10^{-1}$ Torr had been reached. As the sapphire windows are cut from a single crystal, it is necessary to mark the optical axis on the metal flange before welding the window in position. The Raman spectrum of the two orientations of sapphire are shown in Fig. 4.2.

The modified sample area of the Coderg T800 spectrometer at Southampton has a sample table which is adjustable in the x, y and z directions, and the cell is mounted in a cell colder which is bolted down to the sample table. The cell holder accepts both the quartz and sapphire cells, and is pivoted in the sample plane so that the incident angle of the laser beam is adjustable.

4.3 Vacuum and furnace system:

A suitable vacuum system is necessary for handling UF_6 and the activation of adsorbents. A glass vacuum line could not be used for corrosion reasons outlined in section 4.2. The system was built from stainless steel and the layout is shown in Fig. 4.4

Two Metrovac S10 rotary pumps and a 50 mm Edwards Speedivac diffusion pump using Dow Corning no. 704 silicone oil were used. The ultimate vacuum attainable with the system is 10^{-6} Torr. The vacuum is monitored on Pirani/Penning gauges and the adsorbent pressure is monitored on a stainless steel dial gauge, calibrated from 0 to 100 kPa.

The furnace was constructed from a 200 mm length of 50 mm diameter vitreous silica tube wound with nichrome wire of total resistance 44 Ω (at room temperature). The

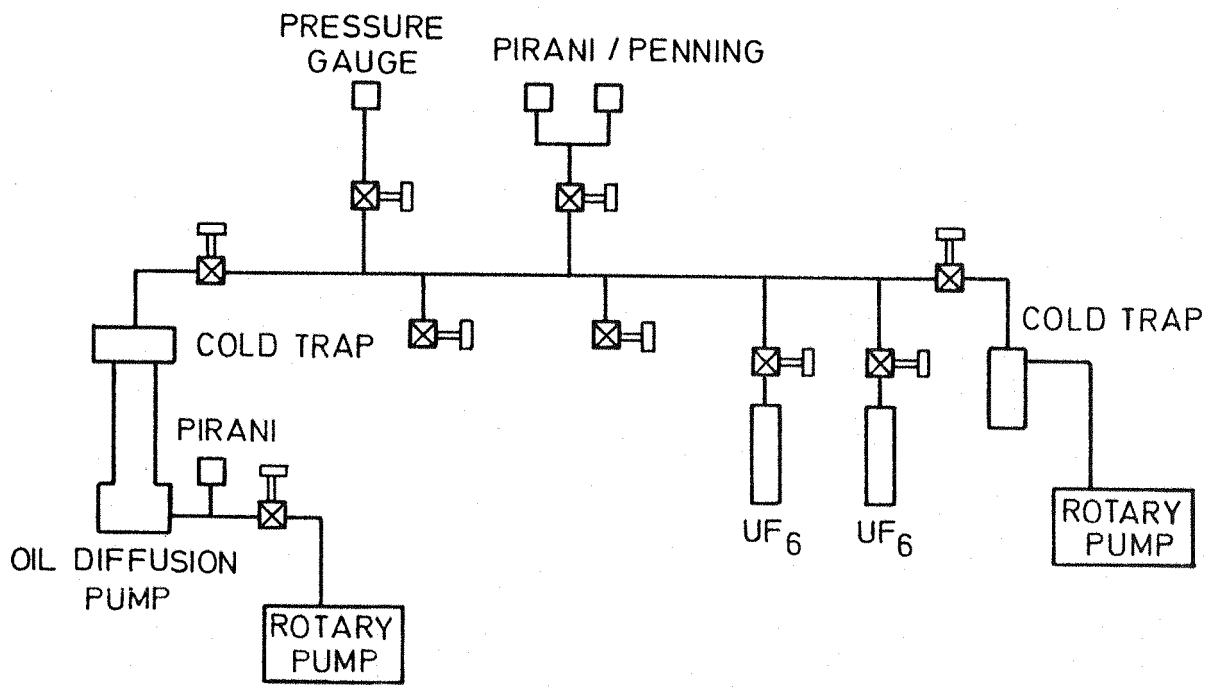


Fig. 4.4

VACUUM SYSTEM

tube and heating element was insulated in a steel box with silica wool and ceramic chips. The temperature of the furnace was controlled by a Type 993 Ether Transitrol controller with a 0 - 1400°C scale using a Pt/Pt 13% Rh thermocouple which was mounted in the furnace at the position of the sample.

4.4 Sample activation and fluorescence

4.4.1 Surface properties on activation

Sample activation is a necessary step in preparing an adsorbent to a state where it is clean and dry using heat and evacuation. Activation at low temperatures (up to 100°C) removes only free and physisorbed water from the surface. Activation at temperatures up to 950°C removes chemisorbed water from the surface and cleans the surface of contaminants, mainly hydrocarbons. Lewis sites are the main product on activating acidic metal oxides at 950°C (see Fig.4.5)

The dehydration of alumina has been well studied and Peri (94) has proposed a model for the surface of γ -Al₂O₃ on dehydration. He used a computer to simulate the removal of hydroxyl pairs from a square lattice. He found that 10% of the hydroxyls could not be removed from the surface even after allowing for defects on the surface. It has been shown (95) that γ -Al₂O₃ activated at 800 - 1000°C does still contain some hydroxyl groups on the surface.

Silica behaves differently on activating at 950°C, and forms strained siloxane bridges (96) instead of Lewis sites (see Fig.4.5). These siloxane bridges are relatively stable towards rehydration of the surface. Silica too does not completely dehydrate and contains about 5% of the hydroxyl groups at 1200°C.

Oxides generally sinter and lose surface area on heating, the amount of surface area lost is important as the surface area at specific temperatures is required to calculate adsorbate coverages. Krieger (97) has shown that alumina can lose ~ 40% of its surface area on heating

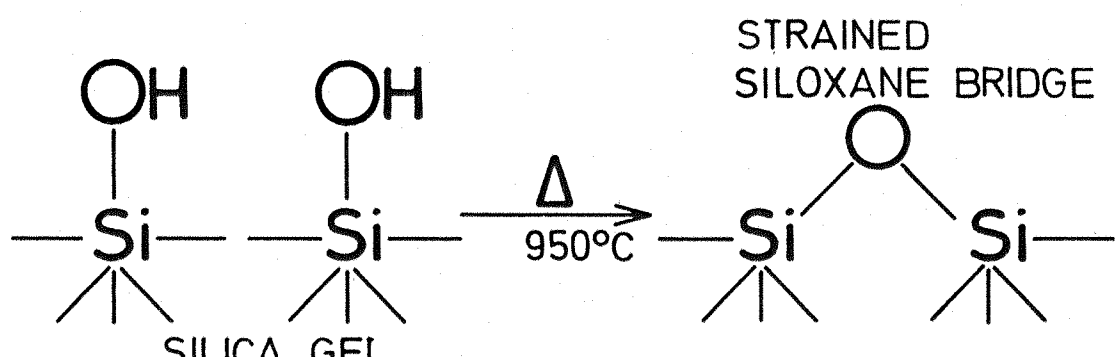
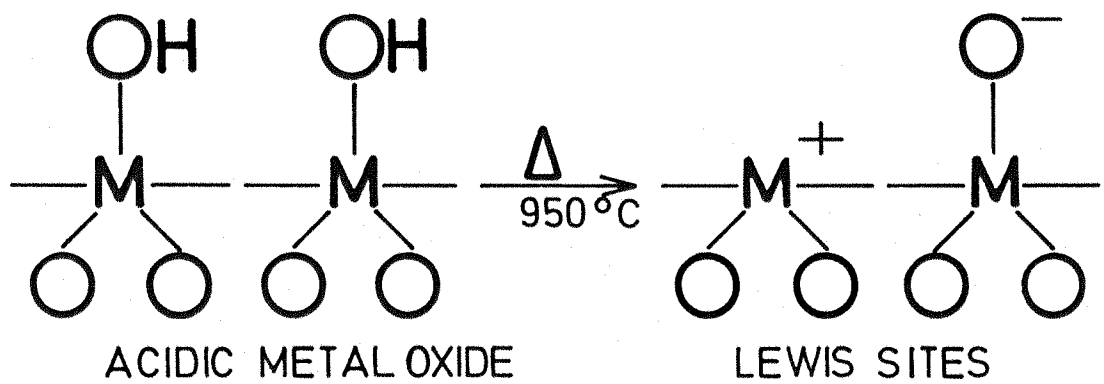


Fig. 4.5 SURFACE SPECIES ON 950°C ACTIVATION

to 950°C. Muroya (98) has shown that the Na^+ concentration in silica gel has a great influence on the surface area of the activated gel. 50 ppm Na^+ results in 65% loss of surface area on activation at 950°C, while 600 ppm Na^+ results in 92% loss of surface area under the same conditions.

4.4.2 Fluorescence and its elimination from oxides.

It has been shown previously (92) that the fluorescence background of alumina increases with activation temperature and reaches a maximum at 550°C, and decreases on further heating. The fluorescence generated on activation between 200° and 800°C is so intense it easily "swamps" the Raman spectra of adsorbed species. This has resulted in activation temperatures of < 200° and > 800°C being used, where the fluorescence is present in manageable intensities.

Silica gel has a similar fluorescence background to alumina (see Fig. 4.6). The maximum fluorescence occurs at 470°C.

Fluorescence arises from the absorption of a photon and re-emission of a new photon at a different frequency after a time interval of $> 10^{-9}$ s (cf. "spontaneous" Raman emission occurs in 10^{-13} s). There are three basic origins of a fluorescence background when dealing with surfaces: hydrocarbon contamination, metal ion impurities in the oxide and surface hydroxyl groups.

It has previously been shown (54) that grease free activation of $\gamma\text{-Al}_2\text{O}_3$ significantly reduces the fluorescence background though not completely. A molecular sieve was used to trap almost all hydrocarbons from the grease used in a glass vacuum line and to prevent back diffusion of oil vapour from the diffusion pump.

Pott and McNicol (99) have shown that Fe^{3+} doped $\gamma\text{-Al}_2\text{O}_3$ has a strong phosphorescence spectrum between 350 and 550 nm. Their results show that $\gamma\text{-Al}_2\text{O}_3$ with < 9 ppm Fe^{3+} has virtually no phosphorescence. These results speculate that metal ion impurities (especially Fe^{3+}) are

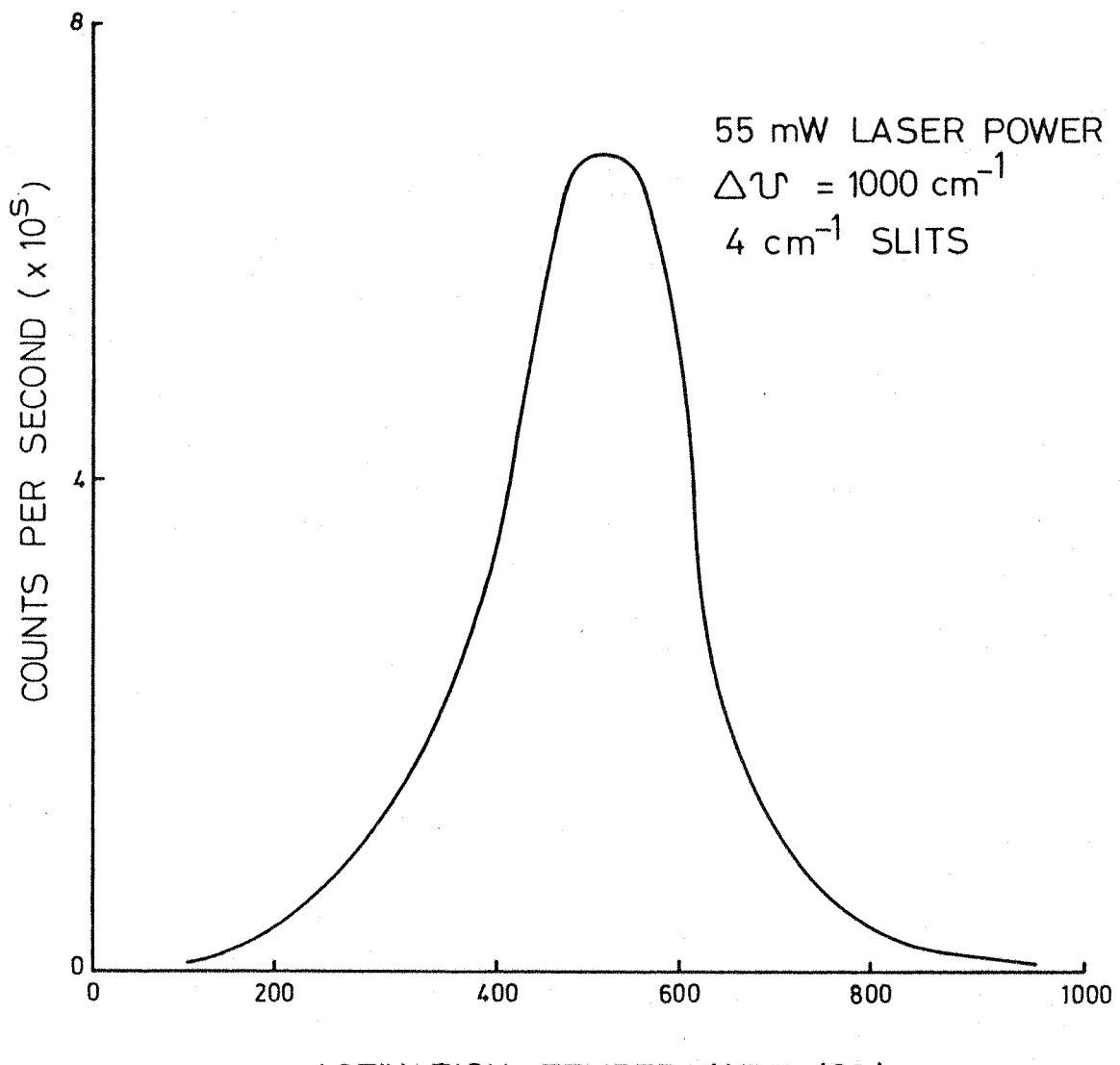


Fig. 4.6 FLUORESCENCE BACKGROUND
OF SILICA GEL

one of the causes of fluorescence in metal oxides. The alumina and silica used here contain typically 200 - 300 ppm Fe^{3+} . To overcome this cause of fluorescence specially prepared high purity oxides are recommended.

Careri et.al. (100, 101) have attributed the fluorescence background of liquid and solid proteins to bound water. They concluded (102) that the fluorescence background from oxide surfaces was due to adsorbed water and noticed that the background increased again on exposing the activated oxide to moist air. Jezirowski and Knözinger (103) have recently shown that the background spectra of MgO and Al_2O_3 are proportional to the hydroxyl concentration on the surface. Thus, high activation temperatures are necessary to decrease this source of fluorescence. However the correlations above may be purely fortuitous.

Fluorescence is normally overcome by activating at $<200^{\circ}C$ or $>800^{\circ}C$. Grease-free activation helps to further reduce the background. Fluorescence can be partially "burnt-out" from a sample by leaving it in the laser beam for several hours during which time the background decreases, but this method is very time consuming. Activating the sample in oxygen has also been found to help.

A method which has been used with some success relies on the spontaneous emission of a Raman photon whereas a fluorescence photon is emitted after $>10^{-9}s$. A mode-locked laser is used to generate a train of 0.5 ns pulses and the output of a fast photomultiplier tube is gated to the duration of the pulse. As a consequence Raman photons are accepted but the majority of the fluorescence photons will not be counted. Fast photomultiplier tubes are unfortunately not as sensitive as normal tubes.

4.5 Coloured adsorbents

White oxides such as Al_2O_3 , SiO_2 , ZnO and MgO have very little heating problems under normal illumination conditions, as the absorption of the laser beam is low.

Coloured oxides such as NiO and Fe_2O_3 do strongly absorb and serious heating effects are encountered which can desorb and decompose adsorbed species. The Raman signal from a coloured surface is low as the Raman scatter is also absorbed by the coloured surface. A number of possible methods are available to increase the Raman signal and decrease the heating effect. The laser line may be changed to one where less absorption occurs. A cylindrical lens should be used to focus the laser to a strip on the sample and reduce the light flux density on the surface (as shown in section 3.3.1). Spinning cells have been used with great success in obtaining spectra from highly coloured compounds. Keifer and Bernstein (104) have used a spinning cell to record the spectrum of $KMnO_4$ and I_2 and have observed many more overtones than is possible in a static system. Other systems such as "spot-wobblers" and rotating refractor plates which periodically move the laser beam in a pattern on the surface to decrease the average light flux density have been used with some success (105).

Chapter 5Adsorption and reaction of UF_6 at oxide surfaces

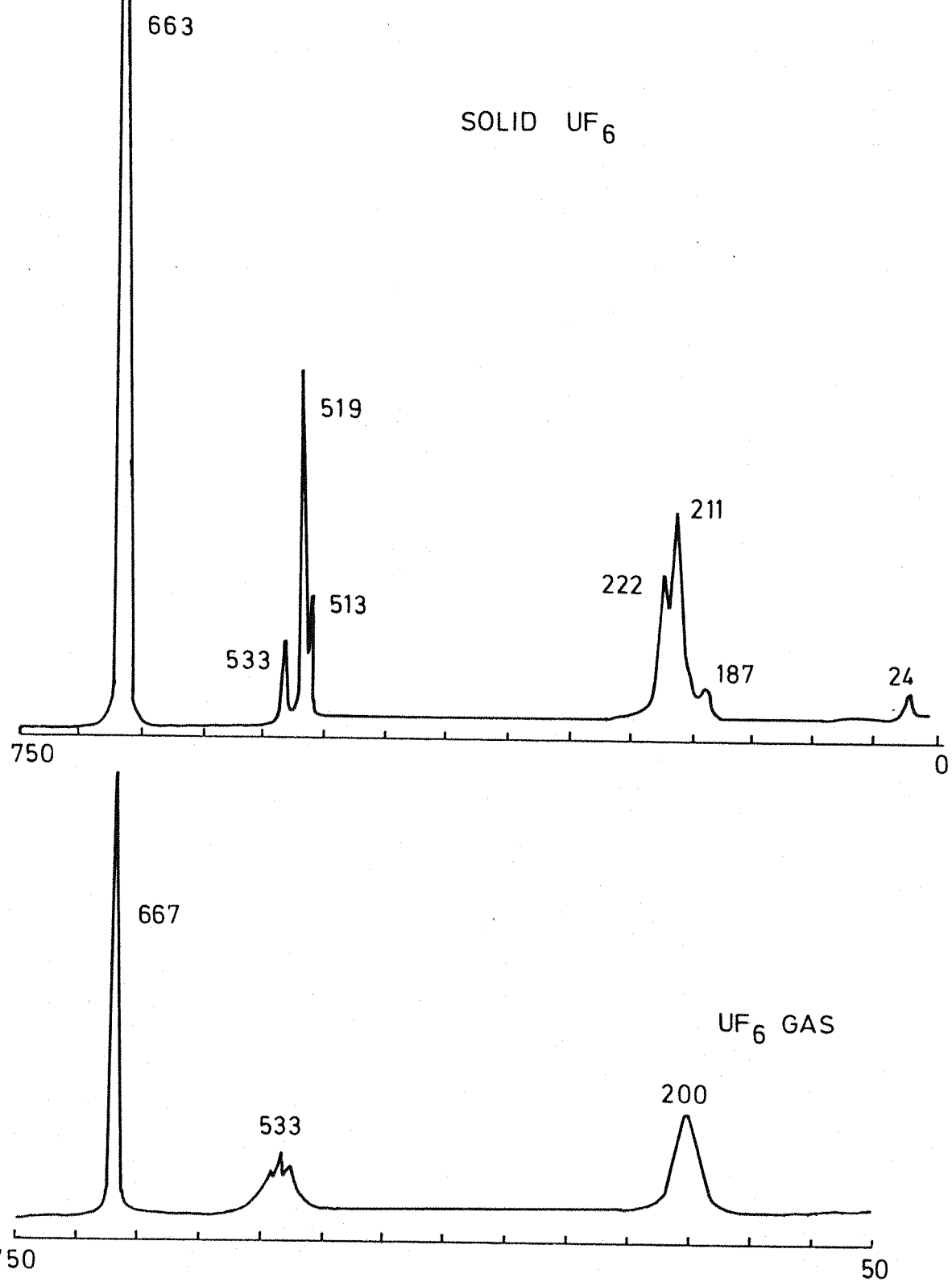
The aim of the investigation is to use Raman spectroscopy to observe the adsorption processes and hydrolysis of UF_6 at oxide surfaces. Further it is intended to apply the optimum optical conditions for surfaces as determined in chapter 3 to enable coloured metal oxide surfaces such as NiO and Fe_2O_3 to be included as well.

5.1 Handling and reactions of UF_6

UF_6 is a solid in the form of lustrous transparent crystals with a vapour pressure of 120 Torr at room temperature, and has a sublimation point of $56.4^\circ C$ at 760 Torr. UF_6 is easily handled in a vacuum system as it sublimes easily at room temperature. The UF_6 molecule is of octahedral symmetry (point group O_h) and the Raman spectrum of UF_6 gas consists of three fundamentals, $\nu_1 (A_1g)$ at 667 cm^{-1} , $\nu_2 (Eg)$ at 533 cm^{-1} and $\nu_5 (F_2g)$ at 200 cm^{-1} and a further weak band at 284 cm^{-1} due to $2\nu_6 (F_2u)$. The Raman spectra of gaseous and solid UF_6 are shown in Fig. 5.1. The spectrum of solid UF_6 shows correlation splitting of UF_6 in the lattice and a lattice vibration at 24 cm^{-1} . The gas spectrum consists of OPQRS branches for the 200 cm^{-1} and 533 cm^{-1} bands and a Q branch only for the 667 cm^{-1} band (106).

1.1 kg of UF_6 was obtained from BNFL (Capenhurst) in a monel cylinder. The UF_6 consisted of depleted material containing 0.35 % ^{235}U . The stated purity was 99 %. The UF_6 was doubly sublimed into an aluminium container and evacuated at $-30^\circ C$ to remove traces of HF. UF_6 used from this container and any excess remaining in the vacuum line was frozen out in a cold trap and disposed of by hydrolysis with water.

Since UF_6 is a strong fluorinating agent it should be kept out of contact with organic materials and any release into the atmosphere results in instant hydrolysis to form UO_2F_2 and HF, and should be handled with caution as both uranium and fluorine are toxic. UF_6 reacts with metals at suitably high temperatures to form metal fluorides. The Raman cell and vacuum line were constructed from stainless



steel as it offers sufficient resistance to attack at room temperature.

5.2 Uranium oxyfluorides

The most widely known hydrolysis product of UF_6 is UO_2F_2 . This is not the only uranium oxyfluoride known as others: UOF_4 , $\text{U}_2\text{O}_3\text{F}_6$ and $\text{U}_3\text{O}_5\text{F}_8$ have been prepared. Otey (107) has tabled the U-O-F system from UF_6 to UO_3 , and is shown in Table 5.1.

These intermediate oxyfluorides of uranium are important in the hydrolysis of UF_6 at oxide surfaces.

Table 5.1

The U-O-F system

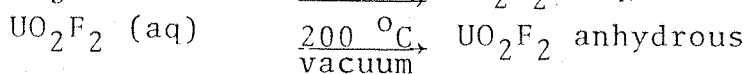
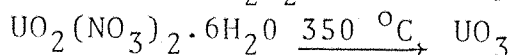
F/U ratio	Compound
0	UO_3 (yellow, orange) $\text{H}_2\text{O} \uparrow\downarrow \text{F}_2$
2	UO_2F_2 (yellow) $\text{H}_2\text{O} \uparrow\downarrow \text{F}_2$
2.67	$\text{U}_3\text{O}_5\text{F}_8$ (yellow) $\text{H}_2\text{O} \uparrow\downarrow \text{F}_2$
3	$\text{U}_2\text{O}_3\text{F}_6$ (yellow) $\text{H}_2\text{O} \uparrow\downarrow \text{F}_2$
4	$\alpha\text{-UOF}_4$ (orange) $\xrightarrow{\text{HF}}$ $\beta\text{-UOF}_4$ (yellow) $\text{H}_2\text{O} \uparrow\downarrow \text{F}_2$
6	UF_6

5.2.1 UO_2F_2

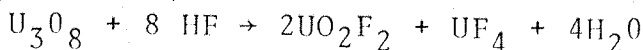
UO_2F_2 is a yellow solid which is formed on hydrolysis of UF_6 with excess water or on exposure of UF_6 to moist air. The crystal structure of anhydrous UO_2F_2 has been determined (108) and is space group $\text{R}3_m$ - D_{3d} . Each uranium is bonded to two oxygen and six fluorine atoms. The mono-, di-, tri- and tetra hydrates of UO_2F_2 are known and have been identi-

fied from their x-ray diffraction patterns (109).

Anhydrous UO_2F_2 has been prepared as follows:



Some U_3O_8 is formed with the UO_3 and fluorination produces some UF_4 .



The UF_4 was filtered from the aqueous UO_2F_2 solution.

Group theoretical consideration shows that for the infinite $(\text{UO}_2\text{F}_2)_\infty$ there should be eight fundamental lattice vibrations, four Raman active (two A_1g and two Eg). The Raman spectrum of anhydrous UO_2F_2 (Fig. 5.2) has only three vibrations.

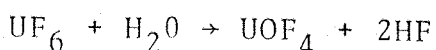
The band at 916 cm^{-1} is the U-O symmetric stretching vibration but the other two bands at 445 cm^{-1} and 181 cm^{-1} do not fit the values that have been previously calculated (107) at 341 and 131 cm^{-1} .

Anhydrous UO_2F_2 exposed to the atmosphere hydrates slowly as can be seen from Fig. 5.3. The hydration is only complete after 25 hours exposure in moist air. The 916 cm^{-1} and 445 cm^{-1} bands are thus characteristic of anhydrous UO_2F_2 , as they disappear on hydration.

The equilibrium hydrate in moist atmosphere was shown to be $\text{UO}_2\text{F}_2 \cdot 3\text{H}_2\text{O}$. 0.5 g of anhydrous UO_2F_2 was allowed to equilibrate for 48 hours in a moist atmosphere and the mass increase noted. The hydrated product was found to contain 14.94 % H_2O on dehydration at 200°C in vacuum and corresponds to $\text{UO}_2\text{F}_2 \cdot 3\text{H}_2\text{O}$ (theoretical 14.93 % H_2O).

5.2.2 UOF_4

UOF_4 is formed in the controlled hydrolysis of UF_6 as follows:



Two methods have been used to prepare UOF_4 .

- Excess UF_6 is vigorously shaken with anhydrous HF containing a controlled amount of water (110,111), and after 10 minutes an orange product is formed.

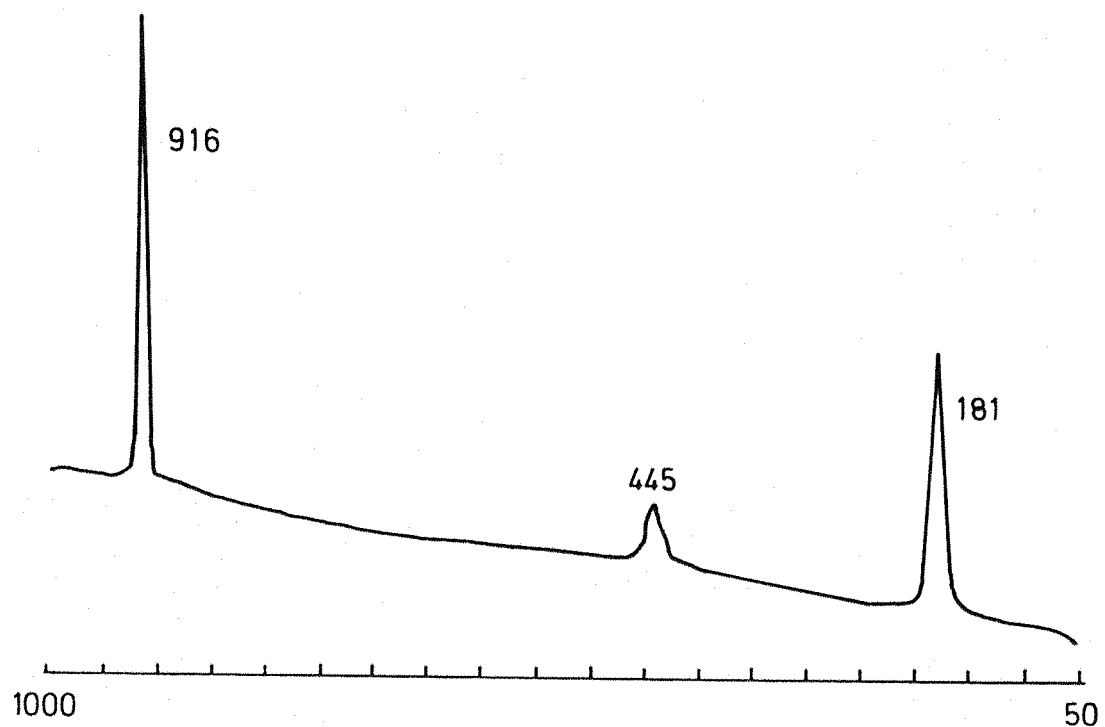


Fig. 5.2 RAMAN SPECTRUM OF ANHYDROUS UO_2F_2

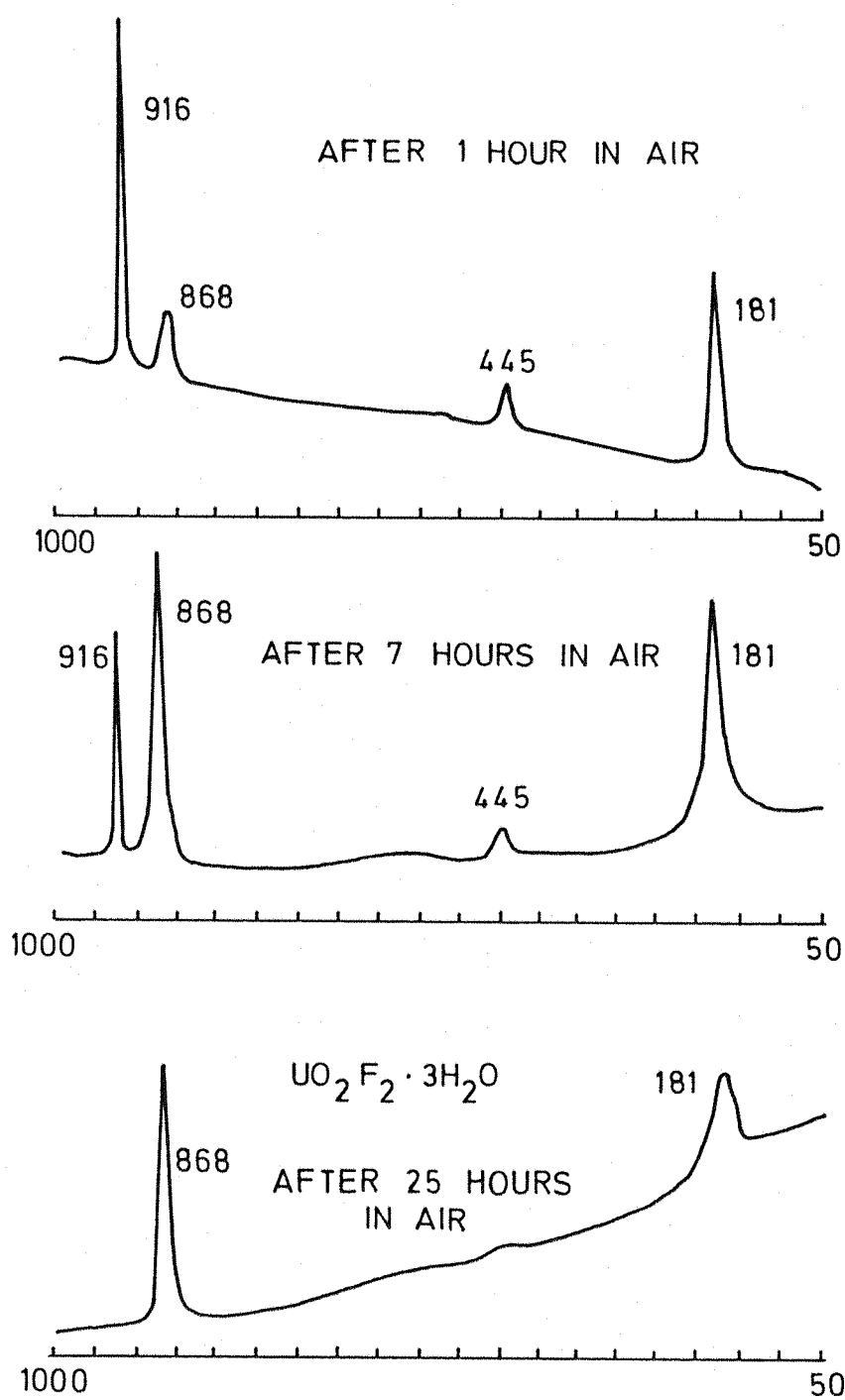
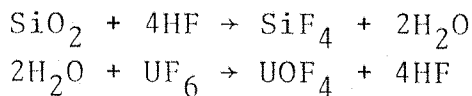


Fig. 5.5 HYDRATION OF ANHYDROUS UO_2F_2

b) Quartz wool is reacted with HF to produce H_2O at a controlled rate in a UF_6/HF medium (112). The HF is cycled through the reaction until all the SiO_2 is used up.



High surface area silica-gel ($750 \text{ m}^2 \text{ g}^{-1}$) was used to prepare UOF_4 and reacted much faster and more evenly than the quartz wool. The mixture after stirring for 4 days produced an orange product. β - UOF_4 is formed on stirring UOF_4 in a HF/UF_6 medium for 10 days (113). The Raman spectrum of UOF_4 is shown in Fig. 5.4. UOF_4 hydrolyses rapidly in air to form UO_2F_2 .

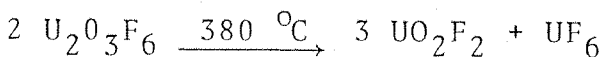


5.2.3 $U_2O_3F_6$

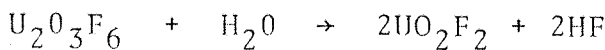
$U_2O_3F_6$ is a pale yellow solid and has not been prepared from the direct-hydrolysis of UF_6 , but rather from the thermal decomposition of UOF_4 (114, 115) as follows:



$U_2O_3F_6$ decomposes to UO_2F_2 on heating to $380 \text{ } ^\circ\text{C}$.

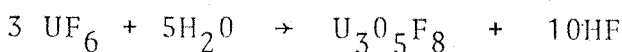


Wilson (114) found that $U_2O_3F_6$ was formed on heating UOF_4 to $> 250 \text{ } ^\circ\text{C}$ in an inert carrier gas, but here it has been found to decompose rapidly to $U_2O_3F_6$ at $190 \text{ } ^\circ\text{C}$ in vacuum. The Raman spectrum of $U_2O_3F_6$ is shown in Fig. 5.5. $U_2O_3F_6$ also hydrolyses in air to UO_2F_2



5.2.4 $U_3O_5F_8$

$U_3O_5F_8$, a yellow solid has been prepared by Otey and Le Doux (107) by the controlled hydrolysis of UF_6 .



They used water vapour/air mixtures to hydrolyse UF_6 at $160 \text{ } ^\circ\text{C}$. Above 0.9 % of the stoichiometric amount of water to form UO_2F_2 , only UO_2F_2 was formed. Below 0.9 %, $U_3O_5F_8$ was formed.

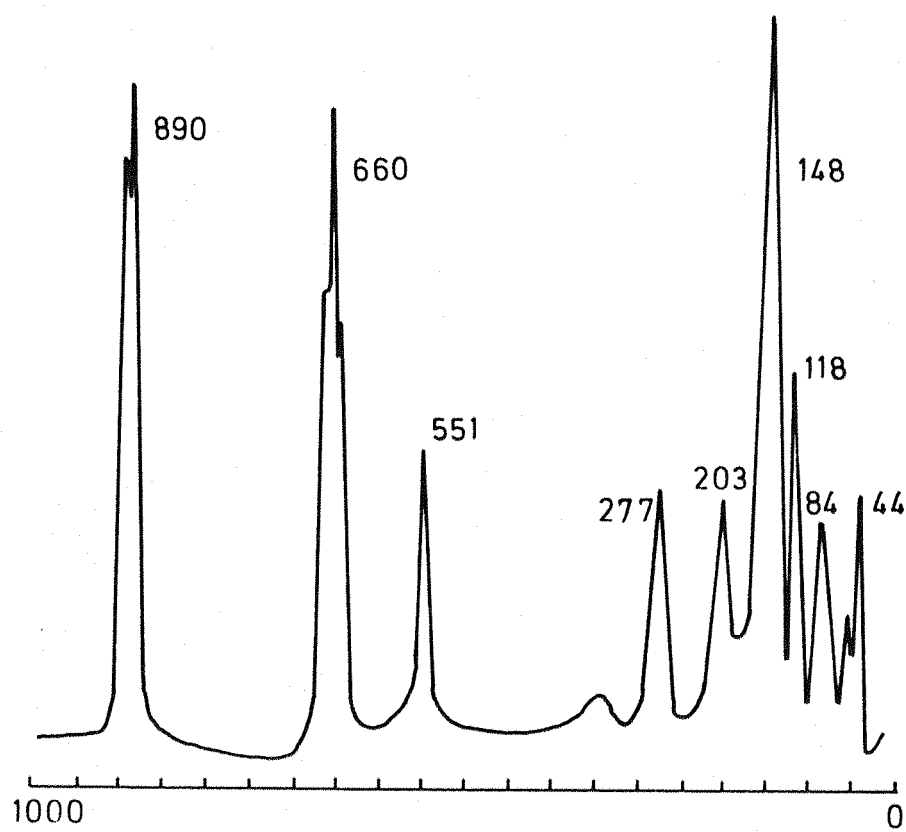


Fig. 5.4 RAMAN SPECTRUM OF UOF_4

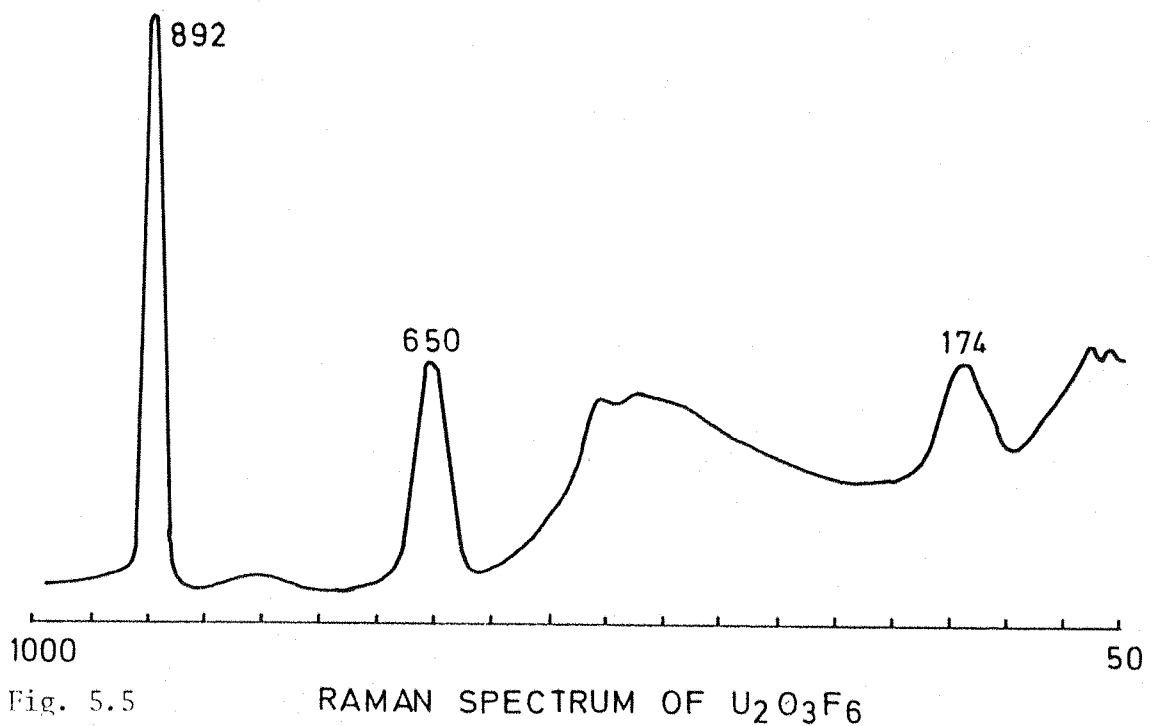
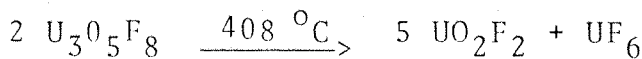


Fig. 5.5

Large quantities of UF_6 are required, and in one experiment Otey and Le Doux reacted 850 kg UF_6 with 9g H_2O to produce 60 g of product. This preparation has not been attempted, and no IR or Raman spectra are available for this compound. $\text{U}_3\text{O}_5\text{F}_8$ decomposes at 408 °C as follows:



Thus $\text{U}_3\text{O}_5\text{F}_8$ cannot be formed from the thermal decomposition of $\text{U}_2\text{O}_3\text{F}_6$ as the $\text{U}_2\text{O}_3\text{F}_6$ decomposes directly to UO_2F_2 at 380 °C. $\text{U}_3\text{O}_5\text{F}_8$ also hydrolyses in air to UO_2F_2 as follows:



5.3 Oxide adsorbents

SiO_2 , $\gamma\text{-Al}_2\text{O}_3$, ZnO , MgO , TiO_2 , NiO and Fe_2O_3 have been used to study the adsorption and reaction of UF_6 .

The SiO_2 , 100/200 mesh chromatographic grade (Silica Gel Ltd). has a surface area of $\sim 775 \text{ m}^2 \text{ g}^{-1}$. The composition as given by the manufacturer is: SiO_2 99.6 %, Fe_2O_3 0.01%, Al_2O_3 0.03 %, Na_2O 0.2 % and CaO 0.04 %.

The $\gamma\text{-Al}_2\text{O}_3$ (P Spence Ltd. grade H) has a surface area of $120 \text{ m}^2 \text{ g}^{-1}$. The maximum impurities are Na_2O 0.4 %, Fe 0.015 %. The MgO , ZnO and TiO_2 were B.D.H. "Analar" grade of > 99 % purity and have relatively low surface areas. The NiO and Fe_2O_3 are also low surface area.

5.4 Adsorption on Silica gel

Samples of silica gel of between 0.5 and 1g were activated at room temperature, 180 °C and 950 °C for each experiment. After activation the cell was cooled while pumping and the adsorbate introduced at room temperature. Pyridine was first used as adsorbate to characterise the surface, then UF_6 adsorbed on a similarly activated sample.

5.4.1 Characterisation of the surface

The Raman spectrum of 23 Torr pyridine adsorbed on room temperature activated silica gel is shown in Fig. 5.6. After evacuation the physisorbed bands at 992 and 1032 cm^{-1} disappear leaving only the bands of hydrogen bonded pyridine at 1009 and 1037 cm^{-1} . The Raman spectrum of pyridine

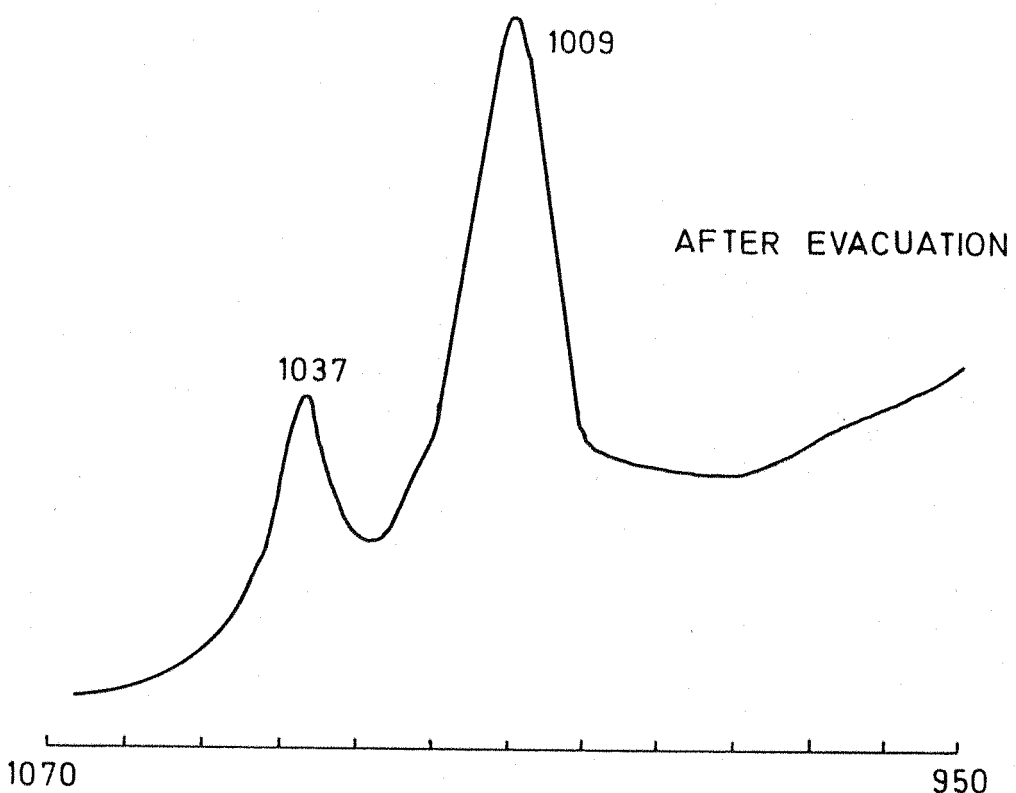
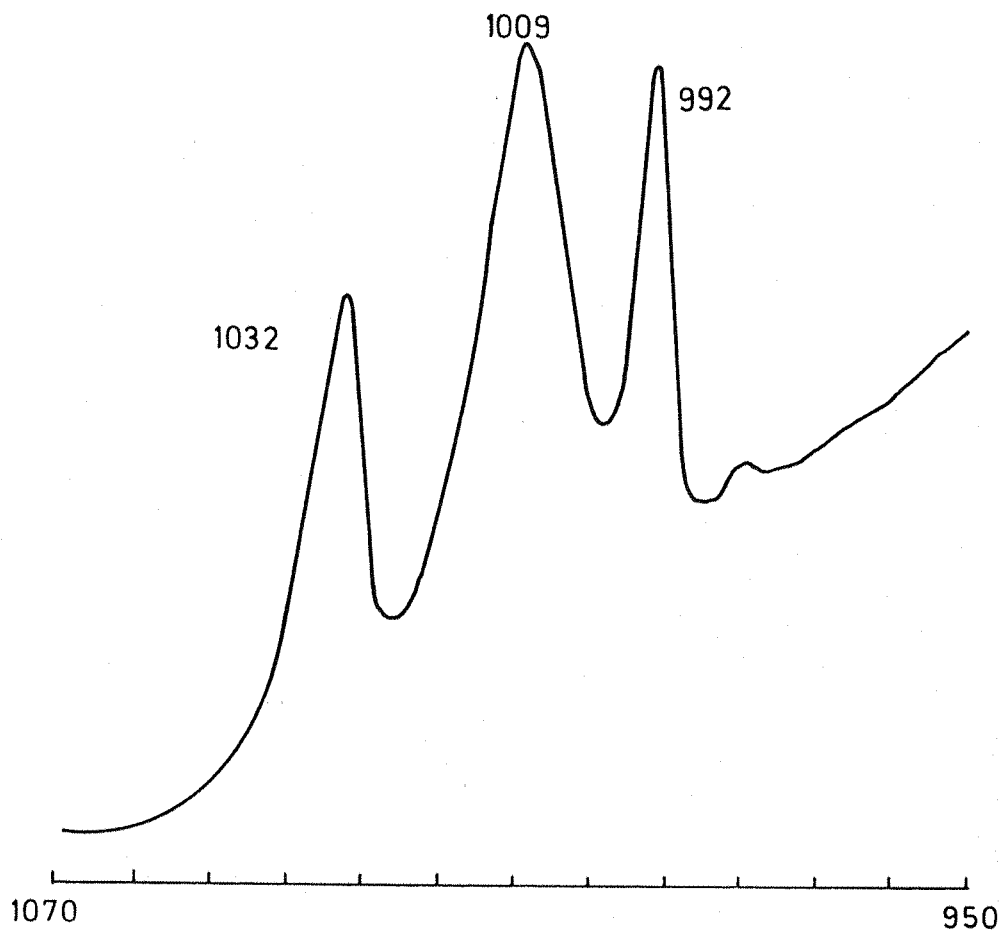


Fig. 5.6 RAMAN SPECTRA OF PYRIDINE ADSORBED
ON ROOM TEMPERATURE ACTIVATED SiO_2

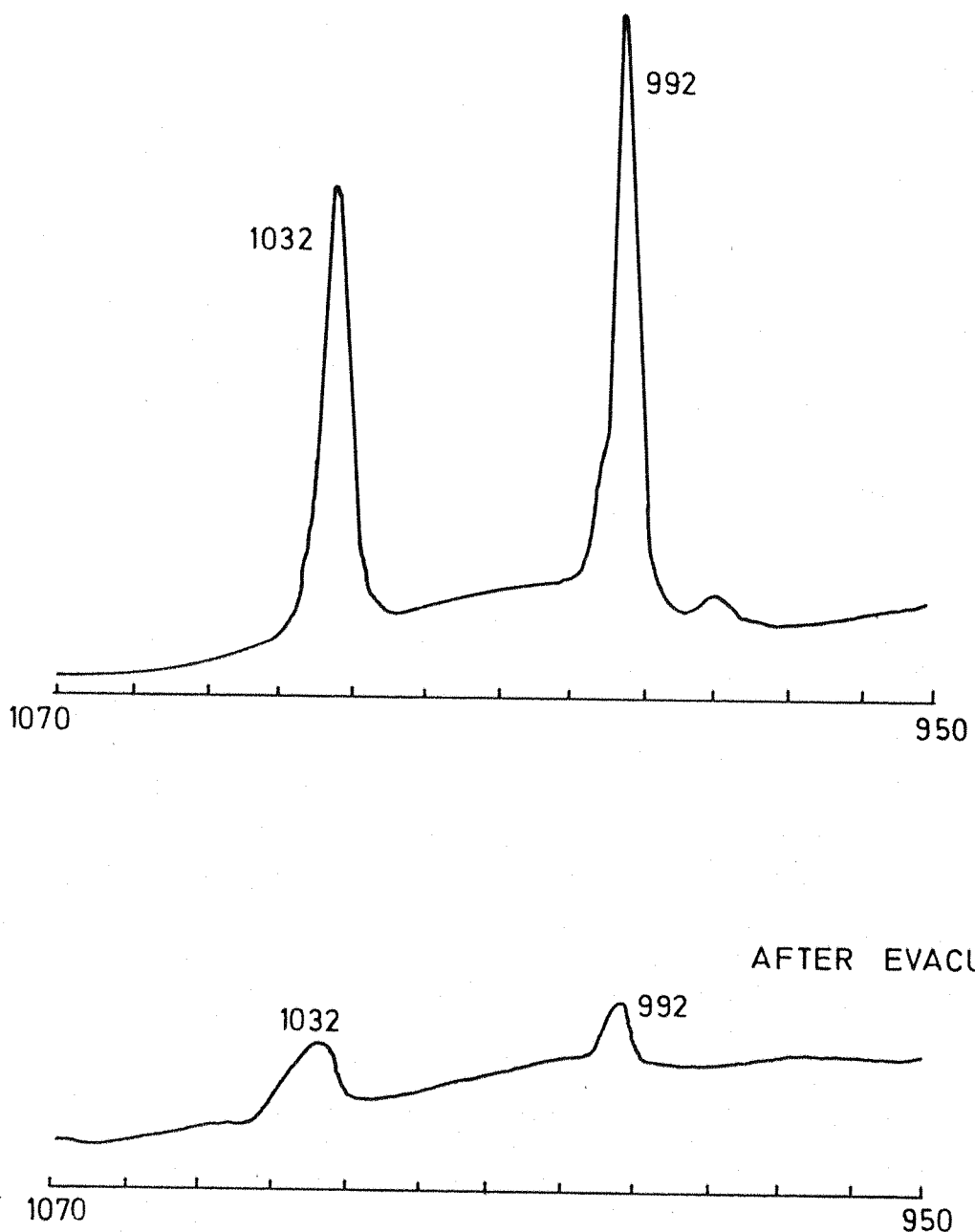


Fig. 5.7 RAMAN SPECTRA OF PYRIDINE ADSORBED
ON 950°C ACTIVATED SiO_2

adsorbed on silica gel activated at 950 °C is shown in Fig. 5.7. Only physisorbed pyridine is observed at 992 and 1032 cm^{-1} , and no Lewis coordinated or hydrogen bonded pyridine is present i.e. there are no surface hydroxyls. This agrees with Morrow and Cody (96) who found only strained siloxane bridges on the surface of similarly activated silica gel.

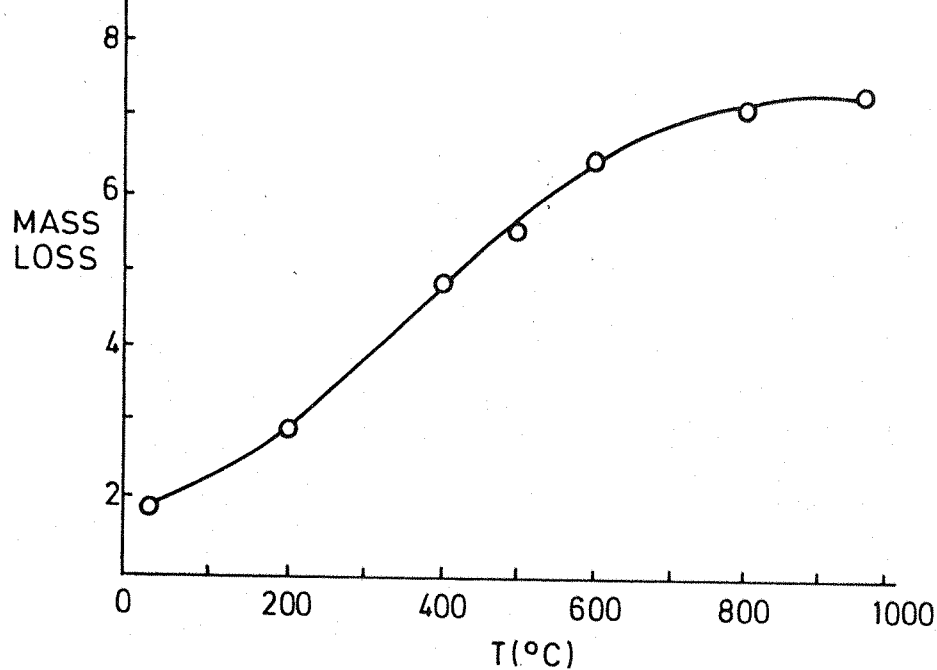
The surface area of the silica gel at 950 °C was calculated from the adsorption isotherm of pyridine (Fig. 5.8) using a cross sectional area of 0.285 nm^2 per pyridine molecule. The calculated surface area is $279 \text{ m}^2 \text{ g}^{-1}$, very much reduced from that at room temperature of $775 \text{ m}^2 \text{ g}^{-1}$ due to sintering. Dzis'ko et.al. (5) have shown that the bound water on silica gel is proportional to the surface area. The mass loss of silica gel versus temperature is shown in Fig. 5.8. Since physisorbed water is removed at 110 °C, the bound water (chemisorbed) is released from 110 °C to 950 °C. Using a cross sectional area for hydroxyl groups of 0.218 nm^2 , the initial surface area is calculated at $748 \text{ m}^2 \text{ g}^{-1}$ which agrees well with the manufacturer's figure of $775 \text{ m}^2 \text{ g}^{-1}$.

5.4.2 Adsorption of UF_6

On introducing 62 Torr UF_6 into a cell containing room temperature activated silica gel, the sample immediately turned a deep yellow and after a few seconds changed to a light yellow colour. The reaction that occurred was strongly exothermic. The Raman spectrum of the sample (Fig. 5.9) shows only bands due to hydrated UO_2F_2 at 874 and 176 cm^{-1} and a further U-O stretching vibration at 836 cm^{-1} . No adsorbed UF_6 is present in the spectrum. A sample of silica gel activated at 180 °C (i.e. only hydroxyl groups on the surface) has the same adsorption phenomena and Raman spectrum as Fig. 5.9. The deep yellow colour is associated with adsorbed UF_6 which rapidly hydrolyses with the surface water and hydroxyl groups on the surface to form UO_2F_2 . The 836 cm^{-1} band is shown to be due to UO_2F_2 bound to the surface in section 5.5.1.

When UF_6 is introduced into a cell containing silica gel activated at 950 °C, a deep yellow colour is produced and deepens with increasing UF_6 pressure.

9.1



γ MONOLAYER = 0.119 g PYRIDINE / g SiO_2

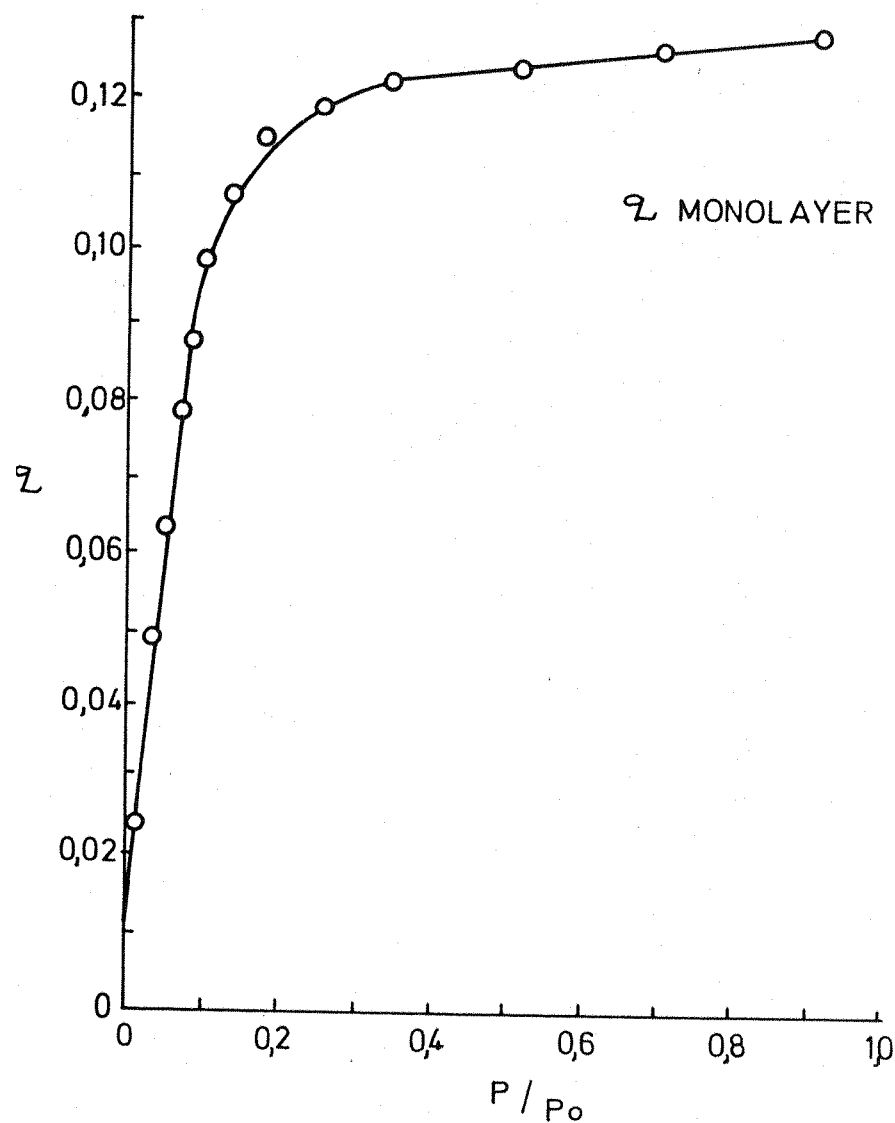


Fig. 5.8 PYRIDINE ISOTHERM AND MASS LOSS OF SiO_2

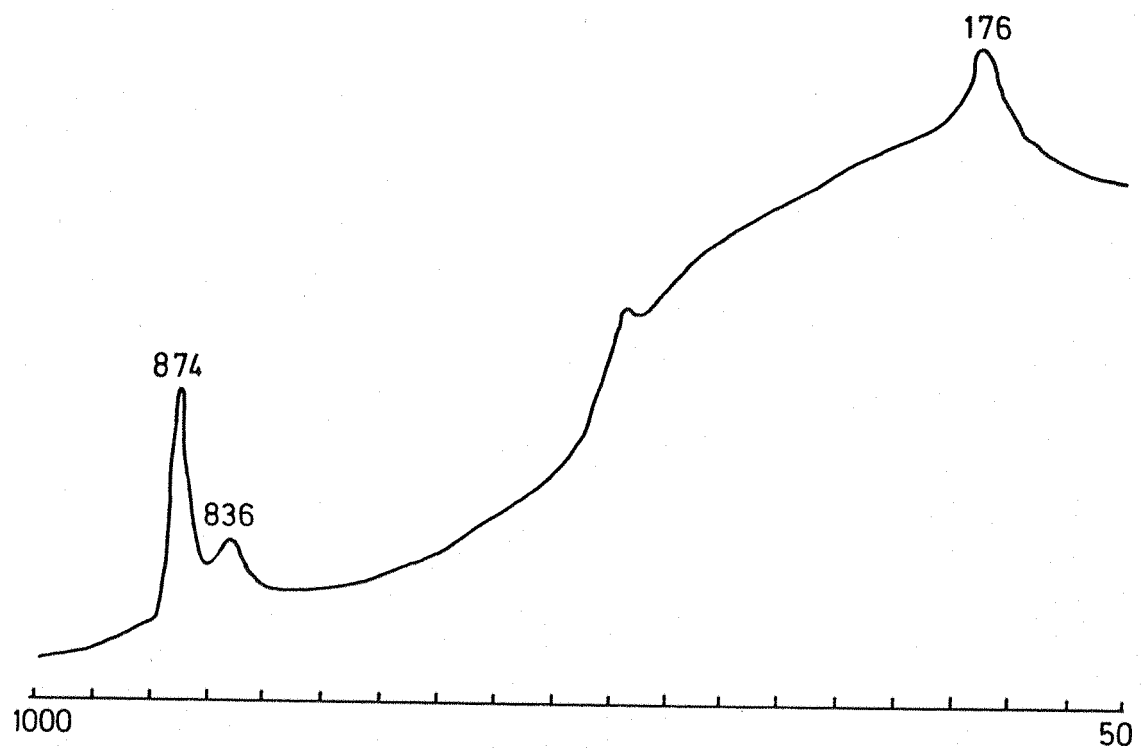


Fig. 5.9 ROOM TEMPERATURE ACTIVATED SiO_2/UF_6

The UF_6 adsorption isotherm at 21°C (Fig. 5.10) is of the Langmuir type. The Raman spectrum at three coverages (Fig. 5.11) shows strongly physisorbed UF_6 bands at 667, 530 and 206 cm^{-1} and a further band at 638 cm^{-1} . On evacuating the sample the physisorbed bands disappeared but not the 638 cm^{-1} band. On heating and pumping on the sample at $> 200^\circ\text{C}$ the yellow colour leaves the silica gel and the 638 cm^{-1} band disappears. This leads to the conclusion that the 638 cm^{-1} band is due to chemisorbed UF_6 .

Solid UF_6 is of $D_2\text{h}^{16}$ space group with 4 molecules per unit cell. This gives UF_6 a cross sectional area of 0.222 nm^2 per molecule. The specific surface area of silica gel activated at 950°C to UF_6 is only $82\text{ m}^2\text{ g}^{-1}$. This is roughly one quarter of the value obtained for pyridine, possibly due to the distribution of active sites on the surface and obstruction from the bulky UF_6 molecule. Hydrolysis products of UF_6 are totally absent in Fig. 5.11, this is expected as the adsorption of pyridine in Fig. 5.7 shows there are no remaining hydroxyl groups on the surface. The monolayer coverage is at $q = 0.201$ ($\text{g UF}_6/\text{g SiO}_2$) from Fig. 5.10. Fig. 5.11 shows that a coverage of 0.05 monolayer is easily detectable. The intensity ratios of the bands are shown in Fig. 5.12.

The chemisorbed band at 638 cm^{-1} is complete at 0.5 monolayer coverage (it is reasonable to assume the Raman cross section of chemisorbed UF_6 will not be different from that of physisorbed UF_6). The 667 and 206 cm^{-1} bands increase linearly with q as expected, and the $667/206$ ratio levels out at $q = 0.06$, below this the chemisorbed component is significant and is included in the 206 cm^{-1} band and not in the 667 cm^{-1} band.

UF_6 thus readily chemisorbs to the siloxane bridges on the surface and is strongly physisorbed as well. This contrasts greatly with the adsorption phenomena of UF_6 on surfaces containing Lewis sites. (section 5.5)

5.5 Adsorption on other non-laser absorbing oxides

Al_2O_3 , ZnO , TiO_2 and MgO are suitable white oxides on which to study adsorption where the heating effects of the laser beam are minimal.

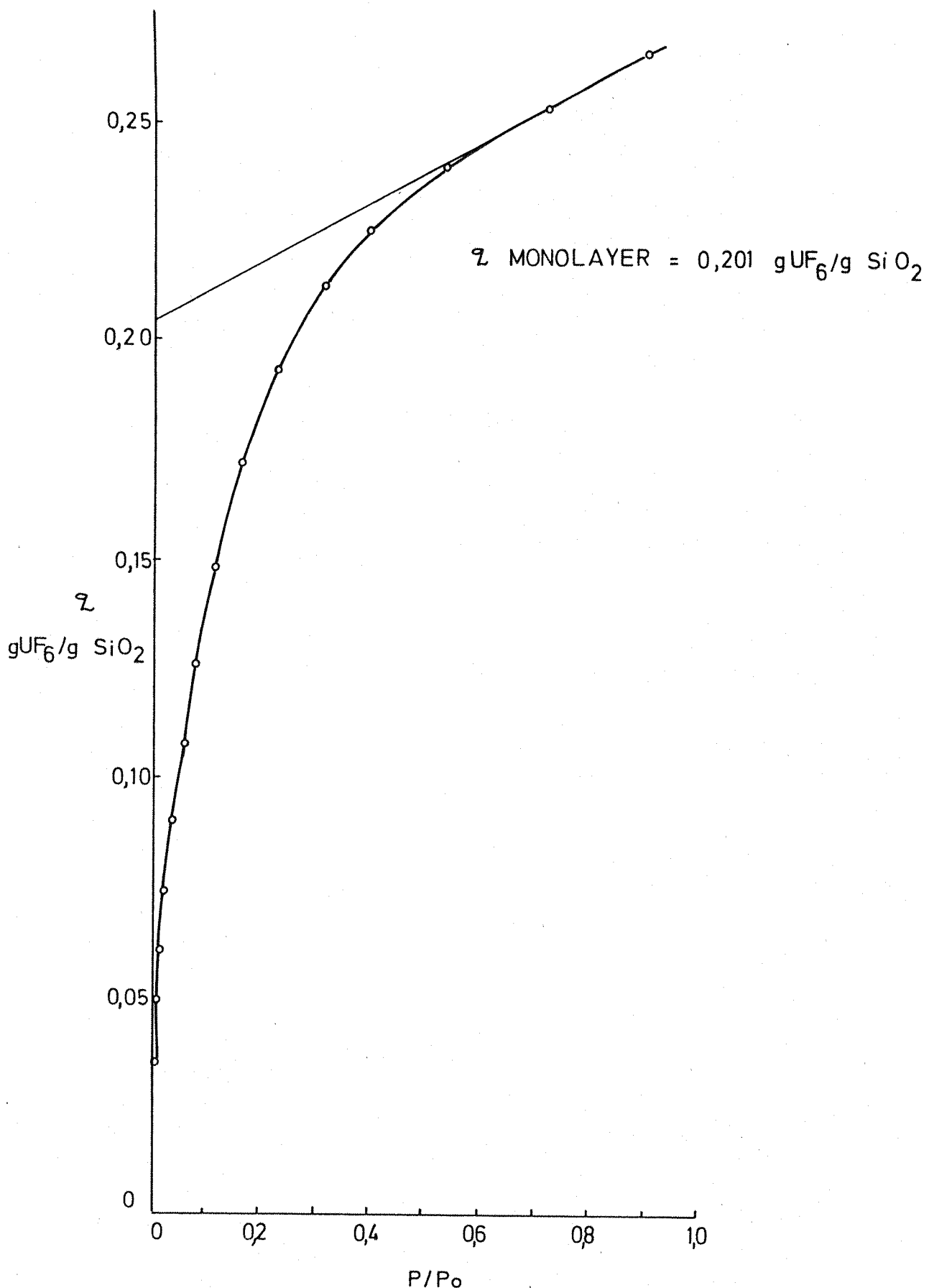


Fig. 5.10 UF_6 ADSORPTION ISOTHERM ON SiO_2

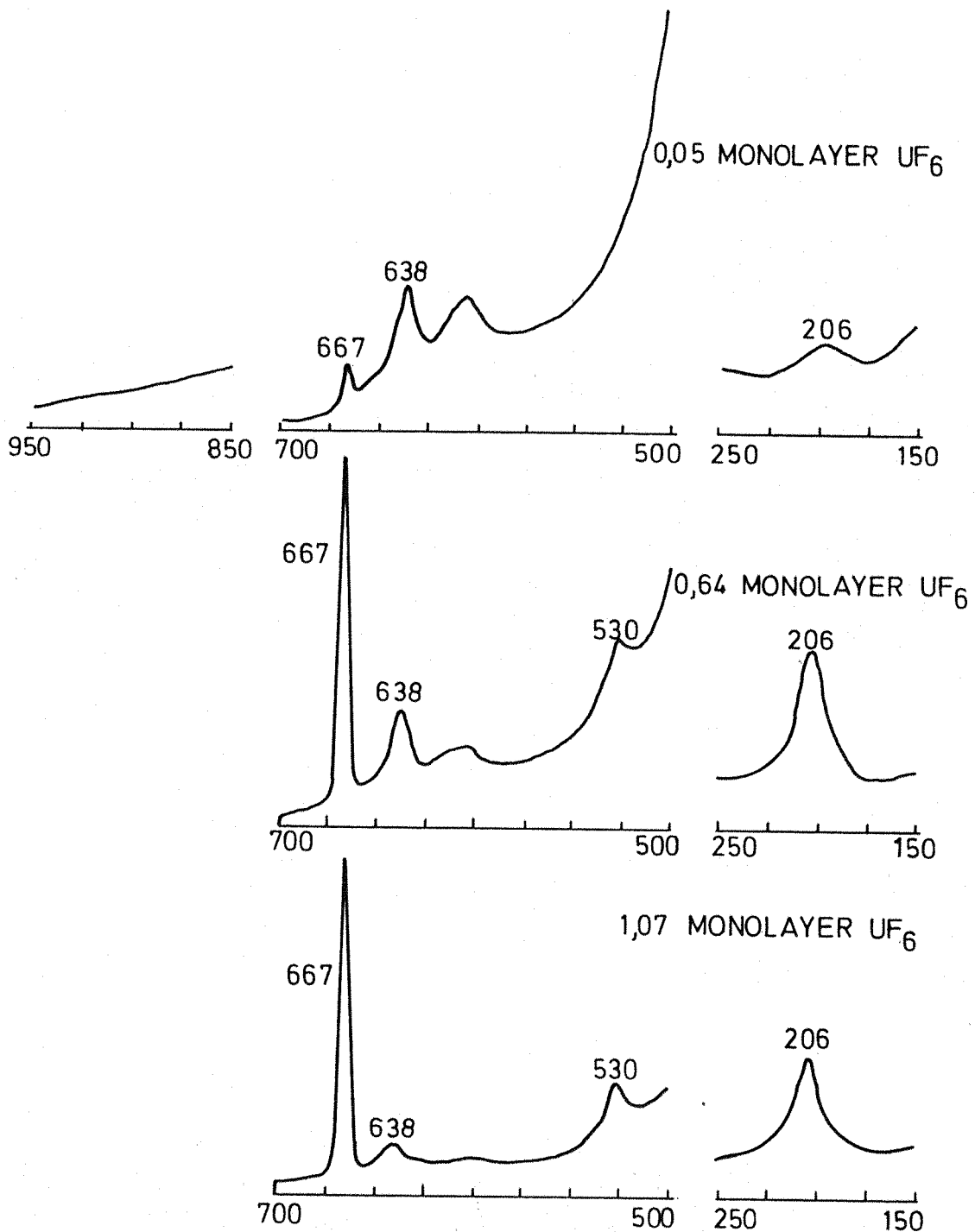


Fig. 5.11 RAMAN SPECTRA OF UF_6 ADSORBED ON 950°C ACTIVATED SiO_2

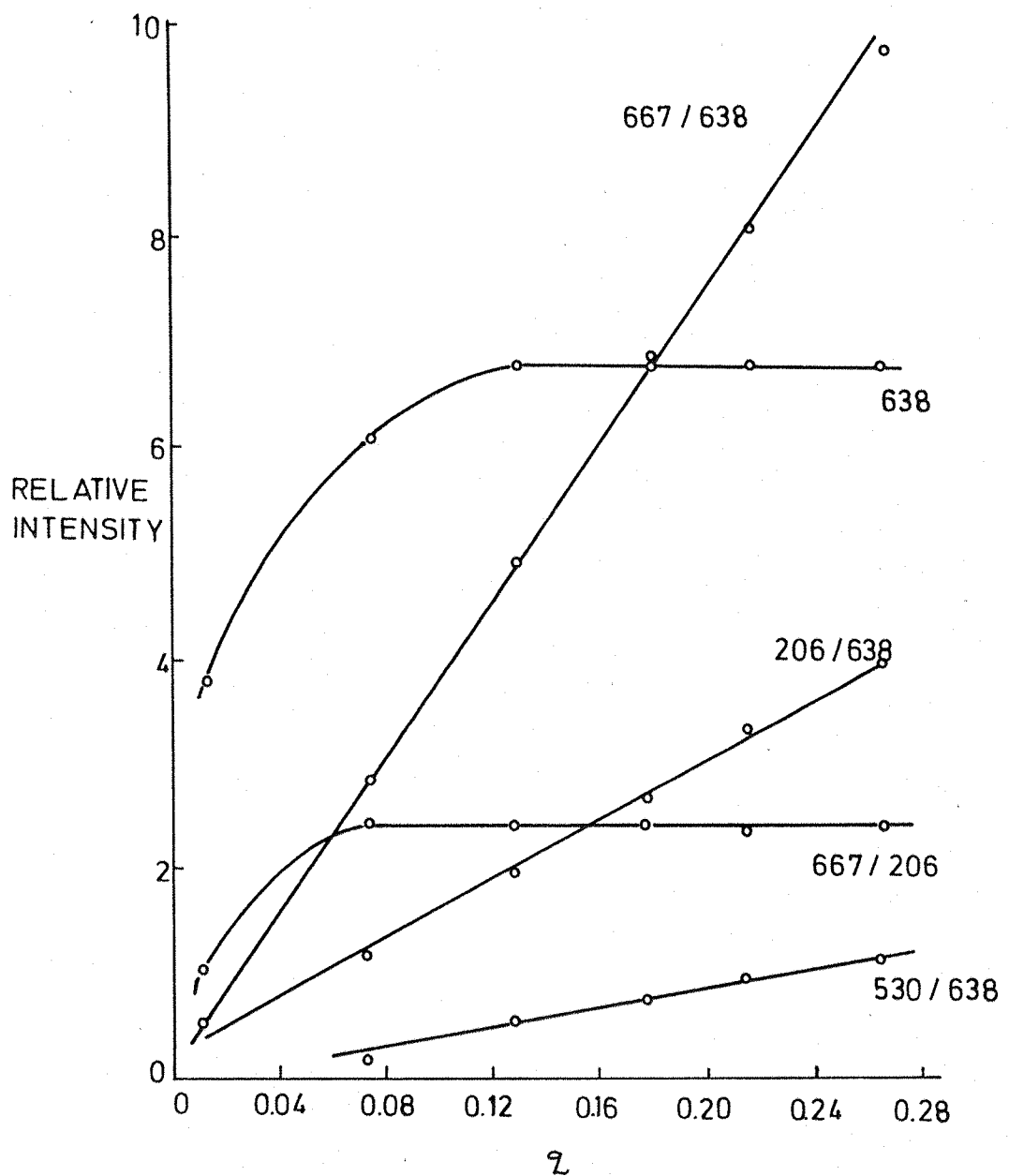


Fig. 5.12

INTENSITY RATIOS OF ADSORBED UF_6 BANDS

5.5.1 $\gamma\text{-Al}_2\text{O}_3$

The adsorption on $\gamma\text{-Al}_2\text{O}_3$ was investigated on samples activated at room temperature and 950°C . The surface area of the room temperature activated $\gamma\text{-Al}_2\text{O}_3$ is $125 \text{ m}^2 \text{ g}^{-1}$ and $75 \text{ m}^2 \text{ g}^{-1}$ after activation at 950°C .

The Raman spectrum of pyridine (23 Torr) adsorbed on room temperature activated $\gamma\text{-Al}_2\text{O}_3$ is shown in Fig. 5.13. The bands at $1\ 000$ and $1\ 034 \text{ cm}^{-1}$ are due to hydrogen bonded pyridine, and the band at $1\ 019 \text{ cm}^{-1}$ due to Lewis coordinated pyridine. Even at this activation temperature there are some Lewis sites present on the surface.

The spectrum of pyridine adsorbed on 950°C activated $\gamma\text{-Al}_2\text{O}_3$ shows only Lewis coordinated pyridine ($1\ 019 \text{ cm}^{-1}$) (Fig. 5.14).

Müller (116) has studied the adsorption process of UF_6 on nickel, copper, polyethylene and Teflon and has shown the process to be reversible. Colvin (117) and Forkos (118) have shown that UF_6 is bound by physical adsorption to the surface of Al_2O_3 . More recently van Schalkwyk and Hendra (119) have studied UF_6 adsorbed on $\gamma\text{-Al}_2\text{O}_3$ and found physisorbed UF_6 and some hydrolysis products on $\gamma\text{-Al}_2\text{O}_3$ activated at 950°C .

$\gamma\text{-Al}_2\text{O}_3$ activated at room temperature for 5 hours turns yellow on admitting 75 Torr of UF_6 into the cell. The Raman spectrum is shown in Fig. 5.15.

The bands at 667 and 206 cm^{-1} are due to physisorbed UF_6 and disappear on evacuation and exposure to air. The 370 cm^{-1} band is characteristic of $\gamma\text{-Al}_2\text{O}_3$. The 893 cm^{-1} band coincides with that of UOF_4 and $\text{U}_2\text{O}_3\text{F}_6$, but the other UOF_4 bands are not present and the strong band at 176 cm^{-1} indicates that the hydrolysis product on the surface is $\text{U}_2\text{O}_3\text{F}_6$ with the 650 cm^{-1} band being obscured by the physisorbed UF_6 band at 667 cm^{-1} . On exposure to air the $\text{U}_2\text{O}_3\text{F}_6$ hydrolyses to UO_2F_2 with bands at 868 and 176 cm^{-1} . The 840 cm^{-1} band which is present even after exposure to air has also been noted by van Schalkwyk and Hendra (119). To determine the origin of this band 0.2 g UO_2F_2 was dissolved

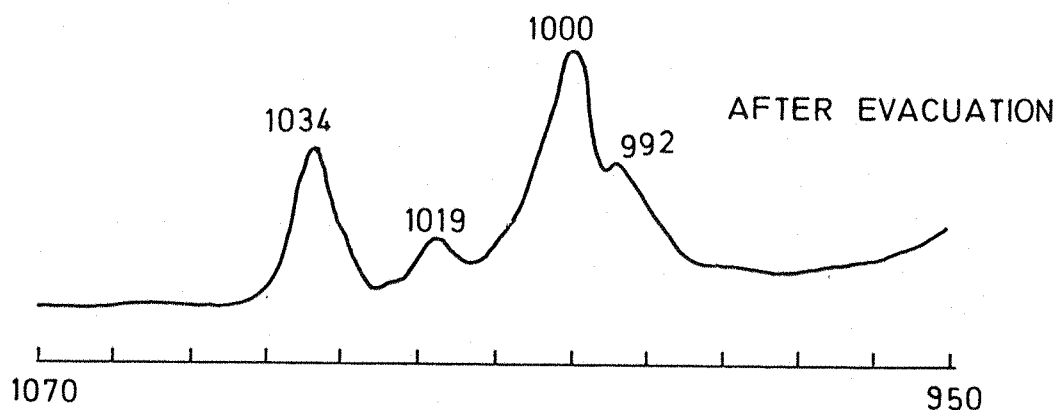
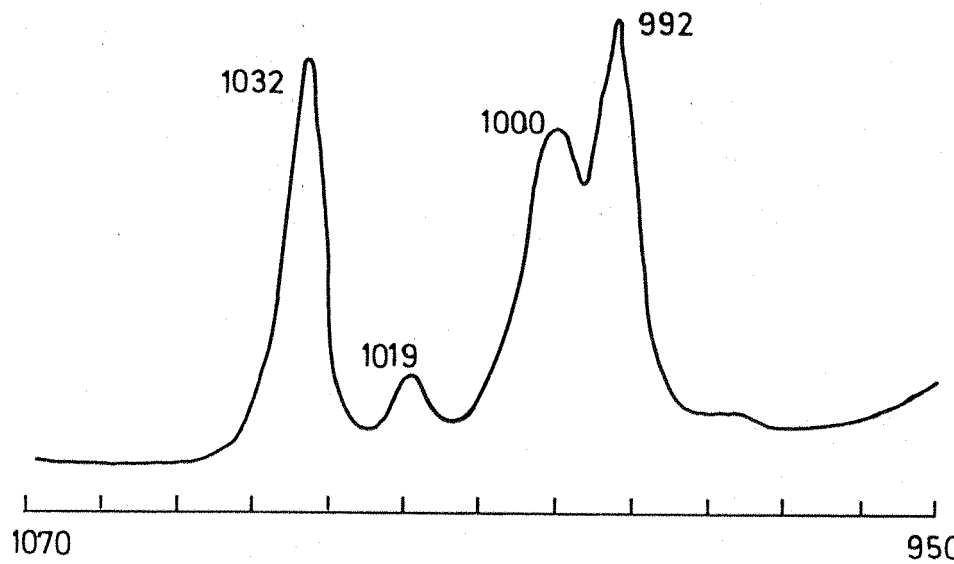
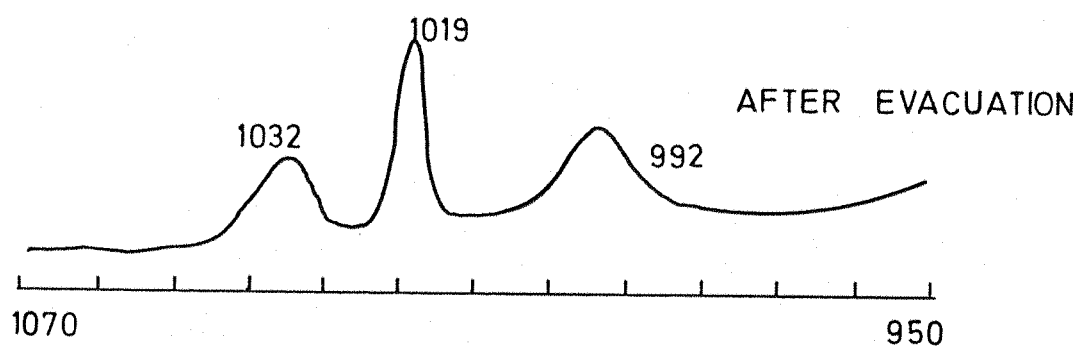
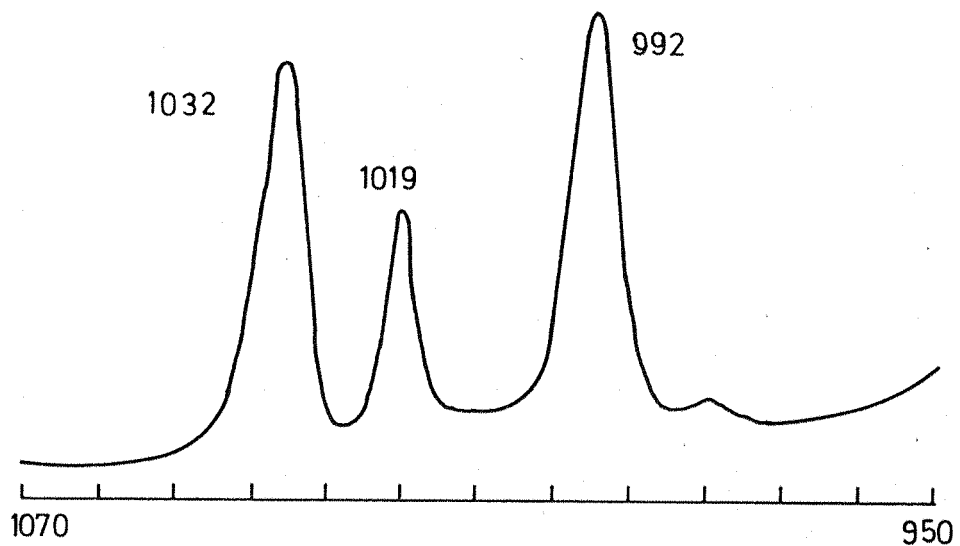


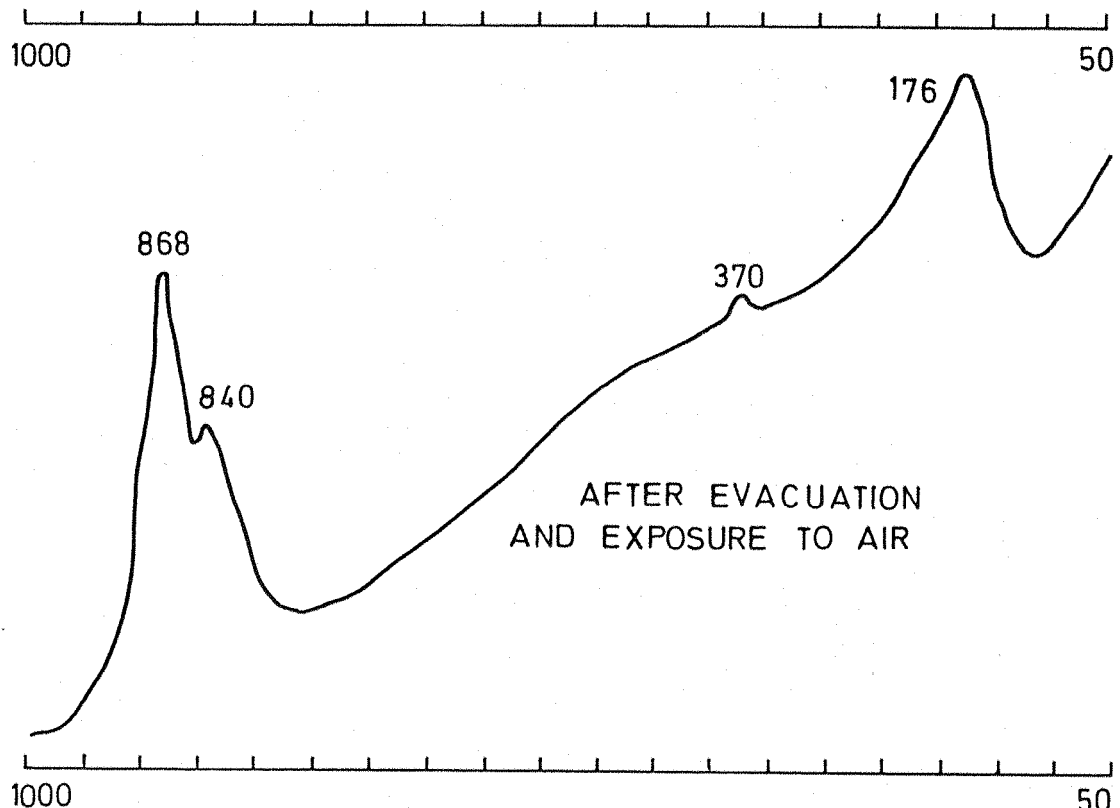
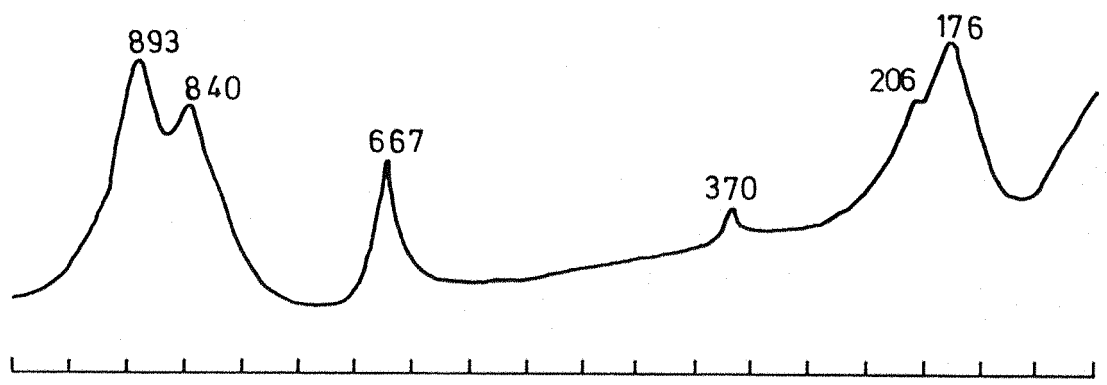
Fig. 5.13 RAMAN SPECTRA OF PYRIDINE ADSORBED ON
ROOM TEMPERATURE ACTIVATED γ - Al_2O_3



RAMAN SPECTRA OF PYRIDINE ADSORBED ON
950°C ACTIVATED γ - Al_2O_3

Fig. 5.14

100



γ - Al_2O_3 ACTIVATED AT ROOM TEMPERATURE / UF_6

Fig. 5.15

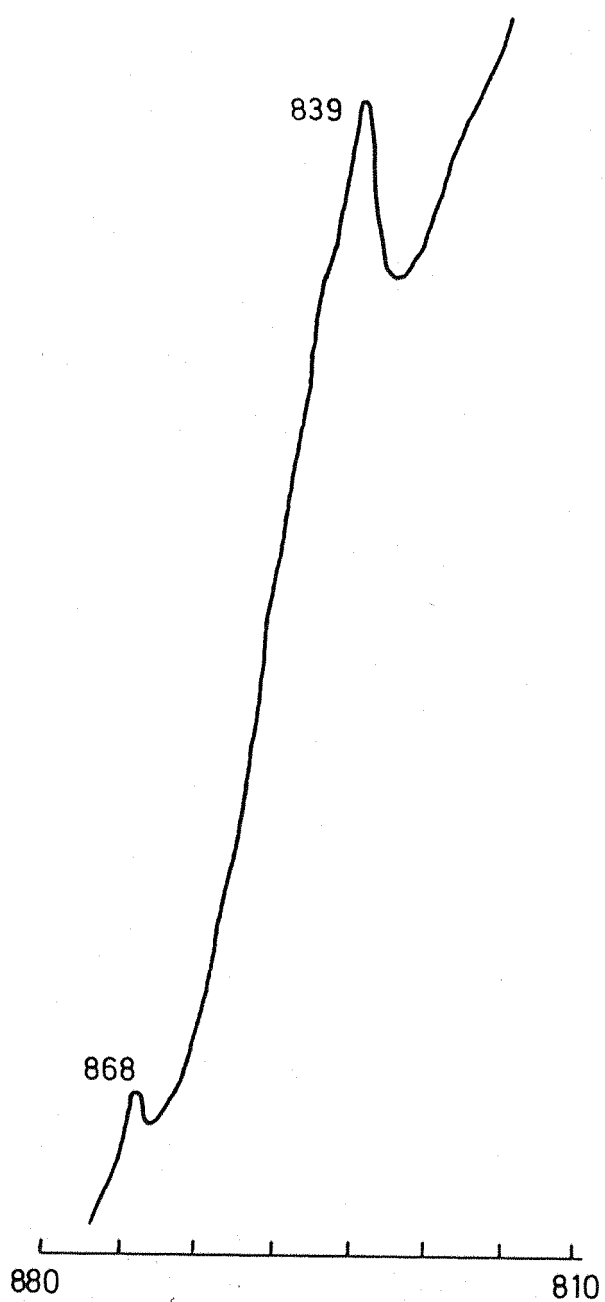
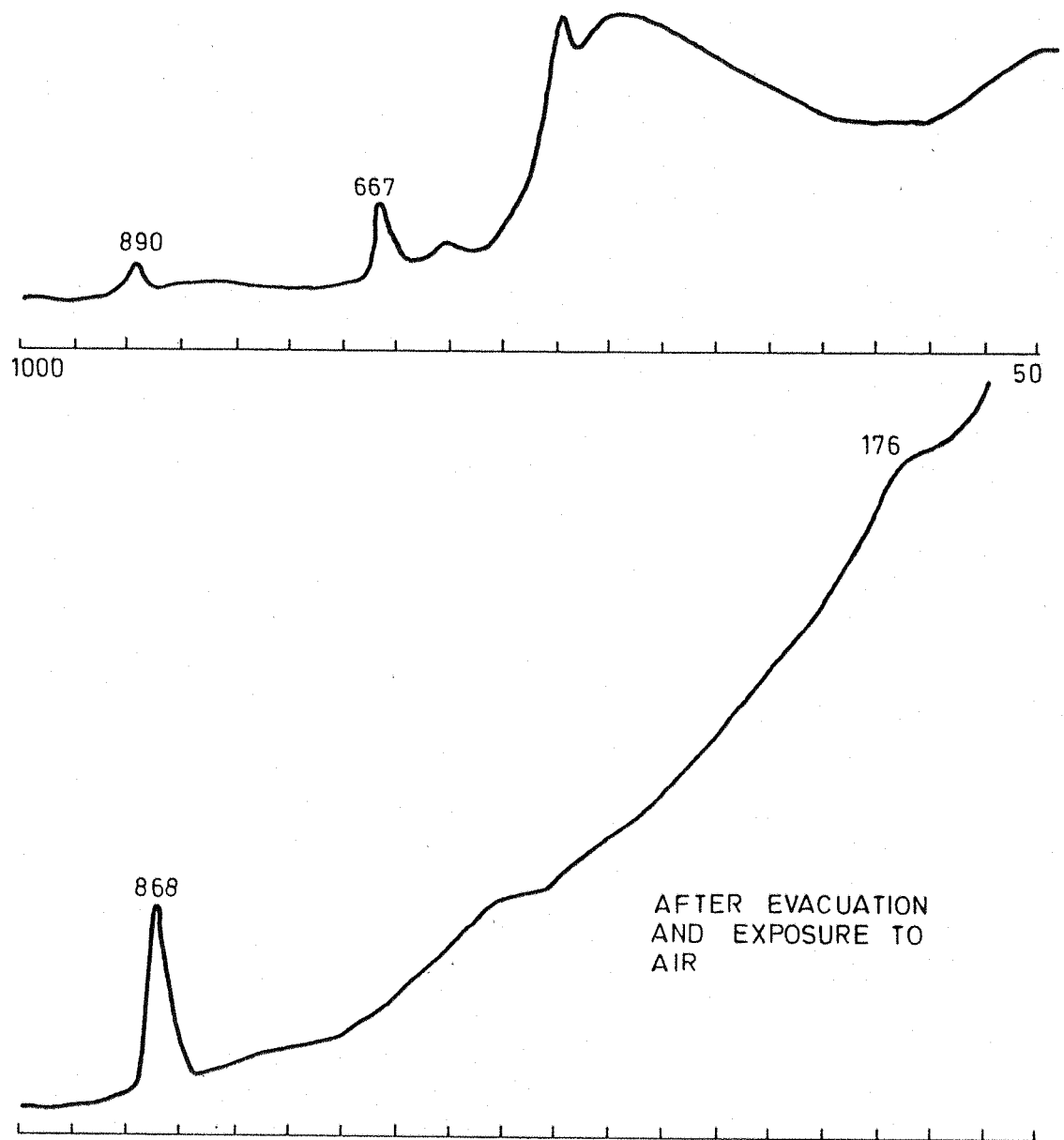


Fig. 5.16 UO_2F_2 ADSORBED ON $\gamma\text{-Al}_2\text{O}_3$



γ - Al_2O_3 ACTIVATED AT 950°C / UF_6

Fig. 5.17

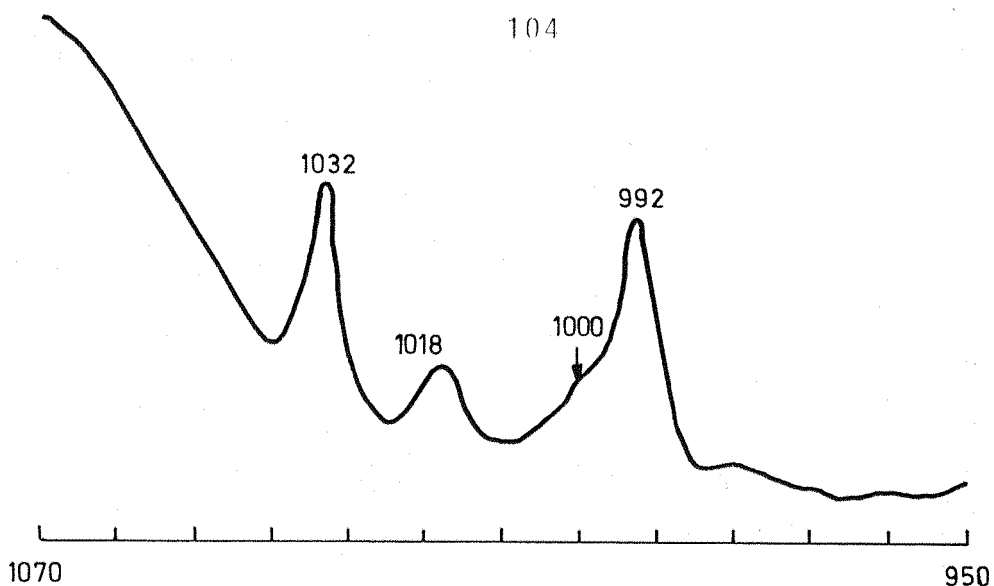
in 2 ml of H_2O then 1 g $\gamma-Al_2O_3$ added. The UO_2F_2 was adsorbed on the $\gamma-Al_2O_3$, and all the UO_2F_2 was removed from the water, and the $\gamma-Al_2O_3$ was yellow. The UO_2F_2 could not be washed off the $\gamma-Al_2O_3$. The Raman spectrum (Fig. 5.16) was recorded after drying in air. The extremely high background is presumably due to the hydroxyls on the $\gamma-Al_2O_3$ surface (102). The band at 839 cm^{-1} is due to UO_2F_2 adsorbed on the surface, and some free UO_2F_2 is also present (band at 868 cm^{-1}).

UF_6 adsorbed on $950\text{ }^\circ C$ activated $\gamma-Al_2O_3$ turned a light brown colour and made it difficult to record spectra, and only 20 mW of laser power was used. The spectra are shown in Fig. 5.17. The bands at 890 and 667 cm^{-1} are weak compared with the normally weak background spectrum of the quartz cell. The weak physisorbed band at 667 cm^{-1} disappears on evacuation and exposure to air. The 890 cm^{-1} band is most probably due to a small amount of $U_2O_3F_6$ formed on the surface, and this hydrolyses to UO_2F_2 on exposure to air. UF_6 is very much less physisorbed on the $950\text{ }^\circ C$ activated surface than on the room temperature activated one. The difference between the two surfaces being a very much larger population of Lewis sites at $950\text{ }^\circ C$ activation, an absence of hydroxyl groups and a $\sim 40\%$ lower surface area. Thus UF_6 is physisorbed much less to a surface covered with Lewis sites. The $U_2O_3F_6$ formed on the surface is due to the small amount of hydroxyls remaining on activating $\gamma-Al_2O_3$ at $950\text{ }^\circ C$.

5.5.2 ZnO

The Raman spectrum of pyridine adsorbed on room temperature activated ZnO is shown in Fig. 5.18. This shows ZnO has a large number of Lewis sites (1018 cm^{-1}) at room temperature activation and significantly less hydrogen bonded pyridine (1000 cm^{-1}) than $\gamma-Al_2O_3$ under the same conditions.

ZnO activated at room temperature turned a light yellow colour on admitting UF_6 to the cell. The Raman spectra are shown in Fig. 5.18. No physisorbed UF_6 was observed due to the abundance of Lewis sites. The bands at 439 , 383 , 335 and 102 cm^{-1} are characteristic of ZnO. The bands at 893 , 647 and 176 cm^{-1} indicate $U_2O_3F_6$ is the hydrolysis



PYRIDINE ADSORBED ON ROOM TEMPERATURE ACTIVATED ZnO

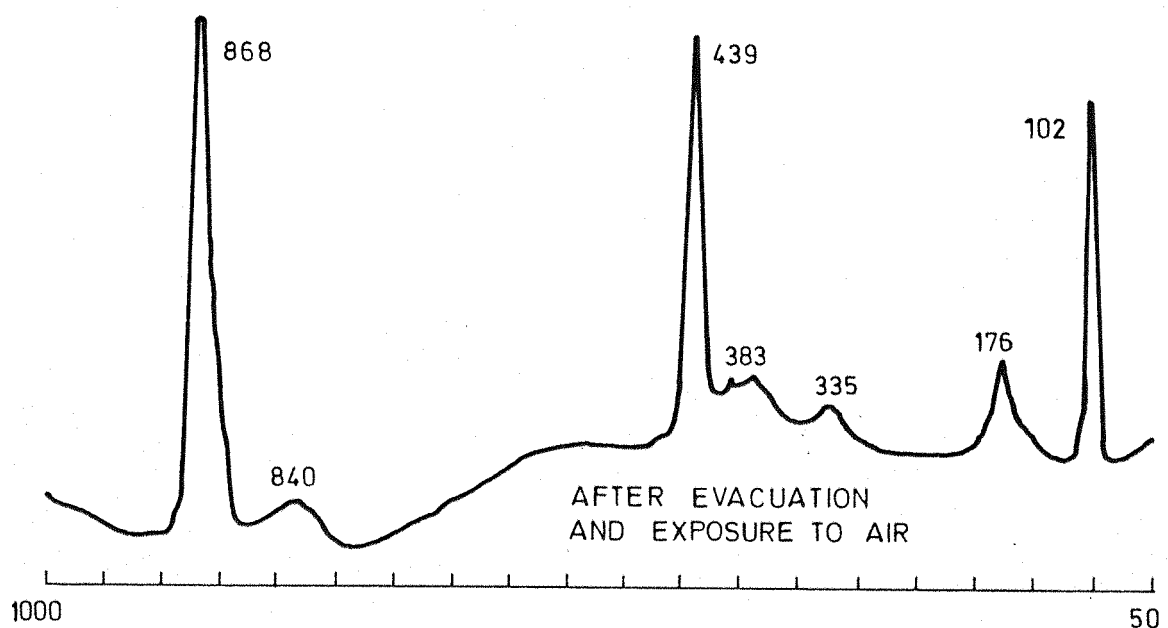
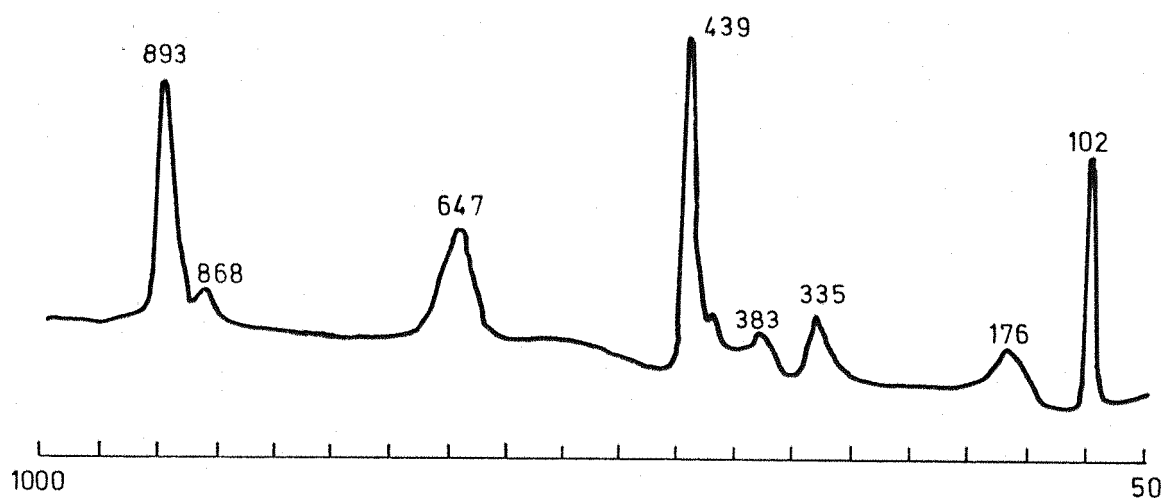


Fig. 5.18 ROOM TEMPERATURE ACTIVATED ZnO / UF₆

product of UF_6 with the physisorbed water and hydroxyl groups on the surface. The band at 868 cm^{-1} indicates that some of the $\text{U}_2\text{O}_3\text{F}_6$ has hydrolysed a step further to UO_2F_2 . On evacuation and exposure to air, all the $\text{U}_2\text{O}_3\text{F}_6$ is hydrolysed to UO_2F_2 (868 and 176 cm^{-1}) and the 647 cm^{-1} band disappears. The band at 840 cm^{-1} attributed to adsorbed UO_2F_2 on the surface is now present.

5.5.3 TiO_2

The study of adsorption of UF_6 on TiO_2 was rendered impossible due to the very strong bands of TiO_2 at 793 w , 640s , 516s , 396s , 320w , 199m and 143vs . With 2 cm^{-1} spectral bandpass and 50 mW laser power, the 143 and 640 cm^{-1} bands exceeded 10^6 and 10^5 counts per second respectively, totally obscuring any bands of UF_6 .

5.5.4 MgO

The low surface area MgO reacts similarly to ZnO in the presence of UF_6 . Hendra, Horder and Loader (93, 70) have shown that MgO shows no chemisorption of pyridine. The Raman spectrum of room temperature activated MgO/UF_6 is shown in Fig. 5.19

The bands due to $\text{U}_2\text{O}_3\text{F}_6$ (893 , 649 and 176 cm^{-1}) and physisorbed UF_6 (667 cm^{-1}) are present. Physisorbed UF_6 is present on the surface as there are no Lewis sites present (93, 70). On evacuation the physisorbed UF_6 is removed and on exposure to air the $\text{U}_2\text{O}_3\text{F}_6$ hydrolyses to UO_2F_2 . The 840 cm^{-1} band due to adsorbed UO_2F_2 is also present.

5.6 Adsorption on laser absorbing coloured oxides

Deeply coloured oxides such as NiO and Fe_2O_3 have severe heating effects in the Ar^+ laser beam. To partially overcome these problems the optics were used at their optimum positions with wide slits and an unfocussed laser beam on the sample.

5.6.1 NiO

The light grey low surface area NiO was activated at room temperature then pyridine adsorbed. After 1 hour of signal averaging in the spectral region 940 to $1\ 080 \text{ cm}^{-1}$ the spectrum showed the presence of Lewis sites ($1\ 016 \text{ cm}^{-1}$) on the surface and no hydroxyl groups, see Fig. 5.20

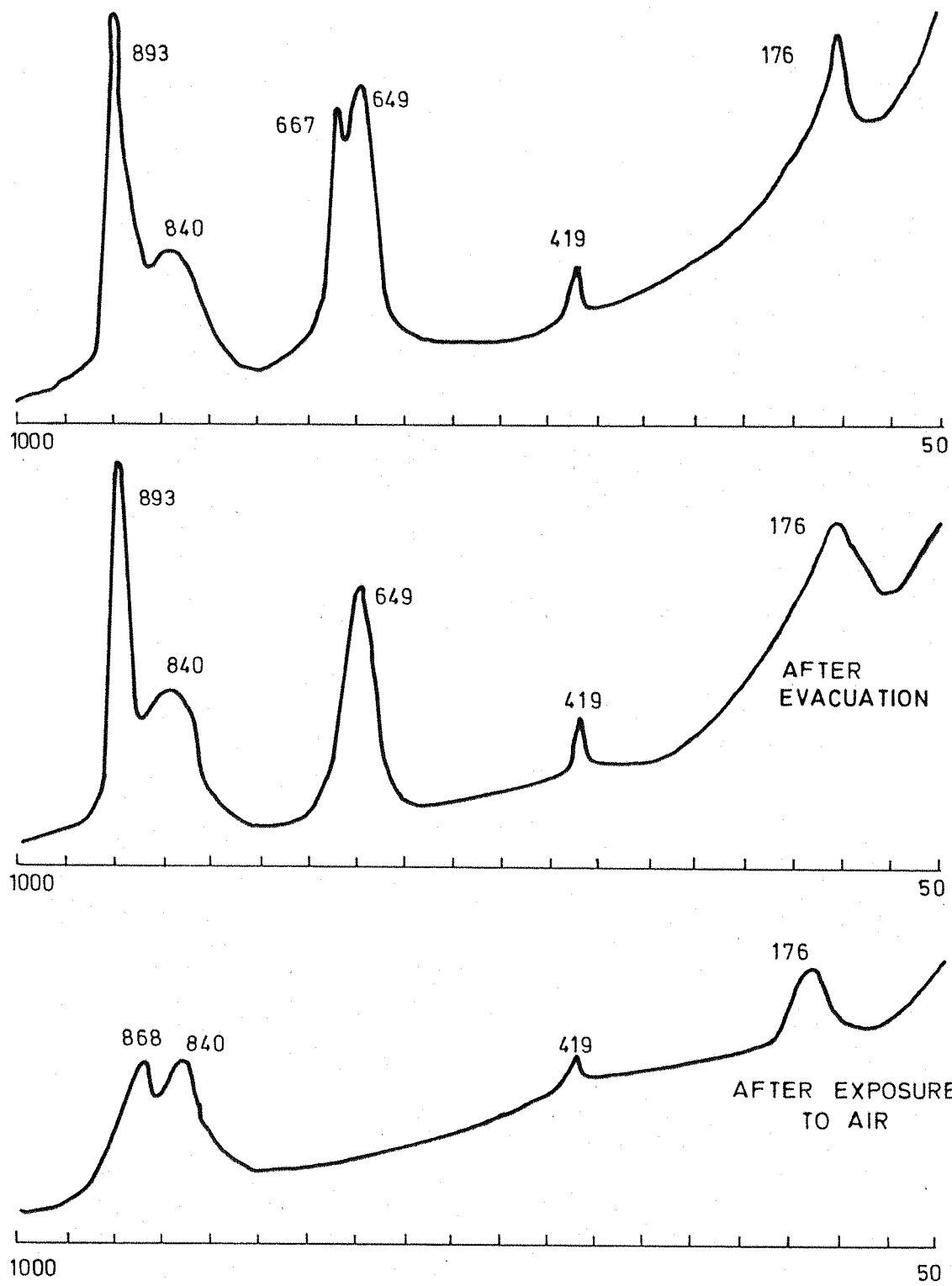


Fig. 5.19 MgO ACTIVATED AT ROOM TEMPERATURE / UF₆

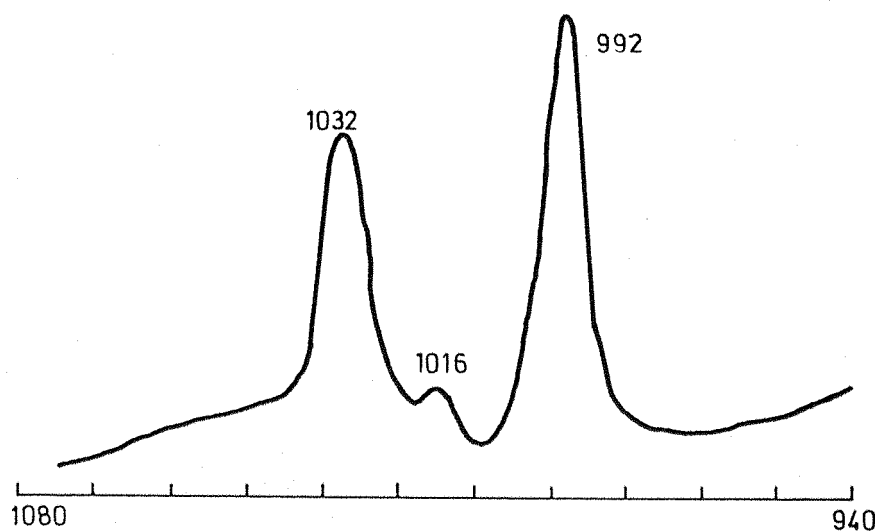


Fig. 5.20 PYRIDINE ADSORBED ON ROOM TEMPERATURE ACTIVATED NiO

Due to the strength of the Lewis coordinated pyridine band, very little UF_6 is expected to physisorb on the surface, and using the identical optical conditions as above, no spectrum of adsorbed UF_6 or hydrolysis products of UF_6 could be observed on the surface after signal averaging for 1 hour.

5.6.2 Fe_2O_3

No bands of adsorbed pyridine were found on a sample of room temperature activated Fe_2O_3 after signal averaging the spectral region $940 - 1080 \text{ cm}^{-1}$ for 1 hour.

The heating effect and absorbtion of the laser beam and Raman scatter makes it difficult to record spectra from coloured oxides. Better results can be expected using a spinning cell and a red laser line.

Chapter 6CONCLUSIONS

The project described here involved the extension of the expertise available at Southampton on the Raman spectra of adsorbed species, and its application to new problems of interest. On the experimental side the following were investigated:

- a) The optimum sample illumination and collection geometry for the study of surfaces and adsorbed species.
- b) The adsorption and reaction of UF_6 at oxide surfaces.

The currently used optics for Raman spectrometers is shown not to be the optimum for surface studies. By using the collection optics at their optimum demagnification of the slits (much lower than that used in commercial spectrometers), a higher Raman signal is obtained as it is collected more efficiently. The decrease in demagnification causes the spectrometer to view a larger area on the surface and since the maximum Raman signal is collected when the slit image is completely illuminated, the light flux density at the surface is greatly reduced especially when a cylindrical lens is used to strip focus the laser beam on the sample. Thus desorption/decomposition problems are greatly reduced. Since Raman scattering is intrinsically a weak effect, the increased signal enables the detection limit to be increased.

The surfaces of metal oxides were characterised with pyridine after activation at various temperatures. Silica gel activated at $950^{\circ}C$ has many siloxane bridges on the surface and strongly physisorbs UF_6 . UF_6 is also strongly chemisorbed to this surface with the totally symmetric U-F vibration shifting downwards by 29 cm^{-1} . Less than 0.05 monolayers of adsorbed UF_6 could be detected on this surface. Surfaces containing Lewis sites showed no chemisorption of UF_6 and very little physisorption.

No fluorination of the metal oxide surfaces could be detected at room temperature but presumably does occur at higher temperatures.

UF_6 reacts with the physisorbed water and hydroxyl groups on the surface to form $U_2O_3F_6$, UO_2F_2 and adsorbed UO_2F_2 . The $U_2O_3F_6$ is formed by the controlled hydrolysis of UF_6 .

on the surface. So far only UOF_4 and $\text{U}_3\text{O}_5\text{F}_8$ have been prepared by the controlled hydrolysis of UF_6 . UOF_4 is noticeably absent from the surface species which is unexplained as it precedes $\text{U}_2\text{O}_3\text{F}_6$ in the hydrolysis of UF_6 .

Since the solid-gas interface is of such importance in industry and nature, further investigation using Raman spectroscopy should bring to light more information about the adsorption and reaction processes occurring at surfaces.

REFERENCES

1. F Haber Z. Electrochem. 20, 521 (1914)
2. G Ehrlich J. Chem. Phys. 34, 29 (1961)
3. G Ehrlich J. Chem. Phys. 34, 39 (1961)
4. J Medema J. Catal. 37, 91 (1975)
5. V A Dzis'ko, A A Vishnevskaya and V S Chesalova Zhur. Fiz. Khim. 24, 1416 (1950)
6. E Robinson and R A Ross Can. J. Chem. 48, 2210 (1970)
7. R W Glass and R A Ross Can. J. Chem. 50, 2817 (1972)
8. R W Glass and R A Ross Can. J. Chem. 50, 2537 (1972)
9. M I Dashevskii, V I Yakerson and A M Rubinstein Dokl. Akad. Nauk. SSSR 225, 123 (1975)
10. R W Glass and R A Ross Can. J. Chem. 49, 2832 (1971)
11. G W Simmons, D F Mitchell and K L Lawless Surface Sci. 8, 130 (1967)
12. B J Hopkins, A R Jones and R I Winton Surface Sci. 57, 266 (1976)
13. H Conrad, G Erth, J Küppers and E E Latta Surface Sci. 57, 475 (1976)
14. K Horn, M Hussain and J Pritchard Surface Sci. 63, 244 (1977)
15. R Feder and G Gafner Surface Sci. 57, 45 (1976)
16. D F Mitchell, P B Sewell and M Cohen Surface Sci. 61, 355 (1976)
17. E J Sheibner and L N Tharp Surface Sci. 8, 247 (1967)
18. P Auger J. Phys. Radium 6, 205 (1925)
19. L A Harris J. Appl. Phys. 39, 1419 (1968)
20. P W Palmberg, G K Bohn and J C Tracy Appl. Phys. Lett. 15, 254 (1969)
21. N C MacDonald Appl. Phys. Lett. 16, 76 (1970)
22. B A Joyce and J H Neave Surface Sci. 27, 499 (1971)
23. P W Palmberg Surface Sci. 25, 598 (1971)
24. M P Hooker, J T Grant and T W Haas J. Vac. Sci. Technol. 13, 296 (1976)



25.	B W Byrum	Rev. Sci. Instrum.	45,	707	(1974)
26.	D Lichtman, R B McQuistan and T R Kirst	Surface Sci.	5,	120	(1966)
27.	R Castaing	Advan. Electron. Electron Phys.	13,	317	(1960)
28.	R L Park and J E Houston	J. Vac. Sci. Technol.	10,	176	(1973)
29.	W Heiland and E Taglauer	J. Vac. Sci. Technol.	9,	620	(1972)
30.	R E Honig	J. Appl. Phys.	29,	549	(1958)
31.	J M Morabito and R K Lewis	Anal. Chem.	45,	869	(1973)
32.	A Benninghoven	Surface Sci.	28,	541	(1971)
33.	S Paletto, M Perdrix, R Goutte and G Guilland	Surface Sci.	35,	473	(1973)
34.	A Benninghoven	Surface Sci.	35,	427	(1973)
35.	H D Hagstrum	Phys. Rev.	150,	495	(1966)
36.	R G Masket and W Bauer	Appl. Phys. Lett.	20,	411	(1972)
37.	J E Mapes and R R Eischens	J. Phys. Chem.	58,	809	(1954)
38.	E P Parry	J. Catal.	2,	371	(1963)
39.	J T Yates, R G Greenler I Ratajczykowa and D A King	Surface Sci.	36,	739	(1973)
40.	P Debye, H R Anderson and H Brumberger	J. Appl. Phys.	28,	678	(1957)
41.	S Tamagusuku	Bull. Kyushu Inst. Technol. Math. Nat. Sci.	12,	71	(1965)
42.	S Tamagusuku	Bull. Kyushu Inst. Technol. Math. Nat. Sci.	13,	21	(1966)
43.	S J Atkinson, C R Brundle and M W Roberts	J. Electron. Spectrosc.	2,	105	(1973)
44.	I D Gay and J F Fritz	J. Phys. Chem.	79,	2145	(1975)
45.	D Freude, D Muller and H Schmiedel	Surface Sci.	25,	289	(1971)
46.	J J Rooney and R C Pink	Trans. Faraday Soc.	58,	1632	(1962)
47.	D J Miller and D Haneman	Phys. Rev. B	3,	2918	(1971)
48.	D F Borofsky and E W Müller	Surface Sci.	10,	177	(1968)

49. B F Lewis, M Moseman and W H Weinberg Surface Sci. 41, 142 (1974)

50. S Brunauer, P H Emmett and E Teller J. Am. Chem. Soc. 60, 309 (1938)

51. R S Hansen, J A Murphy and T C McGee Trans. Faraday Soc. 60, 597 (1964)

52. A G Zettlemoyer and J J Chessick J. Phys. Chem. 64, 1131 (1960)

53. G Karagounis and R Issa Z. Electrochem. 66, 874 (1962)

54. S O Paul M. Phil. Thesis Southampton University (1977)

55. B A Morrow and I A Cody J. Phys. Chem. 80, 1998 (1976)

56. B A Morrow and I A Cody J. Phys. Chem. 80, 1995 (1976)

57. F Koubowetz, H Noller and J Latzel Z. Naturforsch. 31B, 922 (1976)

58. W Schulz and H Knözinger J. Phys. Chem. 80, 1502 (1976)

59. M Tanaka and S Ogasawara J. Catal. 16, 157 (1970)

60. C L Lui and I G Dallalanu Can. Sulphur Sym. Paper. 12 (1974)

61. J H Taylor and C H Amberg Can. J. Chem. 39, 535 (1961)

62. L H Little and C H Amberg Can. J. Chem. 40, 1997 (1962)

63. P J Lucchesi, J L Carter and D J C Yates J. Phys. Chem. 66, 1451 (1962)

64. C V Raman Indian J. Phys. 2, 387 (1928)

65. A Smekal Naturwiss. 11, 873 (1923)

66. P J Hendra and E J Loader Nature 216, 789 (1967)

67. P J Hendra and E J Loader Nature 217, 637 (1968)

68. R O Kagel J. Phys. Chem. 74, 4518 (1970)

69. T A Egerton, A H Hardin, Y Kozirovski and N Sheppard J. Catal. 32, 343 (1974)

70. P J Hendra, J R Hoarder and E J Loader J. Chem. Soc. A 11, 1766 (1971)

71. T A Egerton, A H Hardin, Y Kozirovski and N Sheppard Chem. Comm. 887 (1971)

72. P J Hendra, I D M Turner, E J Loader and M Stacey J. Phys. Chem. 78, 300 (1974)

73. E Buechler and J Turkevich J. Phys. Chem. 76, 2325 (1972)

74. H Jeziorowski and H Knözinger Chem. Phys. Lett. 43, 37 (1976)

75. P J Hendra and E J Loader Trans. Faraday Soc. 67, 828 (1971)

76. C L Angel J. Phys. Chem. 77, 222 (1973)

77. E J Loader J. Catal. 22, 41 (1971)

78. J W Linnett, L D Barrow and A K Bhattacharya J. Raman. Spectrosc. 3, 3 (1975)

79. S P S Porto and D L Wood J. Opt. Soc. Am. 52, 251 (1962)

80. H Kogelnik and S P S Porto J. Opt. Soc. Am. 53, 1446 (1963)

81. J J Barrett and N I Adams J. Opt. Soc. Am. 58, 311 (1968)

82. R R Alfano and N Ockman J. Opt. Soc. Am. 58, 90 (1968)

83. J F James M.N.R.A.S. 137, 15 (1967)

84. G B Benedek and F Fritsch Phys. Rev. 149, 647 (1966)

85. R L Schwiesow J. Opt. Soc. Am. 59, 1285 (1969)

86. W Pilz J. Raman. Spectrosc. 5, 153 (1976)

87. T C Damen, R C C Leite and S P S Porto Phys. Rev. Lett. 14, 9 (1965)

88. S P S Porto J. Opt. Soc. Am. 56, 1585 (1966)

89. J L Koenig and F J Boerio J. Chem. Phys. 50, 2823 (1969)

90. P J Hendra and I D M Turner J. Phys. Chem. 78, 300 (1974)

91. R G Greenler and T L Slager Spectrochim. Acta. 29, 193 (1973)

92. I D M Turner Ph. D. Thesis Southampton University (1974)

93. P J Hendra, J R Horder and E J Loader Chem. Comm. 563 (1970)

94. J B Peri J. Phys. Chem. 69, 220 (1965)

95. J B Peri and R B Hannan J. Phys. Chem. 64, 1526 (1960)

96. B A Morrow and I A Cody J. Phys. Chem. 79, 761 (1975)

97. K A Krieger J. Am. Chem. Soc. 63, 2712 (1941)

98. M Muroya Bull. Chem. Soc. Japan 43, 3453 (1970)

99. G T Pott and B D McNicol Chem. Phys. Lett. 6, 623 (1970)

100. G Careri, V Mazzacurati and G Signoreli Phys. Lett. 31, 425 (1970)

101. G Careri, V Mazzacurati, M Sampoli and G Signoreli Phys.Lett. 32, 495 (1970)

102. G Careri, V Mazzacurati M Sampoli and G Signoreli J.Catal. 26, 494 (1972)

103. H Jeziorowski and H Knözinger Chem.Phys. Lett. 51, 519 (1977)

104. W Kiefer and H J Bernstein Appl.Spectrosc 25, 127 (1971)

105. N Zimmerer and W Kiefer Appl.Spectrosc 28, 279 (1974)

106. R S McDowell, L B Asprey and R T Paine J.Chem.Phys. 61, 3571 (1974)

107. M G Otey and R A Le Doux J.Inorg.Nucl.Chem. 29, 2249 (1967)

108. W H Zachariasen Acta.Crystallogr. 1, 277 (1948)

109. V P Seleznov, Å A Tsvetkov, B N Sudarikov and B V Gromov Russian J. of Inorg. Chem. 17, 1356 (1972)

110. P W Wilson Chem.Comm. 22, 1241 (1972)

111. E Jacob and W Polligkeit Z. Naturforsch.B 28, 120 (1973)

112. R T Paine, R R Ryan and L B Asprey Inorg.Chem. 14, 1113 (1975)

113. J C Taylor and P W Wilson Chem.Comm. 232 (1974)

114. P W Wilson J.Inorg.Nucl.Chem. 36, 303 (1974)

115. P W Wilson J.Inorg.Nucl.Chem. 36, 1783 (1974)

116. L Müller Acta.Chim.Acad. Sci.Hung. 59, 1 (1969)

117. W Colvin Union Carbide Co. Publ no 12315

118. J Forkos Oak Ridge gaseous diffusion plant A3604 Z (1945)

119. G J van Schalkwyk and P J Hendra J.Inorg.Nucl.Chem. 39, 894 (1977)